UC Berkeley
UC Berkeley Electronic Theses and Dissertations

Title

Support Effects in Catalysis Studied by in-situ Sum Frequency Generation Vibrational Spectroscopy and in-situ X-Ray Spectroscopies

Permalink

https://escholarship.org/uc/item/4fv0q7sh

Author

Kennedy, Griffin John

Publication Date

2016

Peer reviewed|Thesis/dissertation

eScholarship.org Powered by the California Digital Library
University of California

Support Effects in Catalysis Studied by *in-situ* Sum Frequency Generation Vibrational Spectroscopy and *in-situ* X-Ray Spectroscopies

By

Griffin John Kennedy

A dissertation submitted in partial satisfaction of the

requirements for the degree of

Doctor of Philosophy

in

Chemistry

in the

Graduate Division

of the

University of California, Berkeley

Committee in charge:

Professor Gabor A. Somorjai, Chair
Professor Martin Head-Gordon
Professor Michael F. Crommie

Fall 2016

Abstract

Support Effects in Catalysis Studied by *in-situ* Sum Frequency Generation Vibrational Spectroscopy and *in-situ* X-Ray Spectroscopies

By

Griffin John Kennedy

Doctor of Philosophy in Chemistry

University of California, Berkeley

Professor Gabor A. Somorjai, Chair

Kinetic measurements are paired with in-situ spectroscopic characterization tools to investigate colloidally based, supported Pt catalytic model systems in order to elucidate the mechanisms by which metal and support work in tandem to dictate activity and selectivity. The results demonstrate oxide support materials, while inactive in absence of Pt nanoparticles, possess unique active sites for the selective conversion of gas phase molecules when paired with an active metal catalyst.

In order to establish a paradigm for metal-support interactions using colloidally synthesized Pt nanoparticles the ability of the organic capping agent to inhibit reactivity and interaction with the support must first be assessed. Pt nanoparticles capped by poly(vinylpyrrolidone) (PVP), and those from which the PVP is removed by UV light exposure, are investigated for two reactions, the hydrogenation of ethylene and the oxidation of methanol. It is shown that prior to PVP removal the particles are moderately active for both reactions. Following removal, the activity for the two reactions diverges, the ethylene hydrogenation rate increases 10-fold, while the methanol oxidation rate decreases 3-fold. To better understand this effect the capping agent prior to, and the residual carbon remaining after UV treatment are probed by sum frequency generation vibrational spectroscopy. Prior to removal no major differences are observed when the particles are exposed to alternating H_2 and O_2 environments. When the PVP is removed, carbonaceous fragments remain on the surface that dynamically restructure in H_2 and O_2. These fragments create a tightly bound shell in an oxygen environment and a porous coating of hydrogenated carbon in the hydrogen environment. This observation explains the divergent catalytic results. Reaction rate measurements of thermally cleaned PVP and oleic acid capped particles show this effect to be independent of cleaning method or capping agent. In all this demonstrates the ability of the capping agent to mediate nanoparticle catalysis.

With this established the hydrogenation of furfural by Pt supported on SiO_2 and TiO_2 was investigated by an approach combining reaction studies with SFG in order to gain molecular level insight into the nature of the metal-support interaction. This is the first instance of SFG being

used to probe the factors governing selectivity in a supported catalyst system. This work revealed that TiO_2 possessed sites, that while inactive without Pt, became highly active for the selective conversion of furfural to furfuryl alcohol. By SFG a TiO_2 bound intermediate species was identified that could explain the highly selective nature of the reaction by Pt/TiO_2. In combination with density functional theory calculations it was determined that furfural bound favorably to oxygen vacancy sites on the TiO_2 surface through the aldehyde oxygen, which in turn activated the aldehyde group for hydrogenation by a charge transfer mechanism. This intermediate could then react with spillover hydrogen from the Pt surface to form furfuryl alcohol.

In an effort to generalize this mechanism to additional molecules and reducible oxides the work was expanded to the hydrogenation of crotonaldehyde with cobalt oxide as an additional support. Reaction studies and SFG study of the Pt/TiO_2, Pt/Co_3O_4, and Pt/SiO_2 catalysts, revealed a reaction pathway for Pt/TiO_2 and Pt/Co_3O_4 which selectively produced alcohol products, crotyl alcohol and butanol, while no alcohol production was observed for the Pt/SiO_2 catalyst. A thorough study of the possible secondary reaction pathways revealed that butanol was formed in a concerted manner, rather than through sequential hydrogenation of the C=C and C=O groups. Sum frequency generation studies revealed that Pt supported on SiO_2 yielded identical reaction intermediates as Pt single crystals, further cementing the passive role of SiO_2. Spectra obtained from the cobalt and titanium oxide supported catalysts revealed adsorption sites exist on the oxide surfaces through which the molecule binds via the aldehyde group. These sites are believed to be the active sites for alcohol production. In the case of Co_3O_4 ambient pressure x-ray photoelectron spectroscopy and x-ray absorption spectroscopy reveal a reduction of the oxide surface under reaction conditions indicating the adsorption sites on the oxide exist on a reduced surface, additional evidence for the site being an O-vacancy.

To better understand the interplay between the formation of the two alcohols a Pt nanoparticle density dependence study was undertaken for the Co_3O_4 case. It was observed that increasing the Pt density, thus increasing the ratio of interface to oxide surface sites, led to an increase in butanol and decrease in crotyl alcohol production. From this it is proposed that butanol forms at the Pt-oxide interface while the crotyl alcohol forms via the spillover mechanism at an oxide site.

Lastly a before undiscovered example of encapsulation of a metal particle by an oxide support is observed for the Pt/Co_3O_4 system by ambient pressure x-ray photoelectron spectroscopy. Under mild conditions an encapsulated state is reached in which the oxide covers the Pt surface, yet does not inhibit reactivity. In fact the total activity of the catalyst increases dramatically and a change in product selectivity was observed. By SFG it is seen that the features of a Pt bound butyraldehyde intermediate increase in intensity, which is directly correlated to a 3-fold increase in butyraldehyde activity.

This work builds on a vast knowledge of catalyst-support interactions in heterogeneous catalysis by applying in-situ techniques to yield a molecular level understanding of the surface processes.

Table of Contents

Acknowledgements **ii**

Chapter 1 Introduction **1**

1.1 Background and Motivation
1.2 The Evolution of Model Catalysts: Single Crystals to Colloidal Nanoparticles
1.3 The Evolution of Surface Science Techniques: Ultra High Vacuum to In-Situ
1.4 Support Effects in Catalysis
1.5 References

Chapter 2 Experimental Methods **11**

2.1 Catalyst Preparation
2.2 Catalyst Characterization
2.3 Catalytic Reaction Studies

Chapter 3 The Role of an Organic Cap in Nanoparticle Catalysis: Reversible Restructuring of Carbonaceous Material Controls Catalytic Activity of Platinum Nanoparticles for Ethylene Hydrogenation and Methanol Oxidation **19**

Chapter 4 Furfuraldehyde Hydrogenation on Titanium Oxide-Supported Platinum Nanoparticles Studied by Sum Frequency Generation Vibrational Spectroscopy: Acid–Base Catalysis Explains the Molecular Origin of Strong Metal–Support Interactions **35**

Chapter 5 Selective Amplification of C=O Bond Hydrogenation on Platinum with TiO_2 as a Support: Catalytic Reaction and Sum-Frequency Generation Vibrational Spectroscopy Studies of Crotonaldehyde Hydrogenation **52**

Chapter 6 In Situ Spectroscopic Investigation into the Active Sites for Crotonaldehyde Hydrogenation at the Pt Nanoparticle Co_3O_4 Interface **67**

Chapter 7 Encapsulation of Pt Nanoparticles by Cobalt Oxide and its Effect on the Hydrogenation of Crotonaldehyde Studied by in-situ Vibrational and X-Ray Spectroscopies **83**

Acknowledgements

The research contained within this dissertation was supported by U.S. Department of Energy, Office of Science, Office of Basic Energy Sciences, Chemical Sciences, Geosciences, and Biosciences Division, under Contract DE-AC02-05CH11231. I received additional support from the Lam Research Graduate Student Fellowship. I am grateful for the opportunity I was afforded as a result of this support.

I must start by expressing my gratitude to Professor Gabor A. Somorjai for providing this amazing opportunity and for his guidance throughout my graduate education. It is a unique opportunity to work for someone with such as strong scientific legacy and a truly unique perspective on research. I was always happy to listen to the stories he would tell of how a breakthrough might come from an unexpected place, or to hear about his personal experiences and how they shaped him into the inspiring person he has become. The emphasis he places on training his students to be complete and capable scientists has left a lasting impact on me, and I am grateful to be able to take that training with me to my next opportunity.

I have an incredible well of gratitude and respect for Robert Baker, without whom, I am convinced, I would not be writing this dissertation today. As my GSI, Robert was infectiously enthusiastic about chemistry and was eager to engage me and the other students of the physical chemistry laboratory course, on a deep scientific level. After that course I joined Robert as an undergraduate researcher where his aptitude as a mentor and scientist were always apparent. It was my work with Robert that inspired me to pursue my graduate education, after being so unsure about what it was I wanted to do with my future. His current success as a professor continues to inspire me and is a testament to the idea that hard work and scientific intuition can bring you great things.

I also want to thank all the researchers whose paths I have crossed as a member of the Somorjai group. Particularly I want to thank Walter Ralston and Gerome Melaet for the hearty sense of comradery I felt over the years. Our lively lunches and engaging scientific conversations will be some of the great memories I will take away from my time as a graduate student. I want to thank Chris Thompson and Lynda Han for their valuable help and guidance through the complexities of sum frequency generation. Yonaton Horowitz, Ji Su and Christophe Deraedt were all great friends over the last few years, I will genuinely miss coming to work and seeing them every day.

I am incredibly grateful to have had Olivia Hayward as my partner and companion for the last 10 years, since before I knew I was a chemist. Her support, particularly during graduate school, has kept me centered and helped me grow into the person I am today. Being able to come home at the end of a hard day to her and our dog Ramona always lifted my spirits and brought great comfort.

Last, but certainly not least, I thank my parents, Gail and Pat, and sister Glyn, for their constant encouragement and support. My parents afforded me the opportunity, and urged me, to explore every interest and possibility that arose throughout my education and my life and were always supportive of the choices I made. They take any chance they get to express how proud they are of what I have accomplished and it has helped me to keep a clear perspective throughout graduate school.

Chapter 1

Introduction

1.1 Background and Motivation

The development of catalytic technology over the course of the last two centuries has made an indelible impact on a wide range of industries and technologies which are at the heart of modern life. The earliest known example of heterogeneous catalysis, in which chemical reactions take place on the surface of an active material, came in 1823 during the development of the "Döbereiner Lamp," an invention of Johann Wolfgang Döbereiner.[1] In this lamp the reaction of Zn metal with sulfuric acid generated hydrogen gas which could be controllably exposed to a piece of Pt sponge. When the hydrogen made contact with the Pt the exothermic adsorption of hydrogen rapidly increased the temperature of the Pt and initiated a reaction with surface bound oxygen which in turn ignited the stream of hydrogen gas to create a flame. Döbereiner is also credited with creating the first ever supported catalyst, an archetype that has become essential in modern catalytic materials, by impregnating pottery clay with Pt sponge.

While Döbereiner's invention may seem quaint, it preceded countless scientific breakthroughs that fundamentally depended on the kinds of surface catalyzed reactions he first took advantage of. Perhaps the most well-known, and arguably most impactful discovery, is that of the Haber - Bosch first posited by Fritz Haber in 1905. In this process iron catalyzes the reaction of N_2 and H_2 to form ammonia, which at the time was an extremely limited, essential agricultural resource. It allowed for an incredible increase in agricultural productivity that in turn enabled rapid growth in other fields. It is believed that without the Haber - Bosch process agricultural production could only support half of the world's current population.

More recently, in the second half of the 20th century, catalysts for the refining, reforming and conversion of petroleum products and other fine chemicals became a primary research focus as the applications for those products are nearly universal. Additionally as natural petroleum and chemical resources become more constrained the efficient conversion of those starting materials by catalysts becomes increasingly important. In the nearly two centuries since Döbereiner's initial discovery, the market for catalysts has grown to a $20 billion per year business and their applications are incredibly varied.

Looking forward, catalysis will undoubtedly play a crucial role in the development of alternative energy sources and particularly in energy storage. The intermittent nature of renewable energy sources, such as solar and wind energy, necessitates a method of effective energy storage and on-demand release. Electrocatalysis and photocatalysis have been growing fields in recent decades as energy storage by chemical conversion has risen to prominence. Ideas

such as Prof. Dr. George Olah's methanol economy,[2] in which the conversion of CO_2 to methanol by electrochemical methods can be used in conjunction with methanol fuel cells to create an adaptable energy supply, have been put forth as possible solutions, but fundamental hurdles remain in the catalytic technology.

Above I have been speaking largely in terms of "catalysis technology" and not "catalysis science" and this is due to the fact that catalytic technologies have been discovered and improved for decades by a trial and error type approach. This approach, as shown above, has yielded enormously important discoveries, but in almost all cases there is a very limited understanding of the molecular level processes that occur on catalyst surfaces. For instance the exact mechanism of the reaction of hydrogen and oxygen on Pt surface, utilized in the Döbereiner lighter was not truly uncovered until very recently.[3] As more difficult problems arise in catalytic applications the need for a scientific approach which can obtain molecular level understanding of these materials will be needed to inform the intelligent development of increasingly complex materials. This disconnect between the technology and the science of catalysis existed in large part because until the second half of the 20th century there did not exist techniques that could adequately characterize surface structure and molecular interactions with surfaces, and thus all catalysis research prior was limited by the "black box." This means one knew what material they were putting in, knew the products being formed, but could not directly inspect the working system. However in the 1960's the development and proliferation of surface science techniques allowed for the first investigations of the structure of catalytic surfaces and their interactions with molecular species.[4] Two problems still remained however, these studies necessitated the use of high or ultra-high vacuum conditions, and simple model systems that were very different from real catalytic materials.[5] In this introductory chapter I will address the progress that has been made to overcome these experimental limitations, ultimately leading to a much more scientific approach to catalysis employed herein, and discuss the types of phenomena that will be studied in the proceeding chapters, namely how metal nanoparticles and oxide support materials work in concert to control catalytic reactions.

1.2 The Evolution of Model Catalysts: Single Crystals to Colloidal Nanoparticles

Conventional catalyst materials have long consisted of active metal nanoparticles typically supported on high surface area oxides. The particles are often prepared by the reduction of metal salts within the pores of the oxide, called incipient wetness impregnation.[6] This process yields nanoparticles with wide distributions in size but the ease of use and the adaptability to numerous metals, oxides, and additives has lent it to wide spread usage. The primary disadvantage of these materials, from the perspective of a surface chemist, is that their complexity and the lack of precise control makes them exceedingly difficult to study on a molecular or atomistic level. Part of the solution to this problem is using model catalysts, ones which share some, if not all, the characteristics of the conventional material, yet allow for more precise control and study.

The first, and simplest, such model for these materials was the metal single crystal.[7] In contrast to the precipitated metal particles, a single crystal surface can have perfectly characterized surface structure based upon which crystal plane is exposed. Beginning in the 1960s and carrying through to the present day studies on single crystal surfaces have uncovered important surface phenomena, including understanding the energetics of the adsorption of numerous molecules on specific types of surface sites, and the rearrangement of numerous metal surfaces in response to gas adsorption, using techniques such as Low Energy Electron Diffraction (LEED), Auger Spectroscopy, Scanning Tunneling Microscopy, and X-Ray Photoelectron Spectroscopy (XPS).[8,9] The major drawback to such model systems is they do not possess the same catalytic properties as the materials they purport to model so it can be difficult to accurately relate the results of single crystal work to the real working catalyst. The reason for this disconnect is related to one of the most fundamental discoveries from single crystal studies, the fact that the most catalytically active sites on a metal surface tend to be the lowest coordination sites, i.e. kinks and step edges,[10] of which a single crystal typically has few while a nanoparticle has many.

With the development in the last 20 years of colloidal methods for synthesizing nanomaterials, a new archetype for model catalytic systems arose which much more closely resembled the conventional materials with crucial advantages. In the colloidal method organic capping ligands are used to lower the surface energy of crystallites which form in solution thus halting their growth. By changing the conditions (solvent, temperature, capping molecule) under which the particles are synthesized one can carefully tune a number of their properties. The colloidal preparation methods for metal nanoparticles were rapidly developed to allow for increasingly precise control over particle size,[11] shape,[12] and composition,[13] where earlier methods offered little direct control over these properties. Not only were these materials better controlled but, they also functioned catalytically. As such new size dependent catalytic properties could be observed that were previously washed out by wide size distributions. As an example the hydrogenation of benzene was widely believed to be insensitive to nanoparticle size, as controlled by the incipient wetness method, but when studied using colloidally synthesized Pt nanoparticles a clear size dependence was observed.[14] Additionally shape control meant that, much like single crystals, these particles could be synthesized with specific exposed crystal facets, and thus reactivity could be directly correlated with the types of sites on those facets.[15] Furthermore these colloids could be combined with flat or porous support materials to better understand the influence that the support may have.[16]

The fundamental difference between colloidally prepared particles and those formed by the earlier methods is the presence of the aforementioned organic capping ligands. In chapters 3 and 4 this issue is addressed directly. In those chapters the impact of the capping agent and its removal, on catalytic properties and the interaction with support materials is thoroughly investigated.

While the above advances in model systems allowed for a better understanding of the materials and how their microscopic properties related to catalytic ones, the problem remained that the catalytic reactions took place in a “black box,” and no improvement in controlling the starting materials could solve this problem. Fortunately the development of methods capable of

studying these materials *in-situ*, or under real working conditions was occurring in parallel with the development of new materials.

1.3 The Evolution of Surface Science Techniques: Ultra High Vacuum to In-Situ

As stated earlier catalysis science is relatively young when compared to catalysis as a technology and it began with development of techniques which were uniquely sensitive to material surfaces largely motivated by the development of solid state electronic devices. The earliest of these techniques were Low Energy Electron Diffraction (LEED)[17] and Auger Electron Spectroscopy.[18] Respectively these two methods offered access to atomic level surface structure and elemental composition. The surface specificity of both was due to the fact the excitation source and the signal obtained for them came in the form of low energy electrons. When escaping the surface these electron have very small mean free paths in solid materials, on the order of 1 nm or ~2 atomic layers, meaning the incident electrons could not penetrate past the surface and the signal electrons could only escape from the surface. However this strength is also the reason for its critical weakness when it comes to their application to catalysis, they must be performed in ultra-high vacuum (UHV) conditions as the mean free path of those electrons in atmospheric pressures is on the order of microns. This limitation could be partially overcome and methods were developed to introduce low pressures of gases such that adsorption could be initiated and the structure of monolayers of adsorbed molecules could be determined by LEED. An extensive knowledge base of surface and adsorbate structures was formed by these methods and it offers a fundamental understanding of the interactions between molecules and surfaces.[19,20] Several other surface specific characterization methods, such as X-Ray Photoelectron Spectroscopy and Scanning Tunneling Microscopy were developed over the following decades, but came with some of the same limitations as what preceded them, such as the requirement of UHV or applicability to only single crystal surfaces.

A number varieties of vibrational spectroscopies have been developed specifically to tackle the issue of surface sensitivity. The first of which was Infrared Reflectance Absorbance Spectroscopy (IRRAS), in which an infrared beam is reflected off of the surface of interest and the reflected beam is collected, containing information about the molecular species on the surface.[21] However this method is susceptible to interference by absorption of the incident beam by gas phase molecules. Polarization modulated IRRAS (PM-IRRAS) was subsequently developed to overcome this disadvantage and has been rather widely used to study molecular species on a wide range of surfaces and interfaces.[22,23] The remaining drawback for PM-IRRAS however is that it can only be used on very planar surfaces, such as metal single crystals and, as such, is not well suited to study the nanostructured materials used in catalytic applications. For this purpose Sum Frequency Generation Vibrational Spectroscopy (SFG) is well suited. Surface sensitivity is intrinsic to the SFG process, as explained in greater detail in the following chapter, and it is rather agnostic toward both the gas phase molecules and the surface structure with the appropriate cell design. It has even found success in studying real supported metal catalyst powders. Furthermore SFG can be used to study any type of interface. It has found success in applications ranging from

catalysis science, biological interface design, and atmospheric chemistry for this reason.[24,25,26,27,28] In the chapters that follow, SFG is to study catalytic reactions and the effect of residual surface species on the catalytic properties of a number of multicomponent material systems, and in these studies its strengths are revealed.

In recent years technological and engineering developments have allowed researchers to overcome some of the fundamental limitations of those early surface science techniques as well. Most notably XPS has been adapted for use in pressures of a few torr allowing for surface chemical composition and state to be interrogated under reaction relevant temperatures and gas conditions.[29,30] This technique, known as Ambient Pressure XPS is explained in more detail in chapter 2 and utilized in chapters 6 and 7. Furthermore even electron microscopy techniques such as Transmission Electron Microscopy, also conventionally requiring UHV conditions, are benefiting from engineering advances that allow experiments to be conducted in reactive gas atmospheres. With these developments in microscopy, vibrational spectroscopy and XPS there now exist better tools than ever for looking inside the "black box" and understanding the structure, state, and bonding of heterogeneous catalytic surfaces.

1.4 Support Effects in Catalysis

While it is accepted that metal nanoparticles constitute the active component of most catalysts, they would be rather useless without a support, as unsupported metal particles would quickly agglomerate under the harsh conditions of most industrial reactions. A porous support material, typically composed of metal or semi-metal oxides, can serve many purposes, the most basic of which are to increase the available catalyst surface area, by dispersing the particles within the porous network of the support, and help prevent agglomeration by maintaining substantial separation between particles. This is not the sole function of many support materials however. While typically inert on their own for a given reaction, the support can, by many different mechanisms, dramatically alter the catalytic performance of metal particles, or become an integral part of the catalytic process with active sites of its own.[31,16,32,33,34] I will be focusing on a few key examples relevant to the following work.

One of the hallmark studies of metal-support interactions was performed by Tauster and Fung, in which they supported a number of metals on, initially, TiO_2 and studied the adsorption behavior of the materials after reduction at a range of temperatures.[35] They found that following a reduction treatment at temperature of 773 K or above the adsorption of H_2 and CO dropped nearly to zero indicating the available metal surface area vanished, while the total surface area of the catalyst remained unchanged. This effect was termed the strong metal-support interaction (SMSI). They expanded this work to a number of other reducible oxide materials and a body of literature has since been expanded to show that this effect occurs for high surface energy metals paired with low surface energy reducible oxides. Electron microscopy studies followed from Baker[36] and Komaya[37] showing that this reduction in available metal surface area was due to the decoration and encapsulation of the metal by the support which in turn lowers the surface energy

of the system. The question still remained regarding the influence this encapsulation effect might have on the reactivity of the material.

To address this question Boffa et. al.[38,39] embarked on a series of experiments wherein oxide layers of a number of oxides, with submonolayer coverage, were deposited onto a Rh metal substrate and studied for the hydrogenation of CO, CO_2 and ethylene. The ethylene hydrogenation rate predictable fell off linearly with the coverage of the metal by the oxide as the metal surface is believed to be the catalytically active surface. Conversely the rate other two reactions increased, with a maximal rate enhancement at a coverage of 0.5 monolayer. The resulting catalysts exhibited up to a 10 fold increase in activity depending on the oxide. What this result indicated was that the interface existed as a uniquely active site for the reactions of CO or CO_2 with hydrogen. They found that the maximal rate enhancement correlated well with the Lewis acidity of the various materials and concluded that the oxide layers provided sites which could activate the CO and CO_2 molecules. It is important to note that once a full monolayer of oxide was formed the rate for all reactions went nearly to zero, suggesting that both surfaces must be exposed to initiate the rate enhancement. This can be thought of similarly to bifunctional catalysts in homogeneous catalysis work in which two sites exist in the same catalyst and both are crucial for the production of the product molecule. These sites, in some cases, may work simultaneously to produce the product, or they can work by the spillover and migration of surface intermediates between sites.[40] Numerous other studies in recent years have found these type of mechanism to explain other reactions such as the oxidation of CO, and the reforming of alkanes.[41,16]

The prevalence of oxide mediated reactivity can be seen throughout the catalysis literature, yet in most cases a molecular level understanding of the mechanism by which the oxide participates in the reaction is lacking. In the work presented here I have endeavored to combine the advances in model catalytic systems with those in in-situ spectroscopic techniques to gain such an understanding for a range of material and reaction systems.

1.5 Summary of Dissertation

1.5.1 Experimental Methods

Chapter 2 contains a discussion and description of the experimental methods and equipment used in this research. This can be broken up into three primary categories, catalyst preparation, reaction studies, and characterization methods. Methods of catalyst preparation include colloidal synthesis of nanoparticles, deposition of oxide thin films by electron beam and atomic layer deposition, deposition of nanoparticle films by the Langmuir-Blodgett method, and a number of treatment procedures for the removal of the organic cap. Catalytic reactions were carried out in batch-mode gas phase reactors equipped with gas chromatographs for product separation and analysis. Ex-situ characterization methods include x-ray photoelectron spectroscopy (XPS) and transmission electron microscopy (TEM). In-situ methods include sum frequency generation vibrational spectroscopy (SFG), ambient pressure x-ray photoelectron spectroscopy (AP-XPS) and x-ray absorption spectroscopy (XAS).

1.5.2 The Impact of the Organic Capping Agent on Colloidal Nanoparticle Catalysis

Chapters 3 deals wholly and chapter 4 in part with the role of the organic capping agent in the catalysis of Pt nanoparticles. The organic cap is essential in allowing for size and shape control of colloidally synthesized particles however it remained a question if its presence prohibited catalytic reactions from taking place. These particles were studied for ethylene hydrogenation and methanol oxidation and it was found that prior to the removal of the organic cap the particles were active for both reactions. Following removal by UV irradiation the activity for the two reactions diverged, ethylene hydrogenation increased by a factor of ten or more, while the methanol oxidation decrease by a similar magnitude. To understand this effect we studied the structure of the cap before removal and the structure of carbonaceous deposits which existed after removal. It was found that the carbonaceous material remaining after the treatment dynamically restructured under difference gas conditions, H_2 and O_2, which controlled the reactivity. This was found to be the case regardless of capping ligand or removal method. In chapter 4 the removal of the capping agent is studied as it relates to the interaction between the metal particles and their support.

1.5.3 The Role of the Support in the Selective Hydrogenation of Aldehyde Molecules Studied by in-situ Techniques

Chapters 4, 5, and 6 are all concerned with understanding the mechanism by which metal oxide support materials influence the hydrogenation of aldehyde containing molecules using in situ sum frequency generation vibrational spectroscopy and in chapter 6 the characterization tools are expanded to include ambient pressure XPS and x-ray absorption spectroscopies. In chapter 4 the hydrogenation of furfural by Pt supported on SiO_2 and TiO_2 is investigated. It was found that following the removal of the organic capping agent sufficient contact between the oxide and metal was initiated a 50-fold enhancement in the production of furfuryl alcohol was observed Pt/TiO_2, while no significant change in product formation was observed for Pt/SiO_2. Using SFG an intermediate toward the furfuryl alcohol was observed unique to the Pt/TiO_2 catalyst surface that was determined to be a TiO_2 bound species, attached via the aldehyde group. From this, and investigation into the relationship between the reaction conditions and reduction of the TiO_2 surface by observation of the nonresonant component of the SFG signal, it was determined that the furfural molecule bound to the TiO_2 surface and reacted with spillover hydrogen from the Pt surface to form furfuryl alcohol. This was further supported with Density Functional Theory (DFT) calculations which revealed that furfural binds very favorably at Ti^{3+} sites of a reduced TiO_2 surface, and that this adsorption mode activates the aldehyde group for hydrogenation.

Chapter 5 expands on the work in chapter 4 by studying a new reaction, the hydrogenation of crotonaldehyde, on the same catalysts, Pt/SiO_2 and Pt/TiO_2. In this case additional reaction pathways are available to crotonaldehyde as compared to furfural, yet a similar trend is observed. The TiO_2 surface is found to contain sites at which the crotonaldehyde molecule can adsorb via the aldehyde group to form a partial hydrogenation product, crotyl

alcohol, or a full hydrogenation product, butanol. Pt/SiO_2 catalysts produce neither of these alcohol products. Sum frequency generation is employed again to determine the intermediate species attributable to the various component surfaces within the catalyst. It is found that the intermediate for butyraldehyde formed on the Pt nanoparticle surface is identical to a previously observed intermediate on Pt single crystal surface. Additionally it is observed that crotonaldehyde adsorbs on the TiO_2 surface via the aldehyde group, much like in the furfural case, and the aldehyde group is subsequently hydrogenated by spillover H_2. Furthermore, by a thorough study of the possible secondary reactions, it was determined that butanol is formed by a concerted hydrogenation of both unsaturated groups in the molecule, rather than by a sequential reaction scheme.

Chapter 6 further expands on the work in chapter 5 by studying a somewhat unconventional support, cobalt oxide. Pt supported on cobalt oxide is found to show similar catalytic performance and SFG signatures as compared to Pt supported on TiO_2 suggesting a universality of the mechanism of alcohol formation in this, and the previous reaction, by reducible oxide supports. AP-XPS and XAS are used to investigate the state of the oxide support under reaction conditions and it is found that the bulk of the oxide remains in a Co_3O_4 structure while the surface is reduced to only Co^{2+}. This serves as further proof that reduced sites on the oxide surface serve as the active sites for aldehyde group hydrogenation. In addition Pt nanoparticle coverage study was undertaken to understand significance of interface sites versus oxide sites which are active by the spillover mechanism. It was found that as the density of Pt nanoparticles on the support increased, and thus the ratio of interface to oxide sites also increased, the production of crotyl alcohol dropped and the production of butanol rose. This implies that butanol is selectively formed at the interface between the Pt and Co_3O_4, such that both unsaturated groups can be hydrogenated simultaneously, while crotyl alcohol is selectively formed at oxide sites by the spillover mechanism.

Lastly chapter 7 describes the discovery of a previously undocumented example of the SMSI effect in which cobalt oxide is found to encapsulate Pt particles supported on it under surprisingly mild conditions. Studies with AP-XPS revealed that after a reduction in H_2 at 513 K and subsequent oxidation at 573 K the signal from Pt cannot escape from the surface of the catalyst and is completely absent from the spectrum. After initiating this encapsulation ethylene hydrogenation and crotonaldehyde hydrogenation reaction studies were conducted and it was found that there was a slight reduction in available Pt surface area, as determined by ethylene hydrogenation, and a surprising 3-fold increase in the total rate of crotonaldehyde hydrogenation, largely toward the production of butyraldehyde. SFG study reveals a marked increase in intensity of the features assigned to the butyraldehyde intermediate on Pt. Potential explanations are given to explain this increase in butyraldehyde formation but all require further study. The increase in butanol production observed after encapsulation is attributed to the increased number of interface sites. From this study it can be concluded that the SMSI type encapsulation can have a positive effect on reactivity.

1.6 References

(1) Somorjai, G. A.; Li, Y. *Introduction to Surface Chemistry and Catalysis*; Wiley, **2010**.

(2) Olah, G. A. *Angew Chem Int Ed* **2005**, *44*, 2636.

(3) Völkening, S.; Bedürftig, K.; Jacobi, K.; Wintterlin, J.; Ertl, G. *Phys Rev Lett* **1999**, *83*, 2672.

(4) Somorjai, G. A. *Surface Science* **1979**, *89*, 496.

(5) Freund, H. J.; Kuhlenbeck, H.; Libuda, J.; Rupprechter, G. *Topics in Catalysis* **2001**, *15*, 201–209.

(6) Ertl, G.; Knözinger, H.; Weitkamp, J. *Preparation of Solid Catalysts*; Wiley VCH, **1999**.

(7) Goodman, D. W. *Accounts of Chemical Research* **1984**, *17*, 194.

(8) Lang, B.; Joyner, R. W.; Somorjai, G. A. *Surface Science* **1972**, *30*, 454.

(9) Barth, J. V.; Brune, H.; Ertl, G.; Behm, R. J. *Physical Review B* **1990**, *42*, 9307.

(10) Salmeron, M.; Somorjai, G. A. *The Journal of Physical Chemistry* **1982**, *86*, 341.

(11) Clint, J. H.; Collins, I. R.; Williams, J. A.; Robinson, B. H.; Towey, T. F.; Cajean, P.; Khan-Lodhi, A. *Faraday Discuss* **1993**, *95*, 219.

(12) Ahmadi, T. S.; Wang, Z. L.; Green, T. C.; Henglein, A.; El-Sayed, M. A. *Science* **1996**, *272*, 1924.

(13) Wang, Y.; Toshima, N. *The Journal of Physical Chemistry B* **1997**, *101*, 5301.

(14) Pushkarev, V. V.; An, K.; Alayoglu, S.; Beaumont, S. K.; Somorjai, G. A. *Journal of Catalysis* **2012**, *292*, 64.

(15) Narayanan, R.; El-Sayed, M. A. *Nano Letters* **2004**, *4*, 1343.

(16) An, K.; Alayoglu, S.; Musselwhite, N.; Plamthottam, S.; Melaet, G.; Lindeman, A. E.; Somorjai, G. A. *Journal of the American Chemical Society* **2013**, *135*, 16689.

(17) Pendry, J. B. *Low-Energy Electron Diffraction*; **1990**.

(18) Chang, C. C. *Surface Science* **1971**, *25*, 53.

(19) Ogletree, D. F.; Van Hove, M. A.; Somorjai, G. A. *Surface Science* **1986**, *173*, 351.

(20) Kesmodel, L. L.; Dubois, L. H.; Somorjai, G. A. *The Journal of Chemical Physics* **1979**, *70*, 2180.

(21) Hoffmann, F. *Surface Science Reports* **1983**, *3*, 107.

(22) Ozensoy, E.; Meier, D. C.; Goodman, D. W. *The Journal of Physical Chemistry B* 2002, *106*, 9367.

(23) Buffeteau, T.; Desbat, B.; Turlet, J. M. *Applied spectroscopy* 1991, *45*, 380.

(24) Shen, Y. R. *Nature* 1989, *337*, 519–525.

(25) Cremer, P. S.; Su, X.; Shen, Y. R.; Somorjai, G. A. *Journal of the American Chemical Society* **1996**, *118*, 2942–2949.

(26) Bratlie, K. M.; Komvopoulos, K.; Somorjai, G. A. *The Journal of Physical Chemistry C* **2008**, *112*, 11865–11868.

(27) Chen, Z.; Shen, Y. R.; Somorjai, G. A. *Annual review of physical …* **2002**, *53*, 437.

(28) Chen, X.; Clarke, M. L.; Wang, J.; Chen, Z. *International Journal of Modern Physics B* **2005**, *19*, 691.

(29) Grass, M. E.; Karlsson, P. G.; Aksoy, F.; Lundqvist, M.; Wannberg, B.; Mun, B. S.; Hussain, Z.; Liu, Z. *Rev Sci Instrum* **2010**, *81*, 053106.

(30) Ogletree, D. F.; Bluhm, H.; Hebenstreit, E. D. Nuclear Instruments and Methods in Physics Research A, **2009**, *601*, 151.

(31) Vannice, M. A.; Sen, B. *Journal of Catalysis* **1989**, *115*, 65–78.

(32) Hervier, A.; Baker, L. R.; Komvopoulos, K.; Somorjai, G. A. *The Journal of Physical Chemistry C* **2011**, *115*, 22960–22964.

(33) Goodman, D. W. *Catal Lett* **2005**, *99*, 1–4.

(34) Melaet, G.; Ralston, W. T.; Li, C.-S.; Alayoglu, S.; An, K.; Musselwhite, N.; Kalkan, B.; Somorjai, G. A. *Journal of the American Chemical Society* **2014**, *136*, 2260.

(35) Tauster, S. J.; Fung, S. C.; Garten, R. L. *Journal of the American Chemical Society* **1978**, *100*, 170–175.

(36) Baker, R. T.; Prestridge, E. B.; Garten, R. L. *Journal of Catalysis* **1979**, *56*, 390 – 406.

(37) Komaya, T.; Bell, A. T.; Wengsieh, Z.; Gronsky, R.; Engelke, F.; King, T. S.; Pruski, M. *Journal of Catalysis* **1994**, *149*, 142.

(38) Boffa, A.; Lin, C.; Bell, A. T.; Somorjai, G. A. *Journal of Catalysis* **1994**, *149*, 149–158.

(39) Boffa, A.; Lin, C.; Bell, A.; Somorjai, G. *Catal Lett* **1994**, *27*, 243–249.

(40) Conner, W. C.; Falconer, J. L. *Chem Rev* **1995**, *95*, 759–788.

(41) Beaumont, S. K.; Alayoglu, S.; Specht, C.; Kruse, N.; Somorjai, G. A. *Nano Letters* **2014**, *14*, 4792.

Chapter 2

Experimental Methods

2.1 Catalyst Preparation

2.1.1 Thin Film Deposition and Treatment

2.1.1.1 Electron Beam Evaporation – In this work thin films of various oxides were utilized as support materials for Pt nanoparticle catalysts in order to study the influence of the metal – support interaction on catalytic reactions. Two methods were used for the deposition of these materials, electron beam evaporation and atomic layer deposition. Electron beam evaporation utilizes a directed beam of thermally generated electrons to sublimate or melt and vaporize the target material. The target is placed in a crucible liner (typically graphite) and this liner is then placed in a water-cooled hearth. The electron beam is generated by passing a current (on the order of 10-100 mA) through a thin W filament which ejects electrons due to ohmic heating. These electrons are accelerated by a 5 keV potential, applied between the filament and the hearth, and directed to the target by a combination of permanent and electro-magnets. Upon contact with the target the electron beam heats the material, and depending on the material at hand, sublimates or melts and vaporizes the material. The vapor ascends to the top of the deposition chamber to where the substrate is located and deposits onto the substrate. The entire chamber is kept at a pressure below 10^{-5} Torr to prevent electrical arcing and to allow the vapor to ascend to the substrate. The deposition rate and total film thickness are monitored by a quartz crystal microbalance.

2.1.1.2 Atomic Layer Deposition – Films of oxides that could not be reliably prepared by electron beam evaporation were prepared by atomic layer deposition (ALD). Atomic layer deposition is achieved by exposing a substrate to alternating gas phase precursors. In a typical ALD process one precursor is introduced into the deposition chamber and this precursor adsorbs on the substrate in a self-limiting manner, meaning that only a single monolayer may be adsorbed in a given cycle. The residual gas phase precursor is then evacuated from the chamber and a second precursor is added. This second precursor then reacts with the adsorbed molecules of the first and forms a layer of the target material. This cycle is then repeated until the desired thickness is obtained. The self-limiting nature of these processes allows for thin, conformal films, with precise thicknesses to be obtained for a variety of materials. In the case of the work presented here, a plasma assisted ALD is used in which the second cycle consists of oxygen plasma which converts the metal-organic precursor into a metal oxide.

2.1.1.3 Quartz Crystal Microbalance – In the electron beam evaporation method a quartz crystal microbalance is used to monitor deposition rate and film thickness of the deposited material. This is achieved through the use of a quartz crystal resonator, the resonant frequency of which is sensitive to the addition of mass to the crystal surface down to sub-monolayer levels. An oscillating voltage is applied to the crystal tuned to the resonant acoustic oscillation of the quartz substrate. This resonant frequency is inversely related to the total thickness of the quartz plate by the Sauerbrey relation. Thus as material is deposited the resonant frequency decreases. The change in resonant frequency can be measured and related to the mass of deposited material. Using the density of the deposited material and a Z-factor (which describes the degree to which a given material modulates the oscillation of the quartz) the deposited mass can be converted into a film thickness and the mass/time can be converted into a deposition rate.

2.1.1.4 Thermal Annealing – In cases where the as-deposited oxide thin films are oxygen deficient a thermal annealing process was utilized after deposition to ensure a stoichiometric oxide was obtained. Using a tube furnace capable of heating to temperatures in excess of 1,200 K the thin film covered substrates were heated in an oxygen environment to a temperature at which the bulk oxidation would take place.

2.1.2 Preparation of Pt Nanoparticle Based Model Catalysts

2.1.2.1 Colloidal Synthesis of Pt Nanoparticles – The primary synthesis utilized in this work to prepare colloidal Pt nanoparticles is based upon the "polyol method." In this method chloroplatinic acid was dissolved in ethylene glycol, which serves as both the solvent and the reducing agent, along with polyvinylpyrrolidone (PVP), which acts as the capping agent. A solution with a chloroplatinic acid to PVP mass ratio of 1:4 heated to 438 K under an Ar atmosphere for 1 h yields 4.5 nm diameter particles. The temperature and ratio of Pt to PVP can be used to tune particle size. The resulting particles are then precipitated from the ethylene glycol solution using acetone and are subsequently washed by alternating ethanol and hexane solvents to remove excess PVP. The particles can then be stored in ethanol and maintain their size and catalytic activity for months. A second synthetic method was also used to obtain 1.7 nm particles without a capping agent. In this method chloroplatinic acid hexahydrate and sodium hydroxide are combined in a 1:1 mass ratio in ethylene glycol and heated to 433 K for 3 h. The resulting solution is neutralized with 2M HCl to precipitate the particles. These particles can then be treated with ethanol solutions containing a number of different capping agents to yield identical particles with varying capping agents.

2.1.2.2 Langmuir Blodgett Deposition – In order to deposit the colloidally synthesized Pt nanoparticles on the two-dimensional thin film based supports the Langmuir Blodgett (LB) method was used. In this method the Pt nanoparticles are dispersed in a hydrophobic solvent, such as chloroform, and dropped onto a water filled trough such that the solution disperses on the surface of the water. The solvent is then allowed to evaporate over the course of thirty minutes and the evaporation is monitored by a surface tension probe. With the particles dispersed in a film on this water surface two Teflon barriers are then used to compress the film

while the surface tension is monitored. The barriers compress until a compact monolayer of particles is observed, as indicated by a leveling off of the surface tension relative to the change in water surface area. Once the desired surface tension is reached the two dimensional substrate is pulled out from under the water surface and the nanoparticle film is transferred to it. Additionally this method can be used to tune the density of particles present on the substrate which can be shown to impact the catalytic performance of the composite material.

2.1.2.3 Capping Agent Removal by UV Irradiation – Irradiation of the nanoparticle film by UV light resulted in the removal of the organic capping agent from the Pt particles. The removal of this capping agent increases the available number of Pt surface sites and initiates contact between the Pt particles and the oxide support. The apparatus consists of two low pressure mercury lamps (Lights Sources Inc., model number GPH357T5VH/4P) which emit two wavelengths, 184 and 254 nm, contained in a clean aluminum box. The lamps run parallel to one another and the sample is placed 1 cm below the lamps. The UV light removes the cap by the combined action of photochemical decomposition and oxidation by ozone produced by the 184 nm wavelength. By varying the UV exposure time it is possible to control the degree of cap removal.

2.2 Catalyst Characterization

2.2.1 Transmission Electron Microscopy

Nanoparticle size and film densities were determined using a JEOL 2100-F 200 kV Field-Emission Analytical Transmission Electron Microscope. Analysis of the collected images was performed using the ImageJ software package.

2.2.2 X-Ray Photoelectron Spectroscopy

X-Ray photoelectron spectroscopy (XPS) was used to characterize the surface composition and surface oxidation states of the various catalyst materials. Fundamentally XPS works by irradiating a sample with a monochromatic x-ray source which in turn ejects a core level electron whose kinetic energy can be measured. Using the kinetic energy of the photoelectron and the energy of the incident x-ray the binding energy of the electron can be determined. The binding energies of core electrons are characteristic to given elements and thus the technique can be used to determine the elemental composition of a given surface. Furthermore small shifts in the binding energy of a given core electron are characteristic of the oxidation states of the element and thus the oxidation state can be determined. Since this technique is reliant on the detection of relatively low energy photoelectrons (100-1000 eV) it is inherently surface sensitive as the mean free path of an electron in this energy range is on the order of 1 nm, or approximately 10 atomic layers.

The kinetic energy of the photoelectrons is typically measured by a hemispherical analyzer. Photoelectrons enter the analyzer and are exposed to a magnetic field which bends their trajectory. Based upon the strength of the magnetic field and the kinetic energy of the electron

it will reach the detector at a different position and thus the kinetic and binding energies can be determined.

In a typical XPS system an Al or Mg x-ray source is used. This operates by bombarding the Al or Mg source with electrons generated by a filament and accelerated by a high voltage toward the source. Upon collision with the source the electrons excite core electrons in the metal, the relaxation of which produces x-rays of a specific energy.

Another consequence of the short mean free paths of the ejected electrons is that, conventionally, XPS requires ultra-high vacuum conditions for operation. The development of a differentially pumped hemispherical analyzer in combination with the high x-ray flux available at synchrotron light sources has allowed XPS experiments to be conducted in the presence of reactive gases up to 1 Torr in pressure and has been called Ambient Pressure XPS (AP-XPS). The differentially pumped analyzer consists of a small aperture nose cone which can approach the sample surface to within a millimeter, in order to minimize the path in the higher pressure gas. Between this cone and the hemispherical analyzer there are a series of chambers, each of which is pumped using a turbomolecular pump, and each containing magnetic electron lenses to focus the photoelectron beam to the analyzer. In this work AP-XPS experiments were conducted at the Advanced Light Source at Lawrence Berkeley National Laboratory, Beamline 9.3.2, and conventional high vacuum XPS was done using a commercial system (Physical Electronics, PHI 5400 ESCA/XPS) with an Al anode source producing 1486.6 eV x-rays, in the Molecular Foundry at Lawrence Berkeley Nation Laboratory.

2.2.3 Sum Frequency Generation Vibrational Spectroscopy

Sum frequency generation (SFG) vibrational spectroscopy is a non-linear optical spectroscopic technique that allows for the selective probing of molecules on surfaces or at interfaces, in contrast with bulk vibrational spectroscopies such as Raman scattering and infrared absorption. In this work SFG was utilized to obtain the vibrational spectra of adsorbed reactant molecules and intermediates on catalyst surfaces under working catalytic conditions. Additionally it was used to characterize the organic capping agents on metal nanoparticles and the remaining carbonaceous species present following their removal.

Fundamentally SFG requires the spatial and temporal overlap of two coherent, sufficiently intense input beams at the surface of interest. In the case of this work those two beams are a fixed visible beam (Vis) with a 532 nm wavelength and an infrared beam (IR), tunable from 2600-3600 cm^{-1}. Upon interaction with the surface of interest an output beam (SF) can be produced whose frequency is equal to the sum of the two input frequencies. An energy level diagram is shown in scheme 2.1 that describes the overall process.

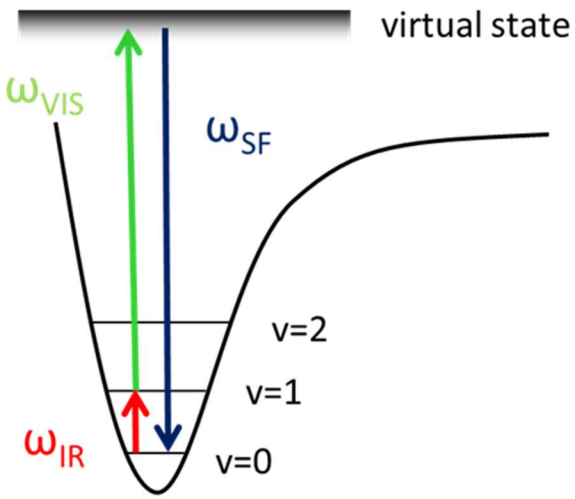

Scheme 2.1

The intensity of the signal is proportional two both input intensities and a quantity $\chi^{(2)}$ which is a tensor that represents the second order polarizability of the sample, as shown in equation 1.

$$I_{SFG} \propto \left|\chi^{(2)}\right|^2 \cdot I_{532} \cdot I_{IR} \qquad \text{Eq. 1}$$

The quantity $\chi^{(2)}$ can be further described as the orientationally averaged molecular hyperpolarizability (β) of N molecules on a surface as shown in equation 2.

$$\chi^{(2)} = N\langle\beta\rangle \qquad \text{Eq. 2}$$

Furthermore hyperpolarizability can be described as the product of the molecular polarizability (α) and molecular dipole moment (μ) shown in equation 3, where a, b and c are the molecular Cartesian coordinates.

$$\beta_{abc} = \alpha_{ab} \cdot \mu_c \qquad \text{Eq. 3}$$

This gives an insight into the nature of the SFG process. Polarizability is probed typically by Raman scattering experiments while the molecular dipole is probed by IR absorption. Thus, most basically, SFG can be thought of as a combined infrared absorption/anti-Stokes Raman event as indicated in scheme 1. Following the rule of mutual exclusion no vibrational mode of a centrosymmetric system can have both nonzero dipole moment and polarizability. Thus for a mode to be SFG active it cannot be part of a system possessing centrosymmetry. This is a condition that is always met at a surface or interface. Additionally this can be explained using a property of the second order polarizability $\chi^{(2)}$ shown in equation 4.

$$\chi^{(2)}_{-I-J-K} = -\chi^{(2)}_{IJK} \qquad \text{Eq. 4}$$

Equation 5 is true for centrosymmetric media,

$$\chi^{(2)}_{IJK} = \chi^{(2)}_{-I-J-K} \qquad \text{Eq. 5}$$

and combining equations 4 and 5 yields equation 6 which states that for centrosymmetric media $\chi^{(2)}$ is necessarily zero.

$$\chi^{(2)}_{IJK} = -\chi^{(2)}_{IJK} = 0 \qquad \text{Eq. 6}$$

Both of these explanations yield the same conclusion, that only regions of broken centrosymmetry can produce an SFG signal. This shows that SFG can be used as a completely surface or interface selective vibrational spectroscopy.

Experimentally this is achieved using an active/passive mode-locked Nd:YAG laser which produces 20 ps pulses of 1064 nm wavelength light at a repetition rate of 20 Hz and a power of 20 mJ/pulse. The 1064 nm principle beam is then used to pump an optical parametric generator/amplifier. The 532 nm beam is produced by a β-barium borate (BBO) crystal by frequency doubling. This 532 nm beam is then used in an optical parametric generation/amplification stage composed of two matching potassium titanyl phosphate (KTP) crystals, which create a signal beam around 600 nm and an idler beam around 1300 nm. The frequency of the signal and idler beams can between by altering the angle of incidence on the KTP crystals. Then the idler is used in a difference frequency generation stage with the original 1064 nm beam. This yields the tunable mid-infrared beam necessary for the experiment. This process yields a 532 nm beam and a tunable infrared beam with energies of 300 μJ/pulse and 250 μJ/pulse respectively. The use of an intense, pulsed light source is necessitated by the fact that the SFG cross section for molecular vibrations is exceedingly small and that the signal intensity is related to both the IR and visible intensities as shown in equation 1. As such, a factor of two decrease in the intensity of both beams would result in a factor of four decrease in signal. By extension if one were to use a laser with longer pulse durations or a continuous wave laser it would require prohibitively high powers, likely causing damage to the sample.

A schematic overview of the full experimental system is shown in Scheme 2.2, highlighting the crucial components described above and showing the beam geometry at the sample stage.

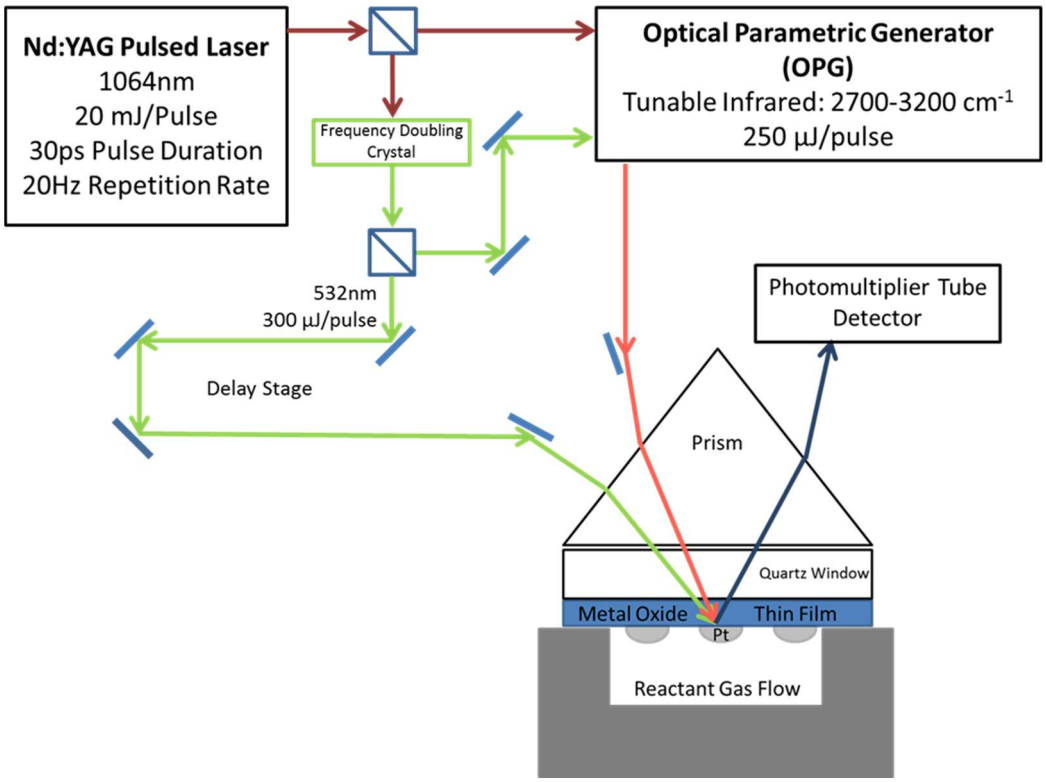

Scheme 2.2

The experiments are performed in a total internal reflection geometry in order to allow for multicomponent thin films to be studied and to remove the influence of infrared absorption by gas phase reactant molecules. The catalysts to be studied are deposited onto a quartz window using the previously described methods. A prism is used to direct the beams to the surface of interest. In order to minimize reflection at the interface between the prism and window a solution was developed in the Somorjai group. This consists of deuterated polystyrene and deuterated decalin. The resulting gel-like mixture has an index of refraction close to that of quartz and by using deuterated molecules there is no interference in the infrared spectral region studied. The reaction cell consists of an Al heating block against which the catalyst surface is pressed to obtain thermal contact. A Kalrez O-ring provides a seal between the heating block and the window. A small recess in the heating block allows for gas to flow over the catalyst surface. The cell is connected to a larger gas reservoir and a metal bellows circulation pump serves to mix the gases and deliver them to the cell. The SF signal is collected by a photomultiplier tube detector and processed using a gated integration system to improve the signal to noise ratio. The signal is collected as a function of the infrared wavelength which is scanned through the energy range of interest to obtain a spectrum.

2.3 Catalytic Reaction Studies

Catalytic reaction studies were performed using two separate but identical stainless steel, gas phase, batch mode reactor systems constructed for this work. Batch mode systems were chosen as they are better suited for measuring reaction kinetics of the two-dimensional catalysts required for spectroscopic investigation. Conventional catalysts utilizing porous three-dimensional support materials offer much higher total surface areas and thus can be used in a flow mode, whereas the two dimensional catalysts have orders of magnitude lower surface areas. The batch mode reactor allows for product molecules to accumulate over time to the point where they can be accurately measured and thus the problem of low surface area can be overcome, while keeping conversion below 10% to avoid the formation of secondary products. The reactor systems consist of a 1 liter reaction chamber, a gas chromatograph (GC) for product identification and quantification, a boron nitride sample heater, a recirculation pump (Senior Flexonics) for gas mixing and delivery to the GC, turbomolecular and mechanical pumps for evacuation of the chamber, and a gas manifold for controlled dosing of gases. In a typical reaction run the catalyst is placed on the sample heater then the chamber is sealed and pumped to 10^{-5} torr while the sample is heated to the reaction temperature. Following this the reactor is sealed from the pumps, gases are introduced, the reactor is sealed from the manifold and the recirculation pump is activated. Over the course of, typically, several hours the reaction is allowed to proceed and small samples of the gas mixture are automatically removed at fixed intervals and analyzed by the GC. Depending on the reaction product the GC can be used with either a flame ionization detector (for organic molecules) or a thermal conductivity detector (for small molecules). By calibrating the GC detector responses for each molecule the peak areas can be converted into partial pressures and from this rates of production can be obtained. A summary schematic of the reactor system is given below in scheme 2.3.

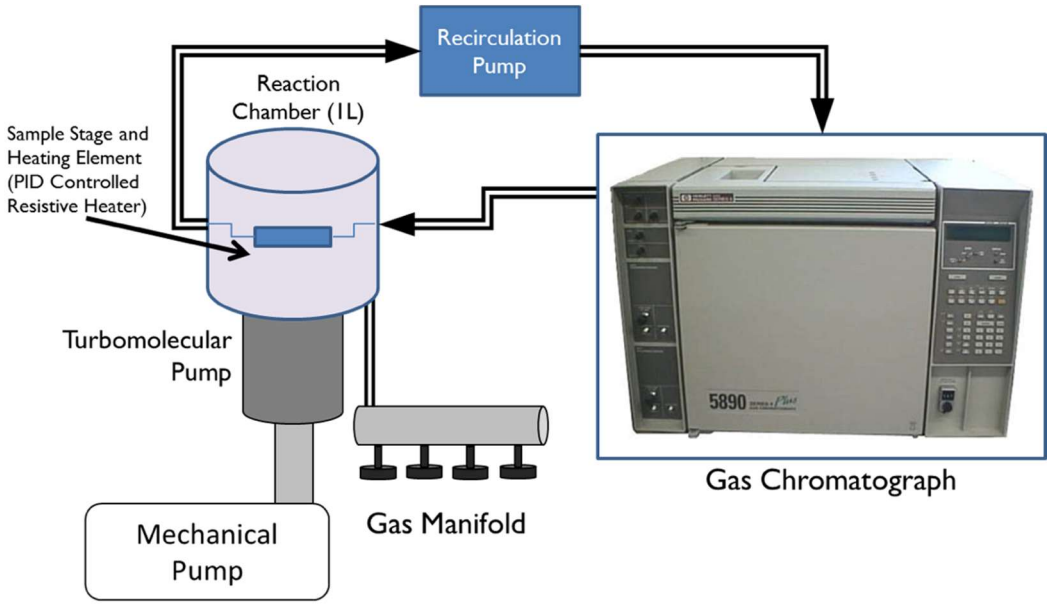

Scheme 2.3

Chapter 3

The Role of an Organic Cap in Nanoparticle Catalysis: Reversible Restructuring of Carbonaceous Material Controls Catalytic Activity of Platinum Nanoparticles for Ethylene Hydrogenation and Methanol Oxidation

3.1 Abstract

Inherent in the colloidal synthesis of nanoparticle catalysts is the presence of an organic capping agent that encapsulates the nanoparticles to prevent aggregation. However, this capping agent often remains present on the nanoparticles during catalytic reaction, and the effect of this coating on catalysis is an important question that will influence the future applications of colloidal nanoparticles. In this study, the structure of poly(vinylpyrrolidone) (PVP) ligands on Pt nanoparticles is probed using sum frequency generation vibrational spectroscopy before and after cap removal by UV light. When the PVP is removed, carbonaceous fragments remain on the surface that dynamically restructure in H_2 and O_2. These fragments form a porous coating around the Pt in H_2 but collapse to a tightly closed shell in O_2. Using ethylene hydrogenation and methanol oxidation as a probe for the catalytic activity of the nanoparticles in H_2 and O_2, respectively, it is shown that the structure of these carbonaceous fragments controls the catalytic activity of the nanoparticles across several orders of magnitude by opening in H_2 and collapsing to block Pt sites in O_2. Kinetic experiments on thermally-cleaned PVP-capped and oleic acid-capped nanoparticles show that these findings apply to multiple capping agents and cleaning methods. This work highlights the dominant role of an organic cap to mediate nanoparticle catalysis and provides one example where capped nanoparticles are dramatically better catalysts than their uncapped analogues.

3.2 Introduction

Traditional methods for catalyst preparation (i.e., incipient wetness and ion exchange) use the reduction of a metal salt inside of a mesoporous oxide[1, 2]. The result is a high surface area catalyst consisting of metal particles with a broad distribution of sizes and morphologies. This type of polydisperse heterogeneous catalyst masks the structure sensitivity inherent in heterogeneous catalysis[3–6] because with this method it is not possible to select nanoparticles of a single size or shape. Recent advances in nanoscience have shown that colloidal synthetic methods can produce monodisperse nanoparticles with well-defined sizes and shapes[7–11]. This advance marked a new era in heterogeneous catalysis where monodisperse nanoparticles serve as model catalysts[12–14] and these catalysts have shown that size and shape control the catalytic activity and selectivity for many reactions[15–21]. These results indicate that colloidal nanoscience is an important tool for the development of new highly selective catalysts necessary to minimize the environmental impact and improve the economic efficiency of numerous commercial chemical processes.

In colloidal synthetic methods, nanoparticles are necessarily encapsulated in an organic polymer or surfactant. This organic coating lowers the surface energy of the nanoparticle to prevent aggregation of the particles[11]; the cap may also help to control the size and shape of the nanoparticles.[22] This gives rise to an important question regarding the effect of the organic cap on the catalytic properties of the nanoparticles. It is traditionally thought that the cap acts as a site blocking agent and lowers the metal surface area available for catalytic reaction.[23] In this light, it has been assumed that colloidal preparation methods are impractical for commercial catalytic applications because the presence of the capping agent decreases the apparent metal dispersion. However, this is an incomplete assumption based on a model that considers the cap as a passive coating rather than a dynamic shell that can adjust under reaction conditions.

It has been observed in the case of Pt–dendrimer complexes that the dendrimer structure, which is highly sensitive to gas/liquid conditions, controls access to the Pt surface.[24] Although the dendrimer blocks the Pt surface in air, it adopts an open structure in water that allows ready access of gasses to the Pt surface. Despite the importance of this effect for nanoparticle catalysis, little effort has been made to directly probe the role of a nanoparticle cap to mediate surface adsorption and catalytic activity. In this work we find that Pt nanoparticles capped with either poly(vinylpyrrolidone) (PVP) or oleic acid (OA) are active for both ethylene hydrogenation and methanol oxidation showing that the organic coating does not prevent nanoparticle catalysis. When the organic coating is removed either by UV light or thermal oxidation, the activity for ethylene hydrogenation increases while the activity for methanol oxidation decreases to almost zero. This surprising result shows that the capped nanoparticles are more active for methanol oxidation than their cleaned analogues.

Because of the high surface energy of metals, it is not possible to maintain a clean metal surface, even under conditions of ultra-high vacuum. With this in mind, it is clear that even catalysts prepared by traditional methods also become “capped” with undefined surface species as these catalysts quickly become contaminated in ambient conditions or during reaction.[25] Accordingly, the capping agent on colloidal nanoparticles represents a well-controlled passivation layer which, as shown here, does not prevent catalysis under reaction conditions. The concept of using an organic coating to increase catalytic activity of a nanoparticle is reminiscent

of homogeneous catalysis where ligands are used to tune the activity and selectivity of single metal ions,[26] and several examples have already shown that similar effects are also possible on metal clusters.[27, 28]

The present work investigates the role of PVP to mediate the catalytic properties of encapsulated Pt nanoparticles. We probe the molecular structure of the PVP cap by sum frequency generations (SFG) vibrational spectroscopy. Ethylene hydrogenation and methanol oxidation then serve as model reactions to probe the catalytic activity in reducing and oxidizing conditions, respectively. Spectral results show that the PVP cap has a strong SFG signal in O_2 atmosphere but disorders in H_2 atmosphere. However, kinetic measurements for ethylene hydrogenation and methanol oxidation show that this capping layer still allows catalysis regardless of the gas conditions. When the PVP is removed by photodecomposition using UV light, carbonaceous fragments remain on the surface that reversibly restructure in H_2 and O_2. In O_2 atmosphere, these carbonaceous fragments form a tightly closed shell around the nanoparticles that blocks catalytic activity, but this shell opens in H_2. As a result, following UV cleaning the nanoparticles are highly active for ethylene hydrogenation but not for methanol oxidation. Kinetic experiments on thermally-cleaned PVP- and OA-capped nanoparticles show similar results indicating that these findings apply to multiple capping agents and cleaning methods. This work highlights the dominant role of an organic coating to mediate nanoparticle catalysis and provides methanol oxidation as one example where capped nanoparticles are dramatically better catalysts than their cleaned analogues.

3.3 Results and Discussion

Figure 3.1a shows the SFG spectra of PVP-capped Pt nanoparticles in sequential gas environments. As the gas environment is initially cycled between H_2 and O_2, the SFG signal is higher in O_2 and decreases in H_2 corresponding to a structural reconfiguration of PVP on the Pt, and this effect has been discussed previously.[32] In summary, because of selection rules, SFG is sensitive not only to the individual molecular susceptibilities, but also to the net susceptibility of the entire ensemble of molecules at an interface. This net susceptibility depends strongly on the relative orientation of molecules at the interface. It is usually assumed that systems showing greater SFG signal intensity have a more highly ordered interface than those showing weaker intensity because a net disorder leads to canceling out of signal from individual molecular oscillators. Accordingly, we assign the loss of signal intensity going from O_2 to H_2 atmosphere as H_2-induced disordering of the PVP. However, after the first H_2/O_2 cycle, the PVP settles into a relatively stable configuration on the Pt, and minimal restructuring occurs as the gas environment continues to change between reducing and oxidizing conditions.

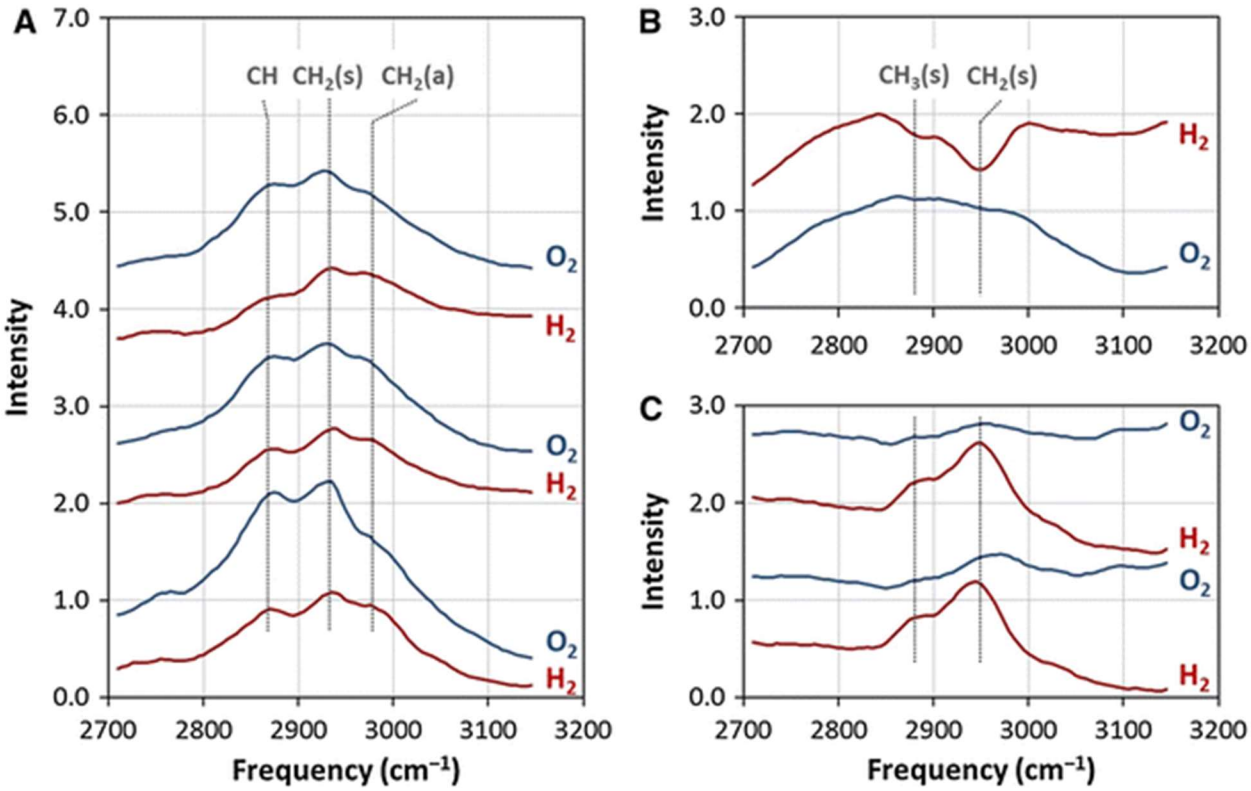

Figure 3.1 SFG spectra of the PVP-capped Pt nanoparticles before UV cleaning (a) and after UV cleaning for 10 min (b and c). Spectra were obtained in 100 Torr of H_2 or O_2 in a background of Ar at 60 °C. A boxcar average over 5 data points improved signal-to-noise. In a and c the spectra are arbitrarily offset for clarity and were obtained sequentially from bottom to top. b Shows the raw spectra with no offset of UV-cleaned nanoparticles first in H_2 then in O_2. The spectrum obtained in H_2 shows a much higher nonresonant intensity with resonant features appearing as dips in the high background. This is a result of the phase mismatch between the resonant and nonresonant contributions of the spectrum. By subtracting the raw spectra from a baseline obtained in Ar, the negative features are inverted to appear positive for clarity (shown in c). Analysis of the resonant features in these spectra shows that before UV cleaning the PVP has a conformation that does not significantly change depending on the gas environment. However, following UV cleaning, carbonaceous fragments are found on the surface that are dynamic and reversibly restructure in H_2 and O_2

This is in strong contrast to spectra shown on identical nanoparticles following UV cleaning to remove PVP from the Pt surface. Figure 3.1b shows the raw spectra of UV-cleaned nanoparticles first in H_2 then in O_2. The spectrum obtained in H_2 shows a much higher nonresonant intensity with resonant features appearing as negative peaks against the high background. This effect, which is common in SFG, is a result of the phase mismatch between the resonant and nonresonant contributions of the spectrum. By subtracting the raw spectra from a baseline obtained in Ar, the negative features are inverted to appear positive for clarity (see Fig. 3.1c). The enhanced nonresonant signal of the UV-cleaned catalyst is a result of H spillover from the Pt resulting in a reduced TiO_2 support, and the effect is completely reversible in O_2. In the

PVP-capped sample, the nonresonant contribution to the spectrum is low even in H_2 because the PVP blocks H spillover to the TiO_2.

It is also evident that the vibrational modes observed following UV cleaning are not the same as those observed from the intact PVP cap. Initially the vibrational modes observed on PVP-capped Pt (see Fig. 3.1a) match closely the assignments previously reported by infrared and Raman for PVP–Pt complexes.[33] Following UV cleaning, the peaks observed are attributable to CH_2 and CH_3 symmetric stretching modes outside of a 5-membered ring. It is also important to note that XPS measurements indicate that the surface C has decreased more than 85 % compared to the fully-capped nanoparticles following UV cleaning. It is not definitive whether the carbonaceous fragments observed by SFG after cleaning are photodecomposition products of PVP, or if they represent contamination of the UV-cleaned Pt surface, which would be unavoidable in ambient conditions. However, it is clear that additional UV cleaning does little to remove these species.

Figure 3.2 shows the catalytic activity of the Pt nanoparticles for ethylene hydrogenation and for methanol oxidation before and after UV cleaning. We selected these two reactions because they operate at low temperature (i.e., 298 and 333 K, respectively) and allowed us to observe the effects of the cap structure on the catalytic activity of the nanoparticles in H_2 and O_2 atmospheres. The PVP-capped Pt nanoparticles are active for both reactions as shown in Fig. 3.2a, b. However, following UV cleaning, the activity of the nanoparticles for ethylene hydrogenation and methanol oxidation diverge. Figure 3.2c, d show that following UV cleaning, the rate of ethylene hydrogenation increases by a factor of 10 while the rate of methanol oxidation decreases by a factor of 3. This represents a 30-fold divergence on the effect of UV cleaning for these two reactions. We note that formaldehyde is also formed at ~30 % selectivity during methanol oxidation. Formaldehyde production is not shown in Fig. 3.2 because it follows the same trend as CO_2.

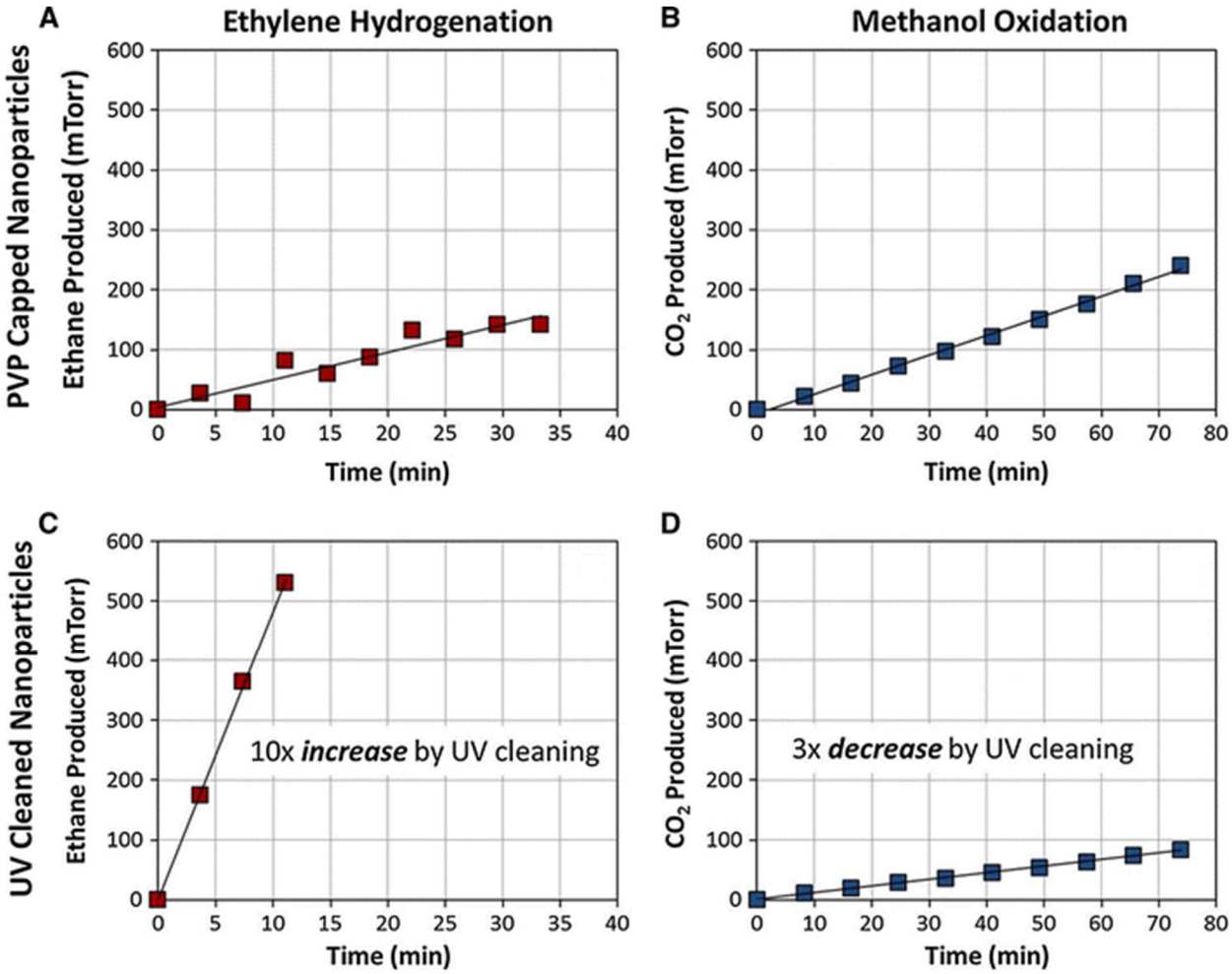

Figure 3.2 Formation of reaction products as a function of time on the Pt nanoparticles for ethylene hydrogenation and methanol oxidation before UV cleaning (a, b) and after UV cleaning for 10 min (c, d). These results show that UV cleaning has a diverging effect on the rates of ethylene hydrogenation which increases by a factor of 10 and methanol oxidation which decreases by a factor of 3. Only CO_2 production is shown for methanol oxidation. However, formaldehyde was also produced as a minor product before and after UV cleaning

Figure 3.3 shows the activity of the catalyst following UV cleaning where the catalyst is cycled several times between ethylene hydrogenation and methanol oxidation. The rates are normalized to the initial rate for each reaction prior to UV cleaning. It can be seen that the rates for both ethylene hydrogenation and methanol oxidation are reversibly affected by the removal of the PVP cap. It is clear from previous studies that the thermal stability of the nanoparticles decreases following cap removal, so the UV-cleaned nanoparticles agglomerate during reaction.[32] Nanoparticle agglomeration results in a loss of Pt surface sites which would lead to a decrease in catalyst activity. However, the ethylene hydrogenation kinetics show that the removal of PVP more than compensates for nanoparticle agglomeration resulting in a tenfold net increase in the reaction rate. Consequently, the loss of activity for methanol oxidation following

UV cleaning cannot simply be a result of nanoparticle agglomeration which would not be reversible between reactions.

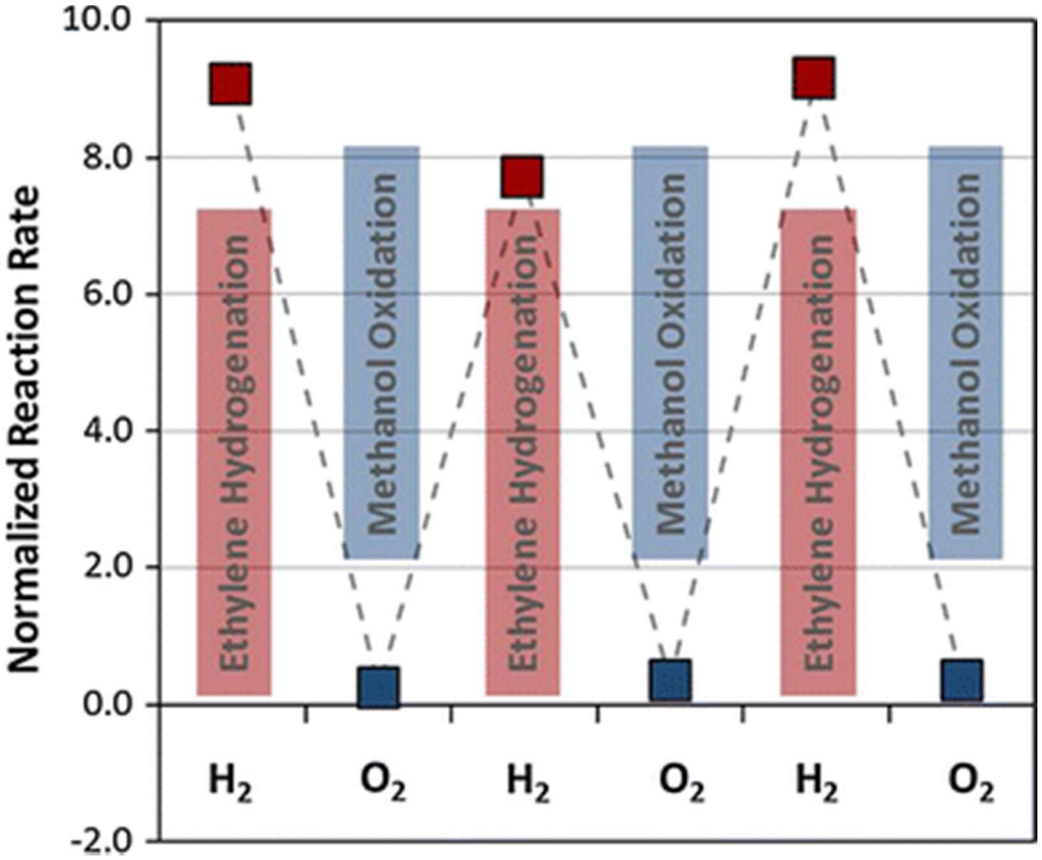

Figure 3.3 The reaction rates for ethylene hydrogenation and methanol oxidation on a single catalyst following UV cleaning for 10 min. The reaction rates are normalized to the initial rate for each reaction before UV cleaning. The results show that the diverging effect of UV cleaning on the two reactions is reversible and appears to correlate with the restructuring of carbonaceous fragments on the Pt surface observed by SFG

In the case of ethylene hydrogenation, the increase in catalyst activity after cleaning is easily understood based on the increased number of Pt sites available following PVP removal. In the case of methanol oxidation, it is surprising that cap removal would have a negative effect on the catalytic activity. It appears that the structure of the carbonaceous fragments observed on the Pt following UV cleaning controls the catalytic properties of the uncapped nanoparticles. We suggest that these carbonaceous fragments which do little to prevent access to the Pt in H_2 atmosphere, collapse to a tightly closed shell around the Pt in O_2 atmosphere.

To confirm this model in which carbonaceous fragments form a porous coating around the Pt in H_2 but collapse to a tightly closed shell in O_2, we used cyclohexene to probe the accessibility of reactants to the Pt surface. Cyclohexene forms a 1,4-cyclohexadiene surface intermediate on Pt.[34] This is a dehydrogenation product of the cyclohexene and forms even in the absence of H_2. The 1,4-cyclohexadiene species has a distinct molecular vibration at 2,760

cm−1 which is spectrally well resolved from any resonant modes of the capping agent. Consequently, cyclohexene represents a suitable probe molecule. To avoid changes in the nonresonant background with changing H_2 pressure, this experiment was performed using Pt nanoparticles supported directly on an SiO_2 prism. Figure 3.4 shows the results of this experiment. When cyclohexene is introduced in the gas phase to UV-cleaned Pt nanoparticles, no 1,4-cyclohexadiene is observed in the SFG spectrum. Only weak features at 2,840 and 2,910 cm−1 appear which we attribute to physisorbed cyclohexene. However, as the H_2 pressure is increased from 0 to 200 Torr, a strong feature at 2,760 cm−1 grows in corresponding to 1,4-cyclohexadiene. Because this feature forms on an atomically clean Pt single crystal surface even in the absence of H_2[34] we conclude that for the UV-cleaned nanoparticles H_2 is needed to open the carbonaceous shell and allow cyclohexene to access the Pt. It is important to note that in this experiment the nanoparticles were pre-reduced with H_2, so that the oxidation state of Pt is not changing during the experiment.

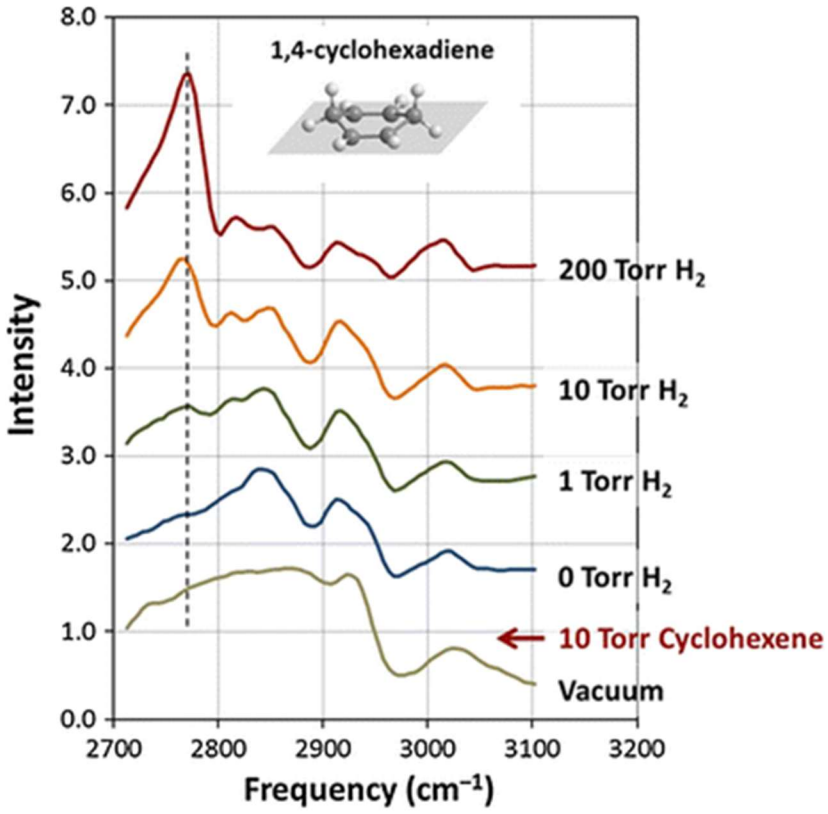

Figure 3.4 SFG spectra of 10 Torr cyclohexene in increasing H_2 pressure on Pt nanoparticles after UV cleaning for 60 min. In this experiment, the nanoparticles are supported directly on a SiO_2 prism. Cyclohexene dehydrogenates on Pt to form a 1,4-cyclohexadiene surface intermediate that is characterized by a strong feature in the SFG spectrum at 2,760 cm−1. This feature is known to form on an atomically clean Pt surface even in the absence of H_2. In this case, the feature is initially absent from the spectrum, but grows in with increasing H_2 pressure. This indicates that H_2 is needed to open the carbonaceous shell on the UV-cleaned Pt nanoparticles and allow cyclohexene to access the Pt

Figure 3.5a shows the effect of UV cleaning time on the activity of the Pt nanoparticles for ethylene hydrogenation and methanol oxidation. The activity for each reaction is normalized to the initial activity of the PVP-capped nanoparticles before UV cleaning. For ethylene hydrogenation the rate increases with increased cleaning time, while for methanol oxidation the rate decreases with increased cleaning time. Following 3 h there is a 200-fold divergence of the rates for these two reactions. This suggests that with increased cleaning, the carbonaceous shell on the Pt nanoparticles becomes tighter and tighter in O_2; however, it can continue to open in H_2 allowing access to the Pt. In fact, the ethylene hydrogenation rate after UV cleaning is slightly greater than expected based on the geometric surface area of the Pt as determined by TEM. This suggests that the carbonaceous fragments have almost no site blocking effect in H_2. Figure 3.5b shows the corresponding C and N surface concentrations as a function of UV cleaning time measured by XPS. After 30 min, the concentration of N is below the limit of detection by XPS. The C concentration also levels off after 30 min to a steady value representing only 10 % of the initial C. Again it is impossible to distinguish if this C is a decomposition product of the PVP or if it is contamination of the cleaned Pt surface.

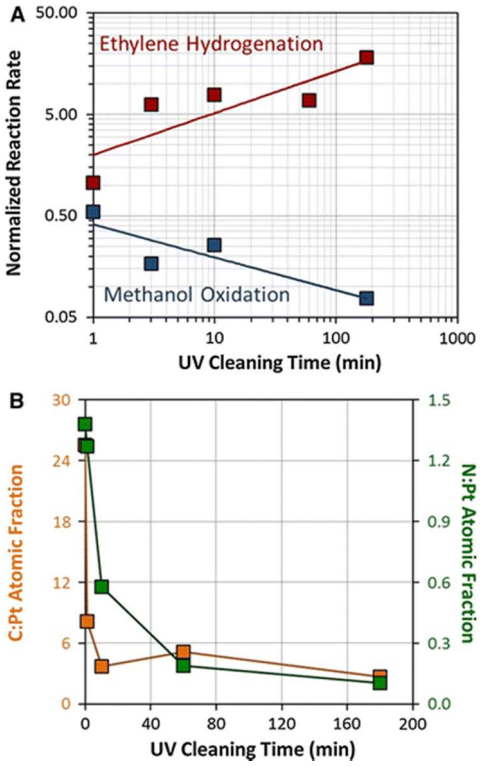

Figure 3.5 (A) Reaction rates as a function of UV cleaning time for ethylene hydrogenation and methanol oxidation. The reaction rates are normalized to the initial rate for each reaction before UV cleaning. The results show that the rates of the two reactions continue to diverge with increased cleaning time, eventually showing a 200-fold difference in activity. (B) C:Pt and N:Pt atomic fractions measured by XPS as a function of UV cleaning time. The N concentration on the surface drops below the limit of detection after 30 min of UV cleaning. The C concentration on the surface also levels off at a value representing only 10 % of the initial C from the PVP capping layer

To determine if the formation of this carbonaceous shell is a general phenomenon, we synthesized Pt nanoparticles using an alternate method where the capping agent is added after synthesis. This allowed us to add different capping agents to identical nanoparticle aliquots to isolate the cap as the sole variable between two nanoparticle samples. For this experiment, PVP and OA were used as capping agents in two separate aliquots, and the activity of these catalysts were monitored for ethylene hydrogenation and methanol oxidation before and after cleaning. In this case, thermal oxidation in a tube furnace was used for cap removal rather than UV cleaning. The OA-capped nanoparticles were cleaned at 473 K, and the PVP-capped nanoparticles were cleaned at 573 K. This temperature for PVP removal is consistent with previous work on the thermal degradation of Pt–PVP complexes.[33] Following cleaning the PVP- and OA-capped nanoparticles showed a 100-fold and 30-fold increased activity for ethylene hydrogenation, respectively.

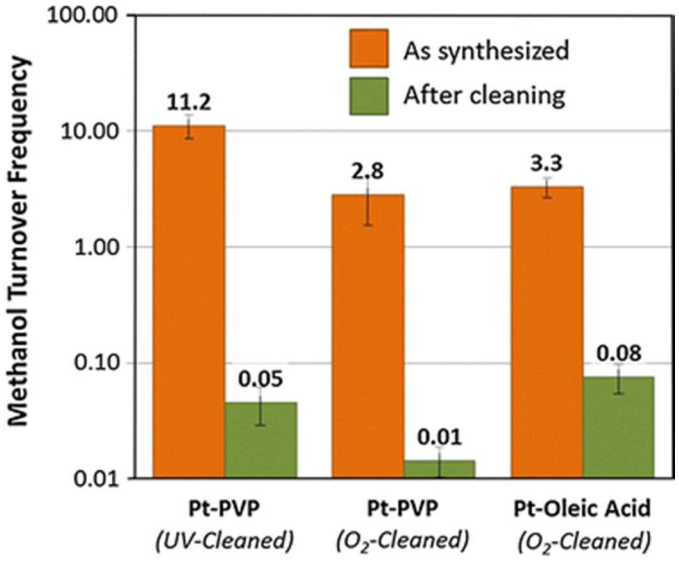

Figure 3.6 Methanol oxidation turnover frequency (TOF) for Pt nanoparticle catalysts before and after cap removal. TOF is given as the number of methanol molecules converted per Pt site per s. The number of platinum sites was determined from the measured rate of ethylene hydrogenation using a known TOF. Consequently, each bar shows the methanol oxidation rate relative to the ethylene hydrogenation rate on the same catalyst. Data is shown for all three types of nanoparticles studied (i.e., UV-cleaned Pt–PVP, thermally-cleaned Pt–PVP, and thermally-cleaned Pt–OA). Noting that this graph is on a log-scale, the Pt activity for methanol oxidation is shown to decrease for each catalyst by a factor of between 50 and 250 following cap removal

Figure 3.6 shows the effect of cap removal on the activity for methanol oxidation. In this figure, the methanol oxidation rate for each catalyst is represented as a turnover frequency normalized to the number of Pt active sites determined by ethylene hydrogenation.[23] Consequently, each bar shows the methanol oxidation rate relative to the ethylene hydrogenation rate on the same catalyst. Data is shown for all three types of nanoparticles studied (i.e., UV-cleaned Pt–PVP, thermally-cleaned Pt–PVP, and thermally-cleaned Pt–OA). Noting that this graph is on a log-scale, the Pt activity for methanol oxidation is shown to decrease

for each catalyst by a factor of between 50 and 250 following cap removal. Because these values are normalized to the catalyst activity for ethylene hydrogenation, this cannot be the result of nanoparticle agglomeration. It seems clear that for methanol oxidation, the capped nanoparticles are dramatically more active than their cleaned analogues, and this finding applies to multiple capping agents and cleaning methods.

3.4 Conclusions

We studied the catalytic activity of PVP- and OA-capped Pt nanoparticles for ethylene hydrogenation and methanol oxidation before and after cap removal. We find that the capped nanoparticles are active for both reactions showing that the organic coating does not prevent nanoparticle catalysis. However, the cleaned nanoparticles are only active for ethylene hydrogenation. The rate of ethylene hydrogenation is substantially higher on the cleaned particles relative to the capped particles, but the rate of methanol oxidation decreases to nearly zero following cap removal either by UV light or by thermal oxidation.

SFG shows that, following cleaning treatments, carbonaceous fragments are still present on the nanoparticles. These carbonaceous fragments are dynamic and reversibly restructure in alternating H_2 and O_2 atmospheres. It appears that a carbonaceous shell forms on the uncapped Pt nanoparticles that is tightly closed in O_2 but becomes permeable in H_2. Using cyclohexene as a probe molecule, we show that following UV cleaning, reactant molecules can only access the Pt when H_2 is present to open the carbonaceous shell.

These results demonstrate the important role of an organic cap to mediate the catalytic properties of nanoparticles. We find that the presence of an organic cap does not prevent catalysis. In fact, for methanol oxidation the capped nanoparticles are more than 10 times more active than their cleaned analogues. Accordingly, the capping agent on colloidal nanoparticles represents a well-controlled passivation layer which does not prevent catalysis under reaction conditions. That this coating may improve catalytic performance for certain reactions argues that the capping agent is a dynamic component of the active catalyst which consists of both a metal nanoparticle and an organic coating.

3.5 Experimental Methods

3.5.1 Nanoparticle Synthesis

The Pt nanoparticles were synthesized from chloroplatinic acid hexahydrate and PVP in a 1:4 mass ratio. In a small beaker, 110 mg of chloroplatinic acid was dissolved in 10 mL ethylene glycol. In a separate beaker, 440 mg of PVP was dissolved in 10 mL of ethylene glycol. Once in solution, the two mixtures were combined into a 50 mL two-neck round bottom flask. The solution was purged under vacuum for 15 min. The vessel was then heated to 438 K for 1 h with vigorous mixing under a flow of argon. The resulting nanoparticles were precipitated with acetone and washed three times with ethanol and hexanes. The nanoparticles were then suspended in chloroform. Transmission electron microscopy (TEM) showed that the particles were 4.6 ± 2.8 nm.

To investigate the effect of different capping agents and cleaning methods on reaction kinetics, Pt nanoparticles were synthesized using an alternate method where the capping agent

is added after synthesis. This allowed us to add different capping agents to identical nanoparticle aliquots to isolate the cap as the sole variable between two nanoparticle samples.[23] In a small beaker, 350 mg of chloroplatinic acid was dissolved in 17.5 mL ethylene glycol. In a separate beaker, 350 mg of NaOH was dissolved in 17.5 mL ethylene glycol. Once in solution, the two mixtures were combined in a 50 mL two-neck flask. The solution was purged under vacuum for 15 min. The vessel was then heated to 433 K for 3 h with vigorous mixing under a flow of argon. Aliquots (2 mL) of the resulting nanoparticles were precipitated with 2 M HCl, and then re-dispersed in 2 mL ethanol containing 10 mg of either PVP or OA. TEM showed that the particles were 1.7 ± 0.8 nm.

3.5.2 Langmuir–Blodgett Deposition

Formation of 2D films of monodisperse nanoparticles to serve as model catalysts is routinely achieved by Langmuir–Blodgett deposition. This technique has been described previously in detail.[12, 29] In short, a suspension of nanoparticles in chloroform is dispersed onto a water surface (18 MΩ). Time is given for the chloroform to evaporate, leaving a 2D dispersion of nanoparticles. The film is then compressed with a mobile barrier, and the surface pressure is monitored as a function of decreasing surface area. The surface pressure corresponds to the density of nanoparticles on the water. When the desired surface pressure is reached, a substrate is pulled out from under the surface of the water, and the film of nanoparticles is deposited onto the substrate. The final density of nanoparticles on the substrate can be controlled by controlling the surface pressure during deposition. A surface pressure of 14 mN/m was used for these studies, and films were deposited using a Nima 611 LB trough. Filter paper served as the surface tension probe.

The substrate used to support the nanoparticles was a TiO_2 thin film (50 nm) deposited on a Si(100) wafer with a thermally grown SiO_2 layer (500 nm). The TiO_2 thin film was deposited on the SiO_2/Si wafer by electron beam evaporation from an oxide source without any substrate heating. Following deposition, the TiO_2 thin film was annealed at 773 K in O_2 to increase crystallinity and ensure a fully oxidized stoichiometry. Analogous samples were prepared for sum frequency generation spectroscopic studies. For these samples, an optically transparent substrate was needed. A sapphire window rather than a Si wafer served as the substrate. A TiO_2 thin film (50 nm) was deposited on the sapphire window by electron beam evaporation, again followed by annealing at 773 K in O_2. The LB technique was then used to deposit a monolayer of the Pt nanoparticles onto the TiO_2 thin films. Electron microscopy showed that the area coverage for Pt on the substrate following LB was 30–50 %.In some cases, TiO_2 used as a Pt support plays an active role in the catalytic chemistry. However, the conclusions reported here are not substrate dependent, and kinetic results have been obtained for identical nanoparticles supported on SiO_2 substrates, and no significant differences were observed.

LB deposition is challenging for OA-capped Pt nanoparticles owing to the high hydrophobicity of the OA. Consequently, for investigating the role of different capping agents, films of the 1.7 nm PVP- and OA-capped nanoparticles were drop cast on a TiO_2 substrate.

3.5.3 Cap Removal

Immediately prior to reaction, the samples were exposed to UV light in air to remove the PVP capping layer. Two low-pressure mercury (Hg) lamps (Lights Sources Inc., GPH357T5VH/4P)

were used as the UV source; the lamps emit at 184 and 254 nm. The two lamps were aligned parallel to each other 2.5 cm apart in a clean Al box. The sample sat 1.2 cm below the lamps. By varying the time of UV exposure, it was possible to control the amount of PVP removed from the Pt nanoparticles. This cleaning is the combined effect of direct photodecomposition of the PVP and oxidation of the PVP by ozone produced from the 184 nm Hg line.[30]

X-ray photoelectron spectroscopy (XPS) was used to observe the removal of PVP from the Pt nanoparticles after UV cleaning. Spectra were obtained using a Physical Electronics system (PHI 5400 ESCA/XPS) with an Al anode source. The analyzer was positioned at 50° relative to sample normal. The C1s, N1s, and Pt4f peak areas were normalized by the appropriate sensitivity factors to obtain the surface C:Pt and N:Pt atomic fractions as a function of UV exposure time. Measurements showed that 90 % of the C was removed from the Pt following 3 h UV exposure.

Thermal cleaning in air was used as an alternative to UV cleaning for drop cast samples. For thermal cleaning, the samples were placed in a tube furnace and heated to a desired temperature for 16 h. The PVP- and OA-capped samples were treated at 473 and 573 K, respectively to remove the two capping agents that show different thermal stabilities.

3.5.4 Sum Frequency Generation Vibrational Spectroscopy

Sum frequency generation (SFG) is a second order, nonlinear process that probes the $\chi^{(2)}$ tensor. Because $\chi^{(2)}$ is zero for centrosymmetric media, SFG is only sensitive to a break in inversion symmetry which usually occurs at a surface or interface.[31] Consequently, SFG is useful for obtaining vibrational spectra of surfaces. In this study, SFG is used to obtain the vibrational spectrum of the nanoparticle capping layer in H_2 and O_2 atmospheres.

For SFG experiments, an active/passive mode-locked Nd:YAG laser (Leopard D-20, Continuum) produces 20 ps pulses at a 20 Hz repetition rate. The fundamental output at 1,064 nm was passed through an optical parametric generator/amplifier to generate a tunable infrared (IR) beam (2,700–3,600 cm−1) and a second harmonic visible (VIS) beam (532 nm). The IR (100 μJ) and VIS (100 μJ) beams were spatially and temporally overlapped on the surface of a sapphire window containing the Pt nanoparticles. The VIS and IR beams were incident on the sample at 40° and 50° degrees, respectively, relative to surface normal. The generated SFG signal was then collected and sent to a photomultiplier tube. A gated integrator was used to enhance the signal-to-noise. To collect a spectrum, the IR beam was scanned across the spectral range of interest. All experiments were performed in the ppp polarization combination.

The beams were directed onto the sample using a sapphire prism as shown in Fig. 3.7. A solution of deuterated polystyrene (d8) in deuterated decalin (d18) served as an index matching liquid between the prism and substrate that did not interfere with transmission of the IR beam at the C–H stretch frequency. The catalyst surface was pressed into thermal contact with an aluminum heating block to heat the catalyst to the desired temperature. A recess in the heating block allowed for the flow of gasses across the catalyst surface. A metal bellows circulation pump provided gas mixing. A gas tight seal was made between the sapphire window and the heating block using a Kalrez O-ring.

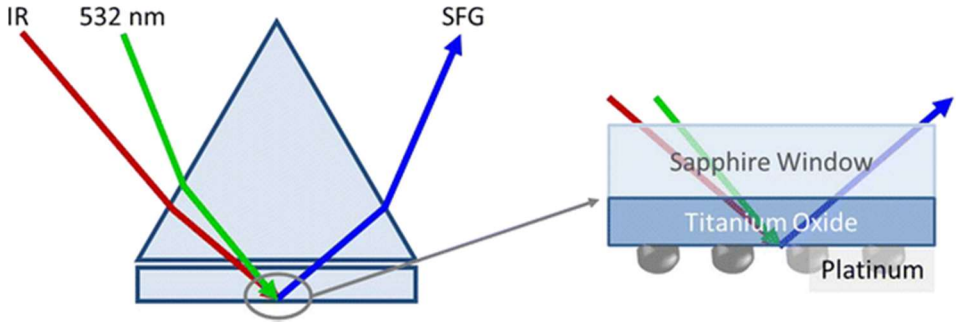

Figure 3.7 Diagram showing how a sapphire prism directed the VIS and IR beams onto the catalyst surface for SFG vibrational spectroscopy. The catalyst was prepared on the back side of a sapphire window and consisted of a thin film of TiO_2 acting as a support for Pt nanoparticles

3.5.5 Kinetic Measurements

A stainless steel batch mode reactor was used to determine the reaction rates for ethylene hydrogenation and methanol oxidation on the Pt nanoparticle catalysts before and after UV cleaning. The catalyst temperature was controlled with a boron nitride substrate heater. A metal bellows circulation pump provided gas mixing. For ethylene hydrogenation, gas pressures were 10 Torr ethylene, 100 Torr H_2, and 650 Torr He, and the catalyst temperature was 298 K. For methanol oxidation, gas pressures were 10 Torr methanol, 50 Torr O_2, and 700 Torr He, and the catalyst temperature was 333 K. The methanol was purified by freeze-pump-thawing cycles. Each catalyst was tested for 2 h, and reaction products were monitored as a function of time using a gas chromatograph with a thermal conductivity detector. Rates for ethylene hydrogenation and methanol oxidation were measured on each catalyst before and after cleaning.

3.6 References

(1) Ertl G, Knozinger H, Weitkamp J (eds) Preparation of solid catalysts. **1999** Wiley, Weinheim

(2) Tsoncheva T, Dal Santo V, Gallo A, Scotti N, Dimitrov M, Kovacheva D, *Appl Catal A Gen* **2011** 406:13

(3) Strongin DR, Carrazza J, Bare SR, Somorjai GA, *J Catal* **1987** 103:213

(4) McCrea KR, Parker JS, Somorjai GA, *J Phys Chem B* **2002** 106:10854

(5) Andersson MP, Abild-Pedersen E, Remediakis IN, Bligaard T, Jones G, Engbwk J, Lytken O, Horch S, Nielsen JH, Sehested J, Rostrup-Nielsen JR, Norskov JK, Chorkendorff I *J Catal* **2008** 255:6

(6) Kliewer CJ, Bieri M, Somorjai GA, *J Am Chem Soc* **2009** 131:9958

(7) Ahmadi TS, Wang ZL, Green TC, Henglein A, El-Sayed MA *Science* **1996** 1996:272

(8) Peng X, Wickham J, Alivisatos AP, *J Am Chem Soc* **1998** 120:5343

(9) Puntes VF, Krishnan KM, Alivisatos AP, *Science* **2001** 291:2115

(10) Oh M, Mirkin CA, *Nature* **2005** 438:651

(11) Yin Y, Alivisatos AP, *Nature* **2005** 437:664

(12) Song H, Kim F, Connor S, Somorjai GA, Yang P, *J Phys Chem B* **2004**109:188

(13) Rioux RM, Song H, Hoefelmeyer JD, Yang P, Somorjai GA, *J Phys Chem B* **2004** 109:2192

(14) Song H, Rioux RM, Hoefelmeyer JD, Komor R, Niesz K, Grass M, Yang P, Somorjai GA, *J Am Chem Soc* **2006** 128:3027

(15) Bratlie KM, Lee H, Komvopoulos K, Yang P, Somorjai GA, *Nano Lett* **2007** 7:3097

(16) Kuhn JN, Huang W, Tsung C-K, Zhang Y, Somorjai GA, *J Am Chem Soc* **2008** 130:14026

(17) Grass M, Rioux R, Somorjai G, *Catal Lett* **2009** 128:1

(18) Grass ME, Joo SH, Zhang Y, Somorjai GA, *J Phys Chem C* **2009** 113:8616

(19) Kliewer CJ, Aliaga C, Bieri M, Huang W, Tsung C-K, Wood JB, Komvopoulos K, Somorjai GA, *J Am Chem Soc* **2010** 132:13088

(20) Witham CA, Huang W, Tsung C-K, Kuhn JN, Somorjai GA, Toste FD, *Nat Chem* **2010** 2:36

(21) Alayoglu S, Aliaga C, Sprung C, Somorjai GA, *Catal Lett* **2011** 141:914

(22) Zhang Y, Grass ME, Kuhn JN, Tao F, Habas SE, Huang W, Yang P, Somorjai GA, *J Am Chem Soc* **2008** 130:5868

(23) Kuhn JN, Tsung C-K, Huang W, Somorjai GA, *J Catal* **2009** 265:209

(24) Albiter MA, Crooks RM, Zaera F, *J Phys Chem Lett* **2009** 1:38

(25) Lu J, Fu B, Kung MC, Xiao G, Elam JW, Kung HH, Stair PC, *Science* **2012** 335:1205

(26) Gorin DJ, Sherry BD, Toste FD, *Chem Rev* **2008** 108:3351

(27) Li Y, Liu JH-C, Witham CA, Huang W, Marcus MA, Fakra SC, Alayoglu P, Zhu Z, Thompson CM, Arjun A, Lee K, Gross E, Toste FD, Somorjai GA, *J Am Chem Soc* **2011** 133:13527

(28) Mitsudome T, Mikami Y, Matoba M, Mizugaki T, Jitsukawa K, Kaneda K, *Angew Chem Int Ed* **2012** 51:136

(29) Bratlie KM, Komvopoulos K, Somorjai GA, *J Phys Chem C* **2008** 112:11865

(30) Aliaga C, Park JY, Yamada Y, Lee HS, Tsung C-K, Yang P, Somorjai GA, *J Phys Chem C* **2009** 113:6150

(31) Shen YR (2003) The principles of nonlinear optics. Wiley-Interscience, Hoboken

(32) Krier JM, Michalak WD, Baker LR, An K, Komvopoulos K, Somorjai GA, *J Phys Chem C* **2012** 116:17540

(33) Borodko Y, Habas SE, Koebel M, Yang P, Frei H, Somorjai GA, *J Phys Chem B* **2006** 10:23052

(34) Yang M, Chou KC, Somorjai GA, *J Phys Chem B* **2003** 107:5267

Chapter 4

Furfuraldehyde Hydrogenation on Titanium Oxide-Supported Platinum Nanoparticles Studied by Sum Frequency Generation Vibrational Spectroscopy: Acid–Base Catalysis Explains the Molecular Origin of Strong Metal–Support Interactions

4.1 Abstract

This work describes a molecular-level investigation of strong metal–support interactions (SMSI) in Pt/TiO_2 catalysts using sum frequency generation (SFG) vibrational spectroscopy. This is the first time that SFG has been used to probe the highly selective oxide–metal interface during catalytic reaction, and the results demonstrate that charge transfer from TiO_2 on a Pt/TiO_2 catalyst controls the product distribution of furfuraldehyde hydrogenation by an acid–base mechanism. Pt nanoparticles supported on TiO_2 and SiO_2 are used as catalysts for furfuraldehyde hydrogenation. As synthesized, the Pt nanoparticles are encapsulated in a layer of poly(vinylpyrrolidone) (PVP). The presence of PVP prevents interaction of the Pt nanoparticles with their support, so identical turnover rates and reaction selectivity is observed regardless of the supporting oxide. However, removal of the PVP with UV light results in a 50-fold enhancement in the formation of furfuryl alcohol by Pt supported on TiO_2, while no change is observed for the kinetics of Pt supported on SiO_2. SFG vibrational spectroscopy reveals that a furfuryl-oxy intermediate forms on TiO_2 as a result of a charge transfer interaction. This furfuryl-oxy intermediate is a highly active and selective precursor to furfuryl alcohol, and spectral analysis shows that the Pt/TiO_2 interface is required primarily for H spillover. Density functional calculations predict that O-vacancies on the TiO_2 surface activate the formation of the furfuryl-oxy intermediate via an electron transfer to furfuraldehyde, drawing a strong analogy between SMSI and acid–base catalysis.

4.2 Introduction

Strong metal–support interactions (SMSI) refer to the ability of a seemingly inert oxide to have a dominant effect on the catalytic properties of a supported metal nanoparticle.[1-4] Tauster and Fung first used the term SMSI to refer to the dramatic loss of chemisorption sites observed for noble metal catalysts supported on titanium oxide after reduction.[2] In their studies, Tauster and Fung showed evidence for a strong bonding interaction between metal nanoparticles and a reduced titanium oxide support, and they used the term SMSI to refer directly to this bonding interaction.[4] However, because this metal–support interaction is closely linked to the catalytic properties of the metal involved, the definition of SMSI has since expanded to broadly refer to support-induced changes in the catalytic activity and selectivity of metal nanoparticles. SMSI plays an important role to enhance many catalytic reactions, including CO oxidation,[5-9] CO and CO_2 hydrogenation,[10, 11] hydroformylation,[12] and partial hydrogenation reactions.[13-17] The ability of an oxide support to mediate the catalytic behavior of a supported metal nanoparticle is an important area in catalysis with both scientific and commercial significance. However, more than 30 years since its discovery, the mechanism of SMSI catalysis remains an open question.

A number of studies show that the support plays an important role in activating the C=O bond. A correlation of the catalyst activity for C=O bond hydrogenation with the Lewis acidity of the oxide empirically shows that charge transfer between the C=O bond and cationic sites in the oxide controls C=O bond activation.[11, 18-20] This observation points out a similarity between SMSI and acid–base catalysis. In acid–base catalysis, the generation of ionic reaction intermediates determines the reaction rate and selectivity because the charged intermediate is highly active for a specific reaction pathway.[21-23] In SMSI the oxide appears to play a similar role: electron transfer between a reactant molecule and the oxide support leads to the formation of a charged reaction intermediate that may be highly selective to a specific reaction pathway. This hypothesis, which explains why SMSI can dramatically enhance the rate of a single reaction pathway, is confirmed in this study by direct observation of reaction intermediates on supported metal catalysts. These results show that SMSI catalysis is a subclass of acid–base chemistry where the flow of charge determines both reaction rate and selectivity.

In the current study, Pt nanoparticles supported on TiO_2 and SiO_2 serve as catalysts for furfuraldehyde hydrogenation. The Pt/SiO_2 catalyst serves a reference state, because SiO_2 is not SMSI active.[3] We investigate the effects of the support on the catalyst selectivity and correlate kinetic measurements with the surface intermediates observed by sum frequency generation (SFG) vibrational spectroscopy. SFG vibrational spectroscopy has been previously used to observe surface reaction intermediates on metal single crystals and shape controlled metal nanoparticles.[24-27] In this study, SFG is used for the first time to study, at a molecular level, how an oxide support controls the selectivity of a metal nanoparticle.

We find that initially the support has no effect on the reaction kinetics. This is because a layer of poly(vinylpyrrolidone) (PVP) encapsulates the Pt nanoparticles and insulates the Pt from the oxide support. However, by controlled removal of the PVP using UV light,[28] direct contact between the nanoparticles and the oxide support results in a new Pt/support interface. In the case of Pt/TiO_2, this interface leads to a 50-fold enhancement in the formation of furfuryl alcohol, while the Pt/SiO_2 interface has no effect on the reaction kinetics. By SFG we observe that a

furfuryl-oxy intermediate forms on the TiO_2 as a result of a Lewis acid–base interaction with the furfuraldehyde molecule. This furfuryl-oxy intermediate is a highly active and selective precursor to furfuryl alcohol. Spectral analysis reveals that the Pt/TiO_2 interface is required primarily for H_2 spillover from the Pt. Density functional calculations identify O-vacancies on the TiO_2 surface as the catalytically active site and show that the barrier to C=O bond hydrogenation is dramatically decreased as a result of furfural bonding at the reduced Ti3+ sites surrounding an O-vacancy. This represents a detailed molecular understanding of the support-enhanced reaction mechanism for an SMSI catalyst and demonstrates a strong similarity between SMSI and acid–base catalysis.

4.3 Results and Discussion

4.3.1 PVP Cap Blocks Strong Metal–Support Interactions

Although many reaction products exist for furfuraldehyde hydrogenation depending on the pressure and temperature conditions,[17] we observed only four products which we break into two reaction pathways as shown in Scheme 1. The first pathway is decarbonylation to produce furan. Along this same pathway, furan can further hydrogenate to form tetrahydrofuran (THF) or further decarbonylate to form propylene.[27] The second reaction pathway is selective C=O bond hydrogenation to produce furfuryl alcohol.

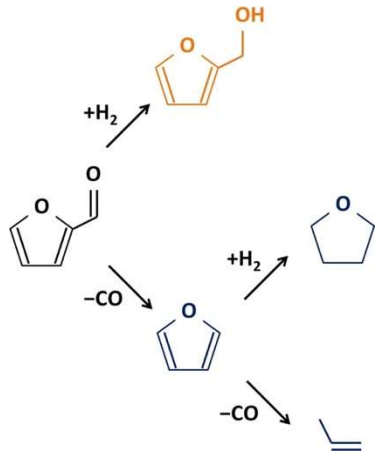

Scheme 1

Figure 4.1 demonstrates that the Pt/TiO_2 interface plays a major role in the production of furfuryl alcohol. Each plot shows the formation of reaction products as a function of time. Parts A and B show the results for PVP-capped Pt nanoparticles supported on TiO_2 and SiO_2, respectively. The PVP-capped particles show identical catalytic activity regardless of the support, indicating that the presence of the PVP cap prevents actual contact between the Pt nanoparticles and the oxide support. Parts C and D show the results for the same catalysts following removal of the PVP cap by UV treatment. The cleaned nanoparticles on TiO_2 show a 50-fold enhancement in the production of furfuryl alcohol which we attribute to the contact between the Pt and TiO_2 following the removal of PVP. However, the cleaned nanoparticles on SiO_2 show similar activity and selectivity to the capped nanoparticles, indicating that the Pt/SiO_2 interface does not play an important role in this reaction

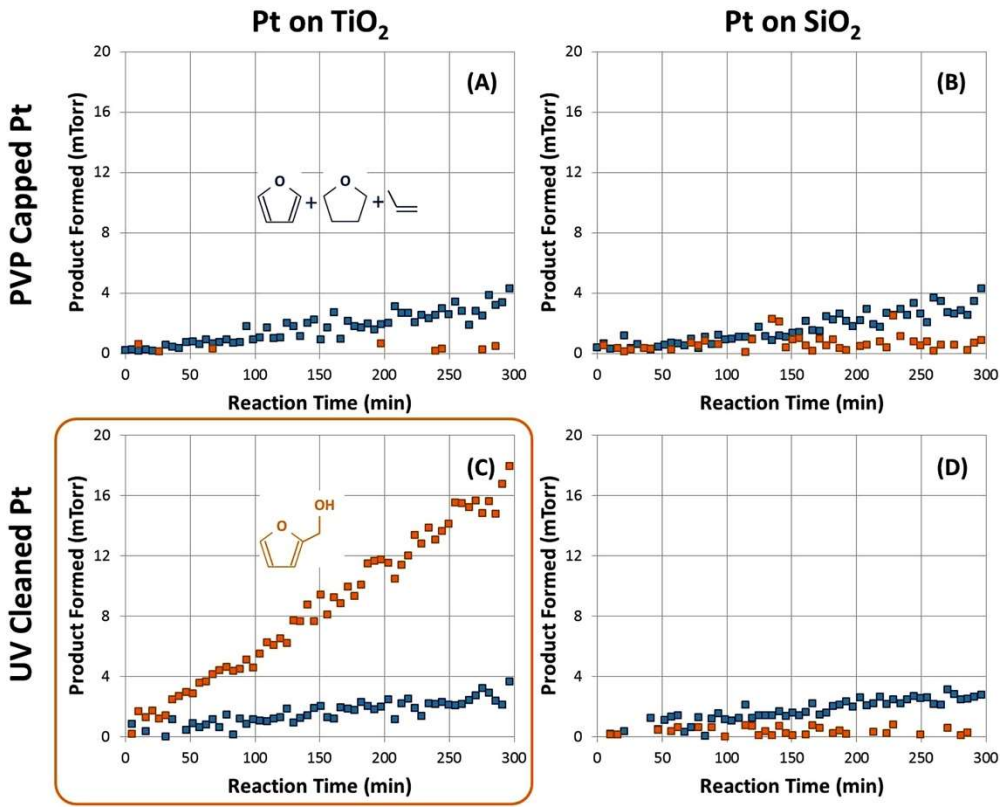

Figure 4.1 Formation of reaction products as a function of time on four Pt nanoparticle catalysts. (A,B) Results for PVP-capped Pt nanoparticles supported on TiO_2 and SiO_2, respectively. (C,D) Results for identical catalysts following 3 h UV cleaning to remove the PVP cap. Furfuryl alcohol is shown in orange, and decarbonylation products (i.e., furan, THF, and propylene) are shown in blue. The support has no effect on the activity or selectivity of the capped particles. However, following UV cleaning, the formation of furfuryl alcohol is selectively enhanced on the Pt/TiO_2 catalyst.

4.3.2 PVP Cap Removal by UV Cleaning

Figure 4.2A shows the C-to-Pt and the N-to-Pt atomic ratios of an LB film of nanoparticles as a function of UV treatment time measured by X-ray photoelectron spectroscopy (XPS). Both C and N signals decrease relative to the Pt signal with UV exposure, indicating that the PVP cap is being removed from the Pt nanoparticles. In this experiment the nanoparticles are supported on a doped Si wafer without any oxide layer to avoid charging during XPS measurements. The activity of the Pt nanoparticles increases by a factor of ~5 with UV treatment time as determined by ethylene hydrogenation, indicating that more Pt sites become available as the cap is removed. The number of active sites after UV cleaning does not vary between TiO_2 and SiO_2 showing that the UV cleaning does not depend on the nanoparticle support. Figure 4.2B schematically depicts the effect of UV cleaning on the supported nanoparticles. As the PVP cap is removed, two important effects are observed: (1) the number of accessible Pt sites increases, so the activity of the catalyst for ethylene hydrogenation increases, and (2) the Pt nanoparticles come into contact

with the oxide support. Electron microscopy shows that size and shape monodispersity of the UV-cleaned nanoparticles is lost during reaction because the uncapped nanoparticles are not as thermally stable as the PVP-capped nanoparticles.

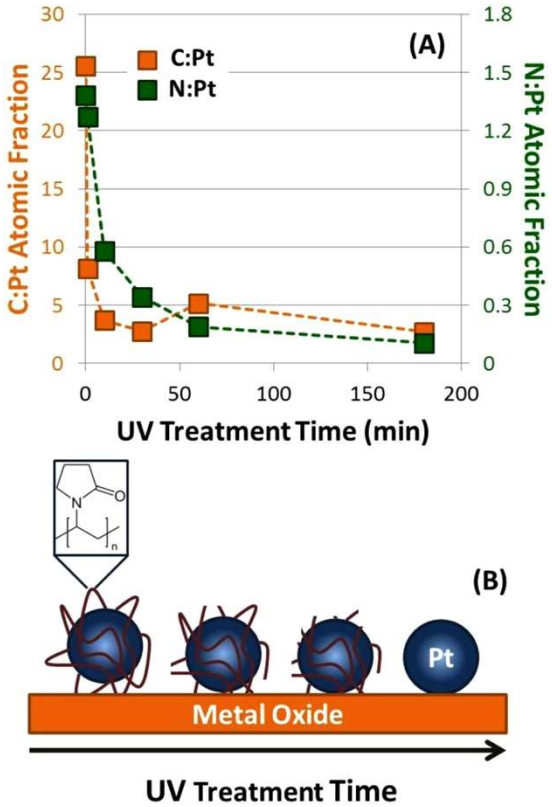

Figure 4.2 (A) C:Pt (orange) and N:Pt (green) atomic fractions for PVP-capped Pt nanoparticles as a function of UV cleaning time measured by XPS. Results indicate removal of the PVP cap from the Pt nanoparticles by UV photodecomposition. (B) Schematic showing the effects of UV cleaning on PVP-capped Pt nanoparticles. UV cleaning has two effects on the catalyst: (1) the number of available active sites per nanoparticle increases, and (2) the nanoparticles are brought into close contact with the support.

4.3.3 Role of Pt/TiO_2 Interface on Reaction Kinetics and Selectivity

Figure 4.3 shows TOF of furfuraldehyde to decarbonylation products (i.e., furan, THF, and propylene) and to furfuryl alcohol as a function of UV treatment time for Pt on TiO_2 (A) and SiO_2 (B). The activity of each catalyst is normalized to the number of active sites measured by ethylene hydrogenation. As described above, this method is capable of measuring the number of Pt active sites without respect to Pt structure or support. Consequently, the changes in TOF with UV cleaning time shown in Figure 4.3 are already corrected for the increasing number of Pt sites as the PVP cap is removed. Initially, the PVP-capped Pt does not produce any furfuryl alcohol regardless of the support. However, as the Pt is brought into close interaction with the TiO_2 by UV cleaning, the activity for furfuryl alcohol production increases. Pt supported on SiO_2 does not

produce any furfuryl alcohol outside of measurement error even after extensive UV cleaning. The data show that Pt activity for decarbonylation does not depend on the support, indicating that the oxide/metal interface has no effect on this reaction pathway.

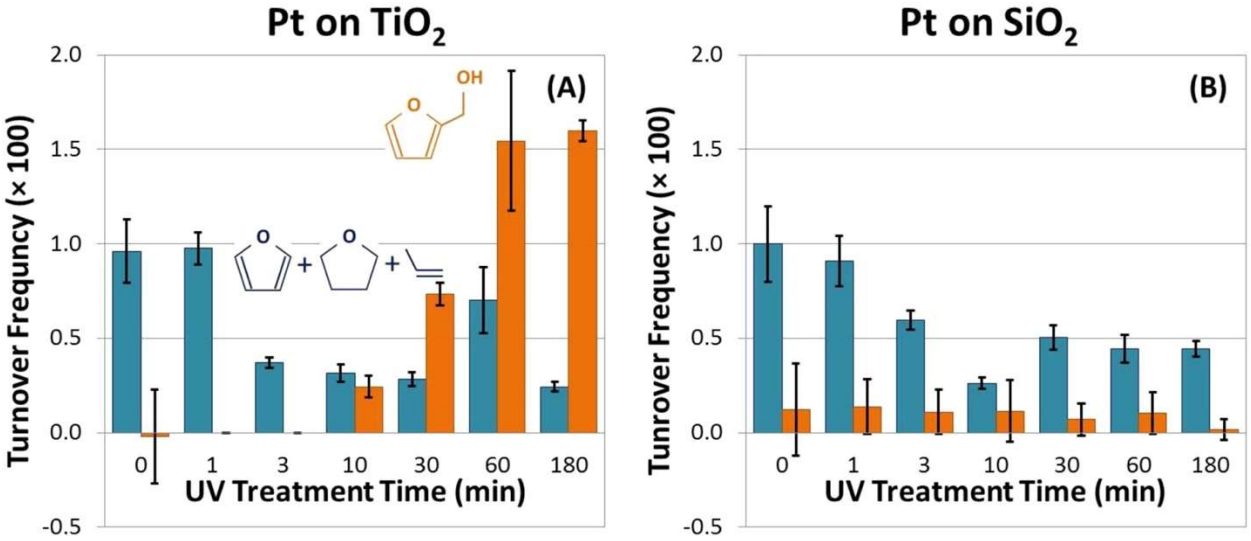

Figure 4.3 Turnover frequency (TOF) of furfuraldehyde by Pt supported on TiO_2 (A) and on SiO_2 (B) as a function of UV treatment time. Orange bars show the formation of furfuryl alcohol, representing selective C=O bond hydrogenation, and blue bars show the combined formation of furan, THF, and propylene, representing the decarbonylation pathway. All TOF values are normalized to the number of Pt actives sites measured by ethylene hydrogenation. Initially, no furfuryl alcohol is produced by Pt on either support. However, with UV cleaning, the formation of furfuryl alcohol is selectively enhanced on the Pt/TiO_2 catalyst.

It is interesting to note that for both supports the rate of decarbonylation decreases following 10 min UV cleaning. Although a rate increase is expected as the PVP is removed by UV cleaning, TOF shown in Figure 4.3 is already normalized to the number of available Pt sites. Consequently, this rate decrease following 10 min UV cleaning does not reflect a change in available Pt sites which is actually increasing. Rather the effect is due to a Pt size dependence for this reaction which results in a decreasing rate of furan formation as nanoparticle size increases.[33] The increase in nanoparticle size after 10 min UV cleaning is caused by nanoparticle agglomeration resulting from a loss in thermal stability following cap removal,[34] and this is confirmed by electron microscopy following reaction.

Figure 4.4 shows the selectivity of Pt supported on TiO_2 (A) and SiO_2 (B) as a function of UV treatment time. The selectivity of the Pt/TiO_2 catalyst for furfuryl alcohol increases with PVP removal, reaching ~90% after 180 min UV cleaning. This is a dramatic change in reaction selectivity changing from ~100% decarbonylation products on the capped nanoparticles to ~90% furfuryl alcohol on the cleaned nanoparticles. The Pt/SiO_2 catalyst shows no effect of PVP removal on the reaction selectivity and produces only decarbonylation products. These results suggest that the Pt/TiO_2 catalyst generates a unique reaction intermediate that is highly selective

toward the formation of furfuryl alcohol. Below we demonstrate by SFG vibrational spectroscopy that the production of furfuryl alcohol correlates with a furfuryl-oxy intermediate that forms on TiO_2, and this furfuryl-oxy intermediate is the selective precursor to furfuryl alcohol.

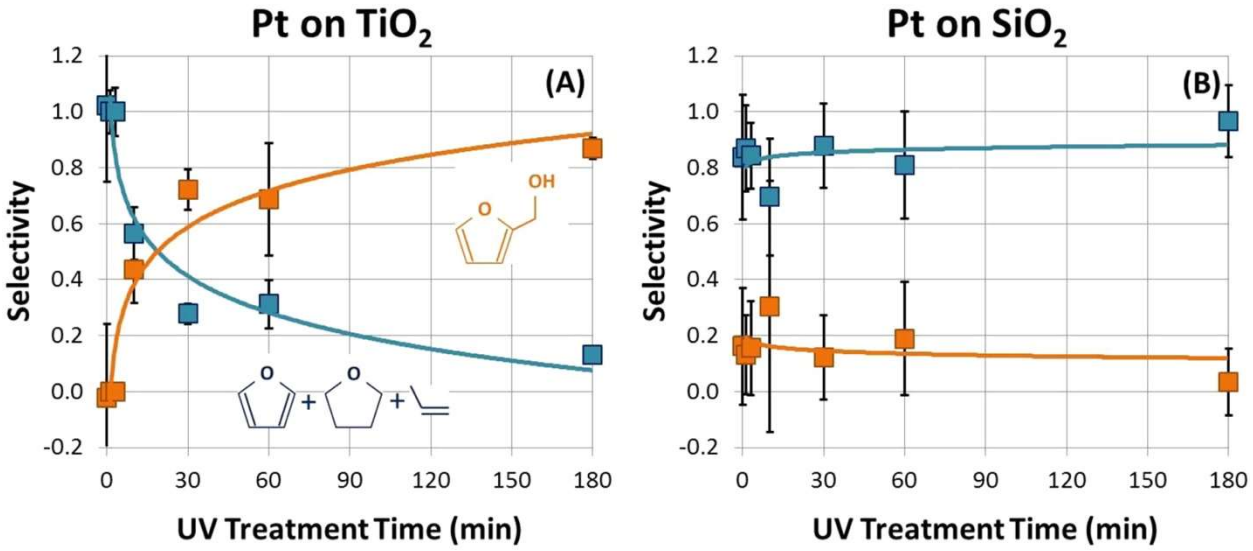

Figure 4.4 Selectivity for furfuraldehyde hydrogenation by Pt supported on TiO_2 (A) and on SiO_2 (B) as a function of UV treatment time. Furfuryl alcohol is shown in orange, and decarbonylation products (i.e., furan, THF, and propylene) are shown in blue. The selectivity of the Pt/TiO_2 catalyst changes dramatically with UV cleaning, going from 100% selectivity for decarbonylation products to ~90% selectivity for furfuryl alcohol. However, the Pt/SiO_2 catalyst is selective only for decarbonylation regardless of UV cleaning time.

4.3.4 Probing Reaction Intermediates by SFG Vibrational Spectroscopy

Figure 4.5 shows SFG spectra of Pt/SiO_2 (A), TiO_2 without Pt (B), and Pt/TiO_2 (C) under reaction conditions following 180 min UV cleaning. The Pt/SiO_2 catalyst shows an intense stretch at 3030 cm^{-1}. This stretch is significantly lower frequency than the aromatic mode for the 5-membered furan ring which appears above 3100 cm^{-1}, and it has been previously assigned in furan hydrogenation as a vinylic stretch.[27] This indicates the presence of an unsaturated furan ring with broken aromaticity. A loss of aromaticity can occur in two ways: The first is partial hydrogenation of the ring to dihydrofuran (DHF) as has been previously observed for furan hydrogenation on Pt single crystals.[27] The second is by an interaction of the furan ring with the catalyst surface via the O atom. In the present study, GC measurements confirm that no DHF forms on this catalyst which is 60% selective to furan, 20% selective to THF, and 20% selective to propylene. Consequently, we assign this vinylic stretch to a furan ring bound to the Pt surface via the O atom as depicted in Figure 4.5A.

At lower temperatures we also observe a stretch at 2765 cm^{-1} (not shown) indicative of the aldehyde C–H stretch. However, this stretch disappears upon heating to 393 K due to decarbonylation of the furfuraldehyde to furan. This process results in CO deposition on the Pt surface which acts as a poison in the subsequent hydrogenation of furan to DHF, THF, or butanol. This explains the relatively low activity of this reaction pathway in furfuraldehyde hydrogenation

compared to previous results for furan hydrogenation where at these pressures and temperatures, THF and butanol would be major products.[27] An additional weak stretch appears in Figure 4.5A at 2860 cm^{-1}. We assign this stretch to the symmetric CH_3 mode from π-bonded propylene which is a 20% product on this catalyst.

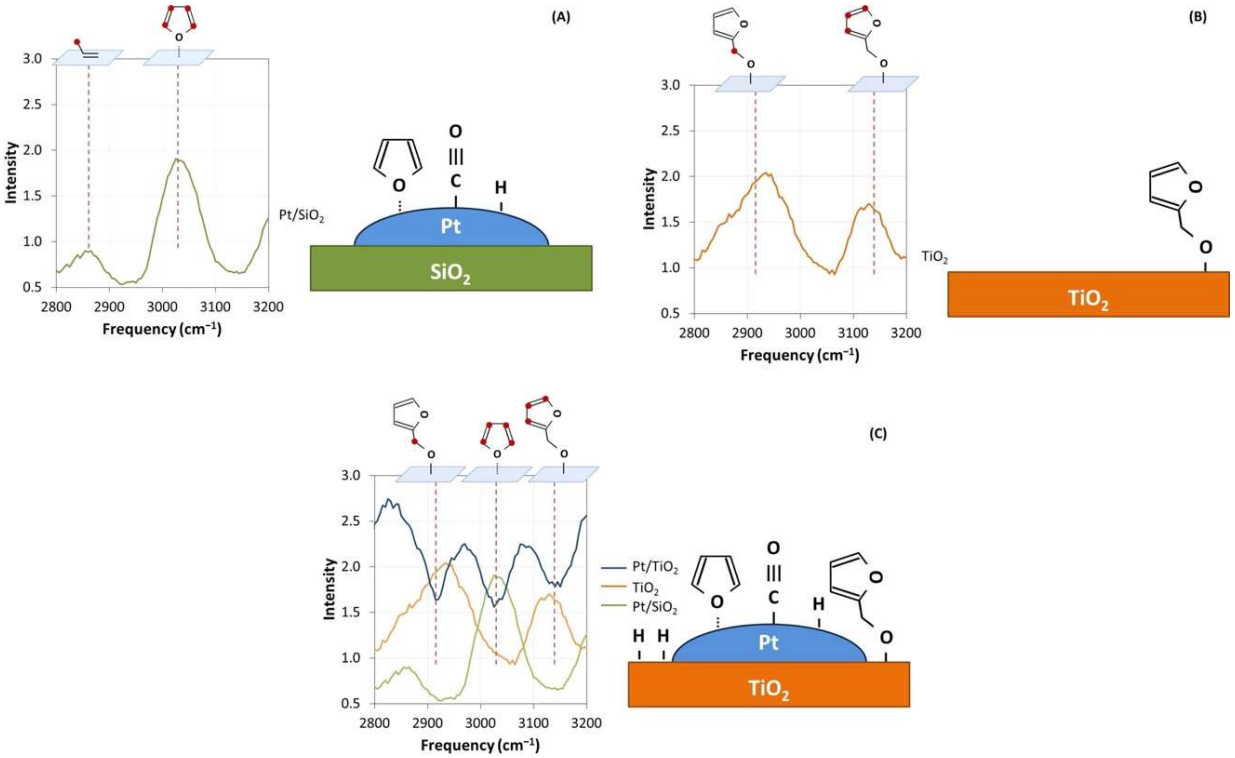

Figure 4.5 SFG spectra of Pt/SiO_2 catalyst (A), TiO_2 support without Pt (B), and Pt/TiO_2 catalyst (C) during reaction following 180 min UV treatment. Next to each spectrum a schematic depicts the surface intermediates represented in the spectrum, and red dots on the molecules above show the C–H bonds responsible for each vibrational mode. The Pt/SiO_2 catalyst (A) shows a strong feature at 3030 cm^{-1} representing the vinylic stretch of furan bound to the Pt surface via the O atom. This intermediate is the result of furfuraldehyde decarbonylation to CO and furan. A weaker stretch at 2860 cm^{-1} represents the CH_3-symmetric mode from π-bonded propylene which is a minor product on this catalyst. The TiO_2 support without Pt (B) shows a strong aromatic feature at 3130 cm^{-1} and a CH_2-symmetric stretch at 2,920 cm^{-1}. This spectrum represents a furfuryl-oxy intermediate resulting from furfuraldehdye bonding to the TiO_2 via the carbonyl O atom followed by the addition of a single H atom to the carbonyl C. This furfuryl-oxy surface intermediate is the precursor to furfuryl alcohol formation. The resonant features on the Pt/TiO_2 catalyst (C) overlap with the features already attributed to a furan intermediate on Pt and a furfuryl-oxy intermediate on TiO_2. This indicates that Pt has a similar reactivity when supported on either oxide, but that H spillover from Pt results in turnover of the furfuryl-oxy intermediate on TiO_2 to furfuryl alcohol. The nonresonant background is much higher for this sample compared to the Pt/SiO_2 and the TiO_2 without Pt, so the resonant modes appear as negative features against the high background.

Figure 4.5B shows the spectrum of TiO_2 without Pt under reaction conditions. This spectrum shows two intense features. The first feature appears at 3,130 cm^{-1} and represents the aromatic stretch of the furan ring. The second feature is a located near 2920 cm^{-1} and represents the CH_2-symmetric mode. This spectrum correlates with a furfuryl-oxy intermediate resulting from furfuraldehdye bonding to the TiO_2 via the carbonyl O atom followed by the addition of a single H atom to the carbonyl C. This furfuryl-oxy surface intermediate is shown schematically next to the spectrum in Figure 4.5B and is the intermediate precursor to furfuryl alcohol formation. Although TiO_2 does not actively dissociate H_2, it is not surprising sufficient H atoms are present to produce a monolayer of furfuryl-oxy surface intermediates. This may be a result of slight H_2 dissociation at defect sites in the polycrystalline TiO_2 film, or the H atoms may come from hydroxyl groups that form on the TiO_2 surface in ambient or during UV cleaning. However, without a continual supply of H atoms from supported Pt nanoparticles, the TiO_2 substrate does not turnover.

Figure 4.5C shows the spectrum of the Pt/TiO_2 catalyst during reaction. In contrast to the spectra obtained on Pt/SiO_2 and TiO_2 without Pt, the nonresonant background of the Pt/TiO_2 sample is quite high, and the resonant modes appear as negative features against the high background. This effect, which is common in SFG, is a result of the phase mismatch between the resonant and nonresonant contributions of the spectrum. In the Pt/SiO_2 sample and TiO_2 sample without Pt, the nonresonant contribution to the spectrum is low, so any phase mismatch is not noticeable. However, the nonresonant component of the Pt/TiO_2 catalyst is much greater resulting in destructive interference with the resonant vibrations. The enhanced nonresonant signal in the Pt/TiO_2 catalyst is a result of H spillover from the Pt resulting in a reduced TiO_2 support. It is well known that in TiO_2, O-vacancies act as electron donors into mid-gap states of the reduced oxide which results in a greatly enhanced surface conductivity.[35] Because the nonresonant contribution to an SFG spectrum is largely the result of free electron motion at the surface of the substrate, it is not surprising that increased TiO_2 conductivity by H_2 reduction results in a dramatic enhancement of the nonresonant signal. This effect is reversible in O_2 as shown in Figure 4.6. Figure 4.6 plots the magnitude of the nonresonant signal in alternating H_2 and O_2 environments (100 Torr) for several catalyst samples. No furfuraldehyde is present during this experiment in which the catalyst is simply cycled between H_2 and O_2 atmospheres and spectra are obtained in each. The catalyst cell is evacuated to <1 mTorr between gases. The nonresonant intensity is determined from the average intensity between 2700 and 2800 cm^{-1}. An effect on the nonresonant signal intensity is only significant for the Pt/TiO_2 catalyst following UV cleaning. The same effect is not observed for the Pt/SiO_2 catalyst and is only weakly observed for the Pt–PVP/TiO_2 catalyst before cap removal. This reflects the non-reducible nature of SiO_2 as well as the necessity of removing the Pt capping agent to enable H spillover to the TiO_2.

The resonant components of the Pt/TiO_2 spectrum during reaction correlate closely with the features observed on the Pt/SiO_2 and the TiO_2 samples, and the Pt/TiO_2 spectrum appears to represent a combination of the spectrum on Pt and the spectrum on TiO_2 as shown in Figure 4.5C. This indicates that Pt has a similar reactivity when supported on either oxide, but that H spillover from Pt results in turnover of the furfuryl-oxy intermediate on TiO_2 to furfuryl alcohol. As shown above by kinetic measurements, this reaction pathway is ~10 times faster than the decarbonylation reaction pathway which occurs only on Pt. This result demonstrates a striking

similarity between SMSI and acid–base catalysis where both processes begin by formation of a unique reaction intermediate that acts as a highly active intermediate in a selective reaction pathway. In the case of SMSI, the TiO_2 support activates the furfuraldehyde molecule to form the highly selective furfuryl-oxy intermediate. The role of the crucial Pt/TiO_2 interface is simply to enable H spillover to this active intermediate.

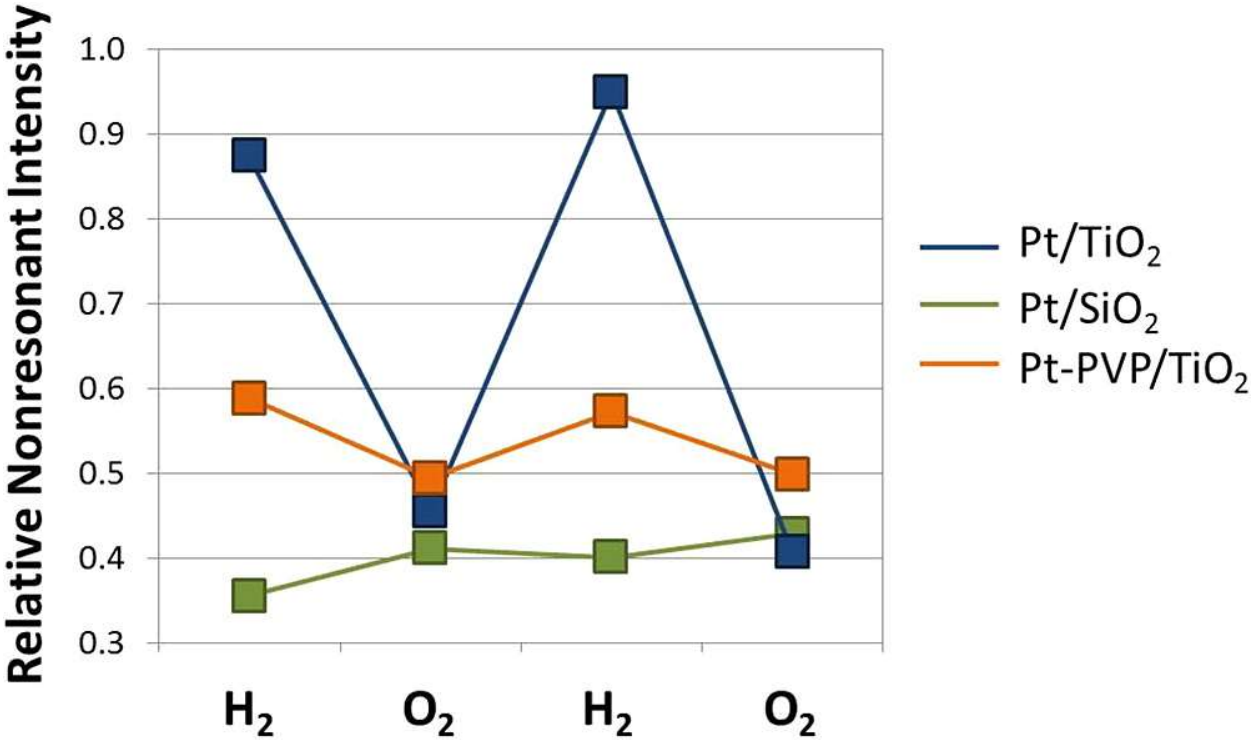

Figure 4.6 Relative nonresonant SFG intensity of a Pt/TiO_2 catalyst (blue), Pt/SiO_2 catalyst (green), and $Pt–PVP/TiO_2$ catalyst in alternating H_2 and O_2 environments (100 Torr) at 333 K. The Pt/TiO_2 and Pt/SiO_2 catalysts were UV-cleaned for 10 min (longer UV cleaning treatments do not change the results shown). The $Pt–PVP/TiO_2$ catalyst was not UV cleaned, so the PVP encapsulated the Pt nanoparticles and prevented contact between Pt and TiO_2. The nonresonant intensity is determined from the average intensity between 2700 and 2800 cm^{-1} where there are no resonant features. For the Pt/TiO_2 catalyst, the nonresonant background changes dramatically in H_2 and O_2. The enhanced nonresonant signal in H_2 is a result of H spillover from the Pt resulting in a reduced TiO_2 support, and this effect is reversible in O_2. The same effect is not observed for the Pt/SiO_2 catalyst and is only weakly observed for the $Pt–PVP/TiO_2$ catalyst before cap removal. This reflects the nonreducible nature of SiO_2 as well as the necessity of removing the PVP cap to enable H spillover from Pt to TiO_2.

4.3.5 Charge Transfer from TiO_2 to Furfuraldehyde

Density functional theory (DFT) calculations indicate that O-vacancies on the reduced TiO_2 surface are the catalytically active sites. Furfuraldehyde binding on the [101] surface of anatase TiO_2 is discussed here; binding on other low-energy surfaces was considered with similar

conclusions. When there is no O-vacancy on the surface, the calculations show that the furfuraldehyde molecule does not bind with either Ti cations or O anions on the surface. However, when there is an O-vacancy on the surface, furfuraldehyde binds to one of the two Ti cations closest to the vacancy site, as shown in Figure 4.7, and the energy of the system decreases by 1.35 eV. The significant energy decrease associated with the binding can be understood considering that the Ti cations near the oxygen vacancy are in the reduced Ti3+ state, so one electron is occupying a high-energy mid-gap state near the conduction band. The binding of furfuraldehyde molecule oxidizes this cation to a Ti4+ state as one electron transfers to the furfuraldehyde molecule. The contour in Figure 4.7 shows the charge transfer during the binding process. The electron transfers from the area around the Ti3+ cation (shown by green contour) to the C=O bond (shown by blue contour). As a new Ti–O bond is formed, the original C=O double bond is changed into a C–O σ bond.

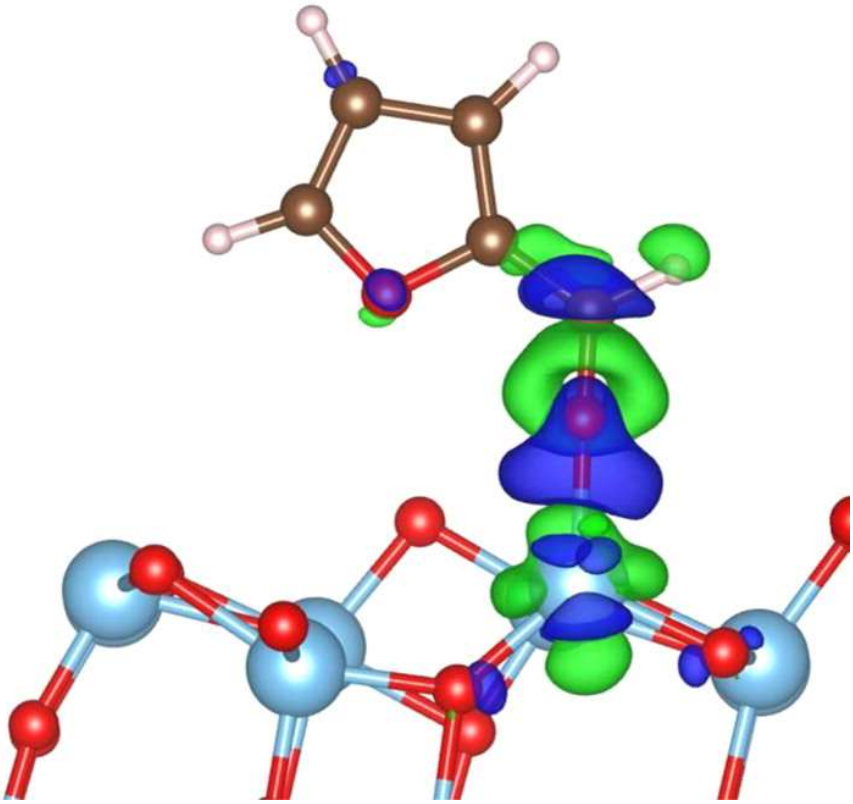

Figure 4.7 Structure plot of a furfuraldehyde molecule binding to a Ti cation near an O-vacancy site on anatase TiO_2 (101), and the charge transfer induced by the surface binding interaction. The filled cyan, red, brown and white circles show the Ti, O, C and H atoms, respectively. The hollow green circles show the site of the O-vacancy (without the vacancy, there should be two O atoms inside the circle). The green contour shows the electron charge loss, and the blue contour shows the electron charge gain induced by the surface binding. In this charge transfer interaction, the Ti atom changes from a 3+ to a 4+ oxidation state, and the furfuraldehyde molecule acquires a negative charge. This negative charge localizes around the carbonyl C, activating it for H addition.

In the final surface binding state, the O atom in the furfuraldehyde molecule is coordinated by Ti and C and is in a stable full-shell state. However, the negative charge localized around the C atom represents a dangling bond, which is very reactive for H binding. A direct calculation shows the energy decreases by 0.2 eV when one H atom leaves the Pt surface and binds with this reactive C atom. Consequently, this step is fast and results in the steady state coverage of furfuryl-oxy intermediates on TiO_2 observed by SFG. This model of furfuraldehyde activation at O-vacancy sites in TiO_2 is also consistent with the experimental data showing that SMSI activity correlates with H spillover which occurs only for the UV-cleaned Pt/TiO_2 catalyst. However, in the case of a free furfuraldehyde molecule (not bound to the TiO_2 surface), there is an energy cost of 2.3 eV for a H atom from the Pt surface to bind to the carbonyl C of a furfuraldehyde molecule. Obviously, this is impossible from a thermodynamic point of view. Furthermore, the calculations show that furfuraldehyde does not bind with a SiO_2 surface. This is in accordance with the experimental observation that the Pt/SiO_2 catalyst is not SMSI active.

4.4 Conclusions

For furfuraldehyde hydrogenation on supported Pt, the oxide support plays a major role to determine the activity and selectivity of the catalyst. This effect, which is common to many reactions, is often referred to as a strong metal–support interaction, but a molecular-level understanding has been lacking notwithstanding the obvious scientific and practical importance. We demonstrate that when Pt nanoparticles make close contact with a TiO_2 support, the Pt/TiO_2 interface results in a new reaction pathway that is highly selective toward furfuryl alcohol formation. SFG vibrational spectroscopy shows that a furfuryl-oxy intermediate forms on TiO_2 and is the selective precursor to furfuryl alcohol. The role of the Pt/TiO_2 interface is simply to enable H spillover to this active intermediate, and this reaction pathway is ~10 faster than the reaction rate on Pt alone. DFT calculations suggest that the formation of the active furfuryl-oxy intermediate is the result of a charge-transfer interaction between the furfuraldehyde molecule and an O-vacancy site on the TiO_2 surface. In this charge transfer interaction, the furfuraldehyde molecule acquires a negative charge that localizes around the carbonyl C, activating it for H addition. These results provide a detailed picture of the molecular and electronic interactions that combine to create the SMSI phenomenon and demonstrate that acid–base interactions are the foundation for highly selective catalysis at the oxide–metal interface.

4.5 Experimental Methods

4.5.1 Catalyst Preparation

To study support effects, two-dimensional model catalysts were prepared by depositing Pt nanoparticles onto two different metal-oxide thin films. SiO_2 and TiO_2 served as the two supports. As synthesized, the Pt nanoparticles were encapsulated in a layer of PVP. This capping layer prevented actual contact between the Pt nanoparticle and the oxide support. However, by photodecomposition of the PVP, the Pt nanoparticles were brought into contact with the oxide support. By controlling the degree of contact between the particle and the support, the effect of the oxide-metal interface on catalytic activity and selectivity was studied.

As previously described, Pt nanoparticles were synthesized from chloroplatinic acid hexahydrate and PVP in a 1:4 mass ratio.[29] In a small beaker, 110 mg of chlorplatinic acid was dissolved in 10 mL of ethylene glycol. In a separate beaker, 440 mg of PVP was dissolved in 10 mL of ethylene glycol. Once in solution, the two mixtures were combined into a 50 mL two-neck round-bottom flask fitted with an Ar flow. The solution was purged under vacuum for 15 min. The vessel was then heated to 438 K for 1 h with vigorous mixing under a flow of Ar. The resulting nanoparticles were precipitated with acetone and washed three times with ethanol and hexanes. The nanoparticles were then suspended in chloroform for Langmuir–Blodgett (LB) deposition. Transmission electron microscopy (TEM) showed that the particles were 4.6 ± 2.8 nm.

Two substrates were used to support the nanoparticles: SiO_2 and TiO_2. For reaction studies, a Si(100) wafer with a 500 nm thermally grown oxide served as the SiO_2 support. The TiO_2 support consisted of a 50 nm TiO_2 thin film deposited on the SiO_2 substrate by electron beam evaporation. Following deposition, the TiO_2 thin film was annealed at 773 K in O_2. Analogous samples were prepared for sum frequency generation spectroscopic studies. For these samples, an optically transparent substrate was needed. A sapphire window rather than a Si wafer served as the substrate. A 50 nm thin film of SiO_2 or TiO_2 was deposited on the sapphire window by electron beam evaporation, again followed by annealing at 773 K in O_2 to ensure oxide stoichiometry.

The LB technique was then used to deposit a monolayer of the Pt nanoparticles onto the metal-oxide supports. This technique has been described previously in detail.[25, 30] In short, a suspension of nanoparticles in chloroform is dispersed onto a water surface (18 MΩ). Time is given for the chloroform to evaporate, leaving a two-dimensional dispersion of nanoparticles on the water surface. The film is then compressed with a mobile barrier, and the surface pressure is monitored as a function of decreasing surface area. The surface pressure corresponds to the density of nanoparticles on the water. When the desired surface pressure is reached, a substrate is pulled out from under the surface of the water, and the film of nanoparticles is deposited onto the substrate. The final density of nanoparticles on the substrate can be controlled by controlling the surface pressure during deposition. A surface pressure of 14 mN/m was used for these studies, and films were deposited using a Nima 611 LB trough. Filter paper served as the surface tension probe. Prior to LB deposition the substrate was cleaned for 1 h in Nochromix solution. TEM showed that the area coverage for Pt on the substrate following LB was approximately 30%. Immediately prior to reaction, the samples were exposed to UV light in air to photodecompose the PVP layer that encapsulated the nanoparticles. Two low-pressure mercury (Hg) lamps (Lights Sources Inc., model number GPH357T5VH/4P) were used as the UV source; the Hg lamp emitted

two lines: 184 and 254 nm. The two lamps were positioned parallel to each other 2.5 cm apart in a clean Al box. The sample was positioned 1.2 cm below the lamps. By varying the time of UV exposure, it was possible to control the amount of PVP removed from the Pt nanoparticles. This cleaning is the combined effect of direct photodecomposition of the PVP as well as oxidation of the PVP by ozone produced by the 184 nm Hg line.[28]

4.5.2 Activity and Selectivity Measurements

A stainless steel batch mode reactor was used to determine the reaction rates and selectivity of furfuraldehyde hydrogenation for Pt supported on SiO_2 and TiO_2 with varying degrees of PVP cap removal. The catalyst was heated with a boron nitride substrate heater to a reaction temperature of 393 K. A metal bellows circulation pump provided gas mixing. Gas pressures were 1 Torr furfuraldehyde, 100 Torr H_2, and 659 Torr He. The furfuraldehyde was purified by freeze–pump–thaw cycles. Each catalyst was tested for 8 h and reaction products were monitored as a function of time using a gas chromatograph with a flame ionization detector. To calculate a turnover frequency (TOF) for each catalyst, it was necessary to determine the number of Pt active sites. Because ethylene hydrogenation is insensitive to Pt structure[31] and support,[11] the number of active sites for each catalyst was determined by measuring the rate of ethylene hydrogenation and normalizing to a known TOF.[32] Ethylene hydrogenation was run on each catalyst following furfuraldehyde hydrogenation in a separate but identical reactor, and catalysts were stored under N2 between reactions. The catalyst temperature for the ethylene reaction was 298 K, and gas pressures were 10 Torr ethylene and 100 Torr H_2 in a background of He.

Turnover frequencies for furfuraldehyde hydrogenation are based on the reaction rate, measured from a fit to peak area versus time, and normalized to the number of active sites as determined by ethylene hydrogenation. Selectivity measurements for furfuraldehyde hydrogenation are calculated as the TOF of a given product normalized to the combined TOF of all products. Error bars represent 95% confidence intervals for these measurements.

4.5.3 Sum Frequency Generation Vibrational Spectroscopy

SFG is a second-order, nonlinear process that probes the $X^{(2)}$ tensor. Because $X^{(2)}$ is zero for centrosymmetric media, SFG is only sensitive to a break in inversion symmetry which usually occurs at a surface or interface. Consequently, SFG is useful for obtaining vibrational spectra of surfaces. In this study, SFG is used to obtain the vibrational spectra of molecules on the catalyst surface during reaction. Comparison of reaction intermediates on Pt nanoparticles supported on SiO_2 and TiO_2 demonstrates that a unique reaction pathway is active on the Pt/TiO_2 catalyst.

For SFG experiments, an active/passive mode-locked Nd:YAG laser (Leopard D-20, Continuum) produced a 20 ps pulse at a 20 Hz repetition rate. The fundamental output at 1064 nm was passed through an optical parametric generator/amplifier to generate a tunable infrared (IR) beam (2700–3600 cm^{-1}) and a second harmonic visible (VIS) beam (532 nm). The IR (100 μJ) and VIS (100 μJ) beams were spatially and temporally overlapped on the back surface of a sapphire window containing the Pt nanoparticles supported on SiO_2 or TiO_2 thin films. The VIS and IR beam were incident on the sample at 40° and 50°, respectively, relative to surface normal. The generated SFG signal was then collected and sent to a photomultiplier tube. A gated integrator was used to enhance the signal-to-noise. To collect a spectrum, the IR beam was scanned across

the spectral range of interest. All experiments were performed in the ppp polarization combination.

The beams were directed onto the sample using a sapphire prism. A solution of deuterated polystyrene (d8) in deuterated decalin (d18) served as an index matching liquid that did not interfere with transmission of the IR beam at the C–H stretch frequency. The catalyst surface was pressed into thermal contact with an aluminum heating block to heat the catalyst to reaction temperature. A recess in the heating block allowed for the flow of reaction gases across the catalyst surface. A metal bellows circulation pump provided gas mixing. A gastight seal was made between the sapphire window and the heating block using a Kalrez O-ring.

4.3.4 Density Functional Theory Calculations

The calculation is performed using the VASP code based on the density functional theory. For the exchange-correlation functional, the generalized gradient approximation (GGA) of Perdew–Burke–Ernzerhof (PBE) is used. The projector augmented-wave pseudopotentials are used with an energy cutoff of 400 eV for the plane-wave basis functions. To simulate the molecule absorption on the TiO_2 surfaces, a slab model is used with 6 Ti–O double layers (about 20 Å thick) and 10 Å vacuum layer, and a 1×2 supercell (about 10 Å × 8 Å) in the x–y plane. The Brillouin zone integration is carried out using 2×2×1 Monkhorst–Pack k-point meshes.

4.6 References

(1) Schwab, G. M. *Trans. Faraday Soc.* **1946**, 42, 689.

(2) Tauster, S. J.; Fung, S. C.; Garten, R. L. *J. Am. Chem. Soc.* **1978**, 100, 170.

(3) Tauster, S. J.; Fung, S. C.; Baker, R. T. K.; Horsley, J. A. *Science* **1981**, 211, 1121.

(4) Tauster, S. J. *Acc. Chem. Res.* **1987**, 20, 389.

(5) Oh, S. H.; Eickel, C. C. *J. Catal.* **1988**, 112, 543.

(6) Zhu, H.; Qin, Z.; Shan, W.; Shen, W.; Wang, J. *J. Catal.* **2004**, 225, 267.

(7) Chen, M. S.; Goodman, D. W. *Science* **2004**, 306, 252.

(8) Goodman, D. *Catal. Lett.* **2005**, 99, 1.

(9) Baker, L. R.; Hervier, A.; Seo, H.; Kennedy, G.; Komvopoulos, K.; Somorjai, G. A. *J. Phys. Chem. C* **2011**, 115, 16006.

(10) Boffa, A. B.; Bell, A. T.; Somorjai, G. A. *J. Catal.* **1993**, 139, 602.

(11) Boffa, A.; Lin, C.; Bell, A. T.; Somorjai, G. A. *J. Catal.* **1994**, 149, 149.

(12) Yamada, Y.; Tsung, C.-K.; Huang, W.; Huo, Z.; Habas, S. E.; Soejima, T.; Aliaga, C. E.; Somorjai, G. A.; Yang, P. *Nat. Chem.* **2011**, 3, 372.

(13) Vannice, M. A.; Sen, B. *J. Catal.* **1989**, 115, 65.

(14) Lin, S. D.; Sanders, D. K.; Albert Vannice, M. *Appl. Catal. A: General* **1994**, 113, 59.

(15) Kijeński, J.; Winiarek, P. *Appl. Catal. A: General* **2000**, 193, L1.

(16) Malathi, R.; Viswanath, R. P. *Appl. Catal. A: General* **2001**, 208, 323.

(17) Kijeński, J.; Winiarek, P.; Paryjczak, T.; Lewicki, A.; Mikołajska, A. *Appl. Catal. A: General* **2002**, 233, 171.

(18) Bracey, J. D.; Burch, R. *J. Catal.* **1984**, 86, 384.

(19) Sachtler, W. M. H.; Shriver, D. F.; Hollenberg, W. B.; Lang, A. F. *J. Catal.* **1985**, 92, 429.

(20) Sachtler, W. M. H.; Ichikawa, M. *J. Phys. Chem.* **1986**, 90, 4752.

(21) Jencks, W. P. *Acc. Chem. Res.* **1980**, 13, 161.

(22) Greeley, J.; Norskov, J. K.; Mavrikakis, M. *Annu. Rev. Phys. Chem.* **2002**, 53, 319.

(23) Olah, G. A.; Molnar, A. *Hydrocarbon Chemistry*, 2nd ed.; John Wiley & Sons, Inc.: Hoboken, NJ, **2003**.

(24) Bratlie, K. M.; Kliewer, C. J.; Somorjai, G. A. *J. Phys. Chem. B* **2006**, 110, 17925.

(25) Bratlie, K. M.; Komvopoulos, K.; Somorjai, G. A. *J. Phys. Chem. C* **2008**, 112, 11865.

(26) Kliewer, C. J.; Bieri, M.; Somorjai, G. A. *J. Am. Chem. Soc.* **2009**, 131, 9958.

(27) Kliewer, C. J.; Aliaga, C.; Bieri, M.; Huang, W.; Tsung, C.-K.; Wood, J. B.; Komvopoulos, K.; Somorjai, G. A. *J. Am. Chem. Soc.* **2010**, 132, 13088.

(28) Aliaga, C.; Park, J. Y.; Yamada, Y.; Lee, H. S.; Tsung, C.-K.; Yang, P.; Somorjai, G. A. *J. Phys. Chem. C* **2009**, 113, 6150.

(29) Kuhn, J. N.; Huang, W.; Tsung, C.-K.; Zhang, Y.; Somorjai, G. A. *J. Am. Chem. Soc.* **2008**, 130, 14026.

(30) Song, H.; Kim, F.; Connor, S.; Somorjai, G. A.; Yang, P. *J. Phys. Chem. B* **2004**, 109, 188.

(31) Schlatter, J. C.; Boudart, M. *J. Catal.* **1972**, 24, 482.

(32) Kuhn, J. N.; Tsung, C.-K.; Huang, W.; Somorjai, G. A. *J. Catal.* **2009**, 265, 209.

(33) Pushkarev, V.; Musselwhite, N.; Ann, K.; Alayoglu, S.; Somorjai, G. Nano Lett. **2012**, 12 (10), 5196–5201.

(34) Krier, J. M.; Michalak, W. D.; Baker, L. R.; An, K.; Komvopoulos, K.; Somorjai, G. A. J. Phys. Chem. C **2012**, 116 (33), 17540–17546.

(35) Seo, H.; Baker, L. R.; Hervier, A.; Kim, J.; Whitten, J. L.; Somorjai, G. A. *Nano Lett.* **2010**, 11, 751.

Chapter 5

Selective Amplification of C=O Bond Hydrogenation on Platinum with TiO_2 as a Support: Catalytic Reaction and Sum-Frequency Generation Vibrational Spectroscopy Studies of Crotonaldehyde Hydrogenation

5.1 Abstract

In this work the hydrogenation of crotonaldehyde by supported platinum nanoparticles is used to determine how the interaction between the metal particles and their support can control catalytic performance. Using gas phase catalytic reaction studies and *in-situ* sum-frequency generation vibrational spectroscopy (SFG) to study Pt/TiO_2 and Pt/SiO_2 catalysts, a unique reaction pathway is identified for Pt/TiO_2 which selectively produces alcohol products. SFG is used to identify surface reaction intermediates. The catalytic and spectroscopic data obtained for the Pt/SiO_2 catalyst shows that SiO_2 has no active role in this reaction. SFG spectra obtained for the Pt/TiO_2 catalyst indicate the presence of a crotyl-oxy surface intermediate. By adsorption through the aldehyde oxygen to an O-vacancy site on the TiO_2 surface, the C=O bond of crotonaldehyde is activated, by charge transfer, for hydrogenation. This intermediate reacts with spillover H provided by the Pt to produce crotyl alcohol.

5.2 Introduction

Enhancement of a metal catalyst's reactivity and selectivity by a seemingly inert metal oxide support has been documented in literature for numerous gas-phase reactions, such as methanol oxidation[1], CO oxidation[2], partial hydrogenation of organic molecules[3-6], CO and CO_2 hydrogenation[7] and hydroformulation[8], on a variety of metals and supporting oxide systems. In some cases, by combining a metal with a metal oxide support the activity of the resulting system can far surpass what would be expected from a simple combination of the two materials. Among a number of explanations for these enhancements, depending on the reaction and catalyst materials utilized, one proposed mechanism of particular interest to this work involves a direct interaction between a reactant molecule and the oxide support and the spillover of a second reactant from the metal. [9,10] In a reducing atmosphere, at elevated temperatures, and in the presence of platinum, metal oxides undergo changes in the surface oxidation state by the formation of O-vacancies, for example, Ti^{4+} is reduced to Ti^{3+}. [11,12] These electron-rich sites interact with adsorbate molecules and activate them toward a certain reaction pathway.[4] Studies of various metal oxide films deposited on metal surfaces have shown that the oxide plays a key role in activating C=O bonds.[7,13] The activity of catalysts for C=O bond hydrogenation in these studies scaled with the Lewis acidity of the oxide, indicating the critical role charge transfer plays the catalytic process. The implication of charge transfer between the support and adsorbate draws a comparison to acid-base catalysis in which the generation of charged intermediate species is the crucial step in determining the activity and selectivity of a reaction.[14,15] In this study it is proposed that intermediates are generated at O-vacancy sites on the TiO_2 surface of Pt/TiO_2 catalysts and that these intermediates are active for the hydrogenation of the C=O group in crotonaldehyde.

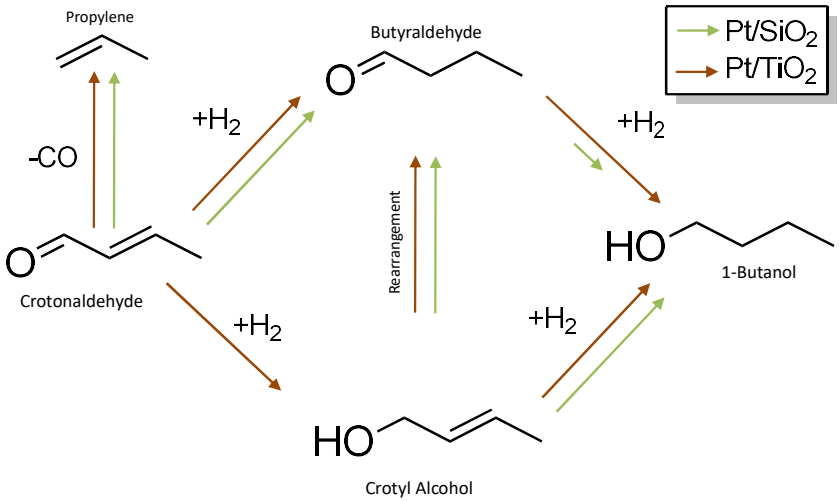

Scheme 5.1 Reaction scheme showing all product pathways observed in the course of reaction studies. Two sets of arrows represent the activity for each pathway for Pt/SiO_2 and Pt/TiO_2. Equal sized arrows indicate no influence of support. Different length arrows represent relative difference between supports for that pathway.

Crotonaldehyde hydrogenation (Scheme 5.1) and hydrogenation of other unsaturated aldehydes have been studied extensively because these reactions have three distinct, competing reaction pathways: decarbonylation to produce CO and propylene, hydrogenation of the C=C bond yielding the saturated aldehyde and the hydrogenation of the C=O bond yielding the unsaturated alcohol.[5,16-18] Selective hydrogenation of the carbonyl bond in such systems without hydrogenation of the C=C bond is of great interest since unsaturated alcohols are useful chemical intermediates for pharmaceuticals and fragrances. However while the hydrogenation of the C=O bond has a 40 kJ/mol lower activation barrier[19] selectively producing the unsaturated alcohol at high rates can be a challenge since hydrogenation of the C=C bond is thermodynamically favored by 35 kJ/mol.[20] Previous work by Kliewer et. al.[19] studying crotonaldehyde hydrogenation on platinum (111) and (100) single crystals shows that the dominant pathways at the temperature used in the present work are C=C bond hydrogenation to form butyraldehyde, and decarbonylation to form propylene, regardless of the crystal face. Based on these results, a C=O bond activating support could drastically alter the activity and selectivity of crotonaldehyde hydrogenation on Pt.

In this study Pt nanoparticle films, deposited onto SiO_2 and TiO_2 substrates, serve as model catalysts for the hydrogenation of crotonaldehyde. This reaction is well suited to probe how the SiO_2 and TiO_2 supports impact, or do not impact, the selectivity and activity toward the various products. By coupling catalytic reaction studies with Sum-Frequency Generation Vibrational Spectroscopy (SFG), a highly surface sensitive technique, it is possible to gain molecular level information about the surface species present on our catalysts under reaction conditions[21-23] and correlate those species to the products formed on each catalyst.

5.3 Results and Discussion

5.3.1 Catalytic Reaction Studies

A Pt/SiO_2 catalyst is used as a reference state under the assumption that SiO_2 has no active role in the catalysis. Inspection of our kinetic results and comparison to previous work, in which crotonaldehyde hydrogenation was carried out on Pt single crystals, give strong evidence that this assumption is valid. Catalytic tests were carried out in a batch-mode gas-phase reactor, and the crotonaldehyde conversion was kept below 15%. Figure 5.1 shows the Turnover Frequency (TOF) for the formation of each observed product of Pt/SiO_2 at 120 °C. Only two products are produced by this catalyst under these conditions: the decarbonylation product propylene (32% of total products), and the C=C bond hydrogenation product butyraldehyde (68% of total products). Neither of the C=O hydrogenation products, 1-butanol and crotyl alcohol, are detected. These results are similar to those of Kliewer et. al.[19] on Pt (111) and (100) single crystals, in which propylene and butyraldehyde are also the two dominant products at 120°C with the alcohol products combined making up less than 5% of all products on both crystal faces. It is

therefore confirmed that SiO_2 has no impact on the catalytic reactions occurring on the Pt nanoparticle surface.

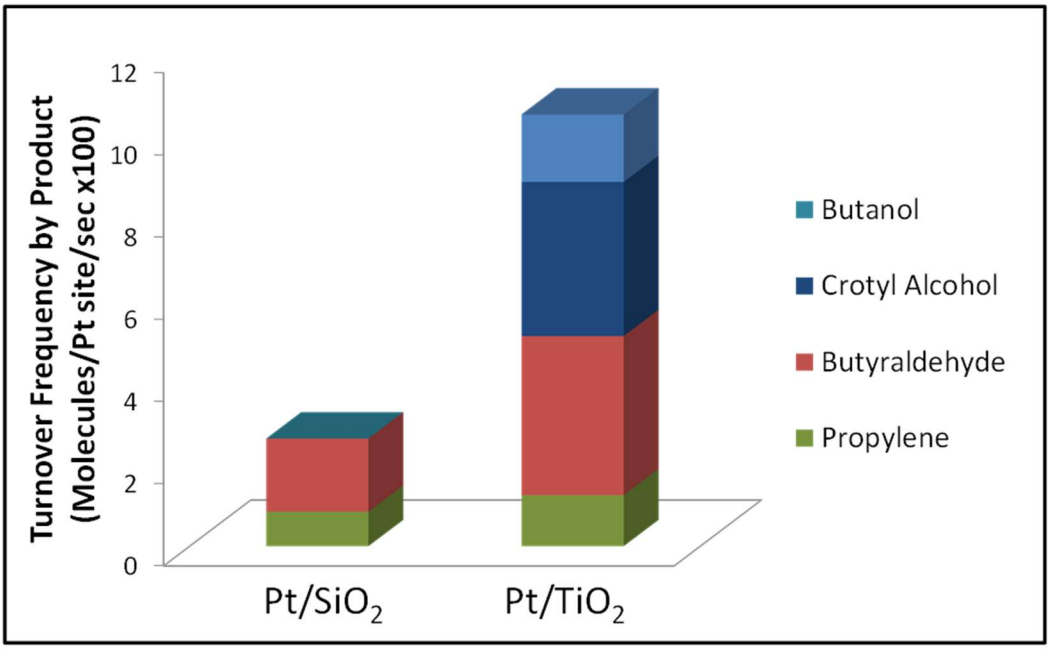

Figure 5.1 *Turnover frequencies for the four observed products are reported for both Pt/SiO_2 and Pt/TiO_2 catalysts. Similar rates of propylene production are observed for both catalysts. Butanol and Crotyl Alcohol production is only observed on Pt/TiO_2 catalysts.*

In contrast, the Pt/TiO_2 catalyst shows dramatically different performance. Under the same reaction conditions for crotonaldehyde hydrogenation, the Pt/TiO_2 catalysts showed a 3-4 fold increase in total activity, mainly from high rates of crotyl alcohol and butanol formation. The combined TOF toward the alcohol products is greater than that for either the propylene or butyraldehyde. The selectivity toward the alcohol products, which is zero for the Pt/SiO_2, is 52% on Pt/TiO_2. Most importantly this change in selectivity is not at the loss of activity toward the other pathways but is due to additional activity, indicating the presence of a new catalytic active site when Pt and TiO_2 are brought into atomic contact, which selectively produces alcohol products. The production of butanol is believed to be from a concerted reaction of both the C=O and C=C bonds of species adsorbed at the interface between TiO_2 and Pt, the alternative being that butanol is formed as a secondary product from the hydrogenation of butyraldehyde or crotyl alcohol. In our case butanol is observed very early on and the rate of its formation does not depend on the concentration of either of the primary products, supporting a concerted mechanism on Pt/TiO_2. Additionally if one were to assume a pseudo-first order rate equation for the formation of the primary products, butyraldehyde and crotyl alcohol, from crotonaldehyde and for the formation of butanol from these primary products (as determined in Figure 5.2), the amount of butanol produced as a secondary product would be below the detection limit of our apparatus. This gives further support to the conclusion that butanol is formed by a concerted process.

Additional catalytic tests were performed in which the partial hydrogenation products, crotyl alcohol and butyraldehyde, were used as reactants in order to further elucidate the influence of the support on the various reaction pathways, the results of which are shown in Figure 5.2. Both catalysts converted crotyl alcohol to 1-butanol with high activity, further showing that C=C bond hydrogenation takes place on Pt with no influence from the support. A rearrangement pathway was also observed, transforming crotyl alcohol to the thermodynamically favored butyraldehyde. This pathway is also independent of support and notably does not occur in the reverse direction to produce crotyl alcohol. This pathway can explain the pronounced increase in the rate of butyraldehyde formation observed on Pt/TiO_2 versus Pt/SiO_2 as crotyl alcohol formed by the Pt/TiO_2 catalyst could be rearranged to make butyraldehyde . The hydrogenation of butyraldehyde shows clear differences between the two catalysts, as activation of the C=O bond greatly enhances the rate of 1-butanol production. Both catalysts convert butyraldehyde to 1-butanol; however the Pt/TiO_2 catalyst does so at about 3x the rate of the Pt/SiO_2. One may then expect to observe 1-butanol from Pt/SiO_2 as a secondary product of crotonaldehyde hydrogenation, which we did not. The reverse of the rearrangement pathway observed for crotyl alcohol hydrogenation is not observed for butyraldehyde hydrogenation on either catalyst, demonstrating that it is not possible to convert the thermodynamically favored initial product into crotyl alcohol, the kinetically favored product.

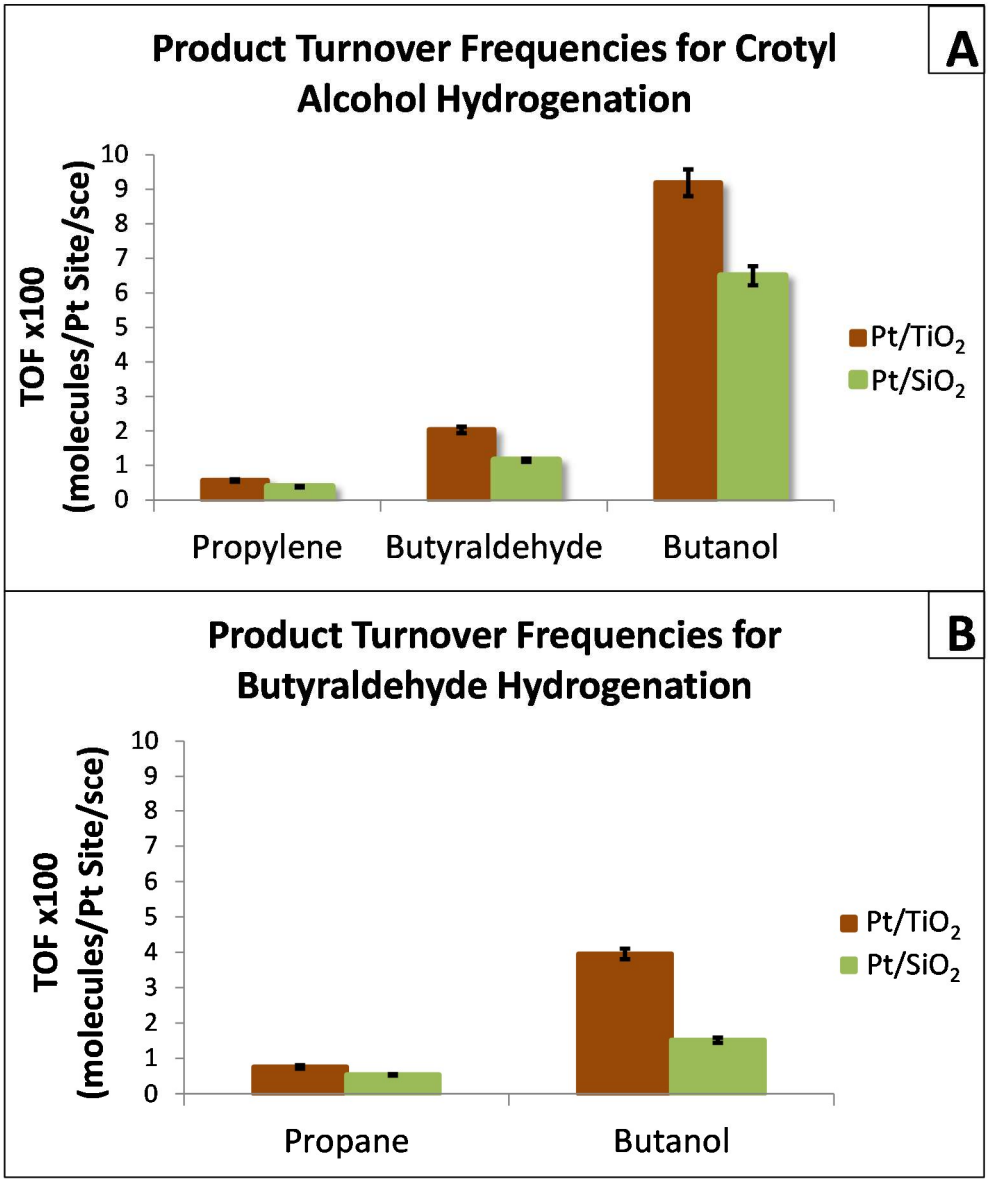

Figure 5.2 Turnover Frequencies for the products of the hydrogenation of (A) crotyl alcohol and (B) butyraldehyde respectively. All reactions are carried out using 1 Torr crotyl alcohol/buteraldeyde, 100 Torr H_2 with 669 Torr at 120°C. In general the Pt/TiO_2 catalyst is more active for all reactions. For crotyl alcohol hydrogenation the selectivity between products is relatively the same for both supporting materials. The impact of C=O bond activation is not seen here as the C=O bond has already been hydrogenated. In the case of butyraldehyde hydrogenation butanol production is roughly 2.5 times greater on the Pt/TiO_2 catalyst, attributable to the activation of the C=O bond by this catalyst. Since butanol is formed on Pt/TiO_2 one might expect to see it as a secondary product in crotonaldehyde hydrogenation, however under these conditions the projected amount of butanol formed would be below the limit of detectability in this system. Rearrangement between crotyl alcohol and butyraldehyde is observed only in one direction, toward the formation of butyraldehyde, the thermodynamically favored molecule.

As shown in figure 5.3, substantial deactivation of the Pt/SiO_2 catalyst is observed over the first 3 hours of reaction. This is likely due to poisoning of the platinum surface by the CO produced by the decarbonylation reaction, reported previously for this reaction on Pt nanoparticles.[9] The catalysts deactivates by roughly 70% for the formation of both propylene and butyraldehyde, determined by comparing the rate during the first 100 minutes and the last 100 minutes. Once a steady state is reached for the formation and subsequent desorption of CO the platinum maintains a constant rate of production for both the butyraldehyde and propylene products. Since CO is a noted poison for Pt catalyzed reactions at these temperatures this reinforces the conclusion that Pt alone is the catalytic material for the C=C hydrogenation and decarbonylation pathways. Reported reaction rates are taken after the initial deactivation period.

Also of note is while a 70% deactivation is observed for the production of butyraldehyde and propylene, the deactivation is only 30% for the production of crotyl alcohol and butanol, leading to the conclusion that the formation of these products is less dependent on the number of Pt active sites. This suggests a spillover mechanism where the active intermediate for crotyl alcohol and butanol is formed on the oxide surface and subsequently reacts with atomic hydrogen spilling over from the platinum surface. This hypothesis is supported by the following vibrational spectroscopic data.

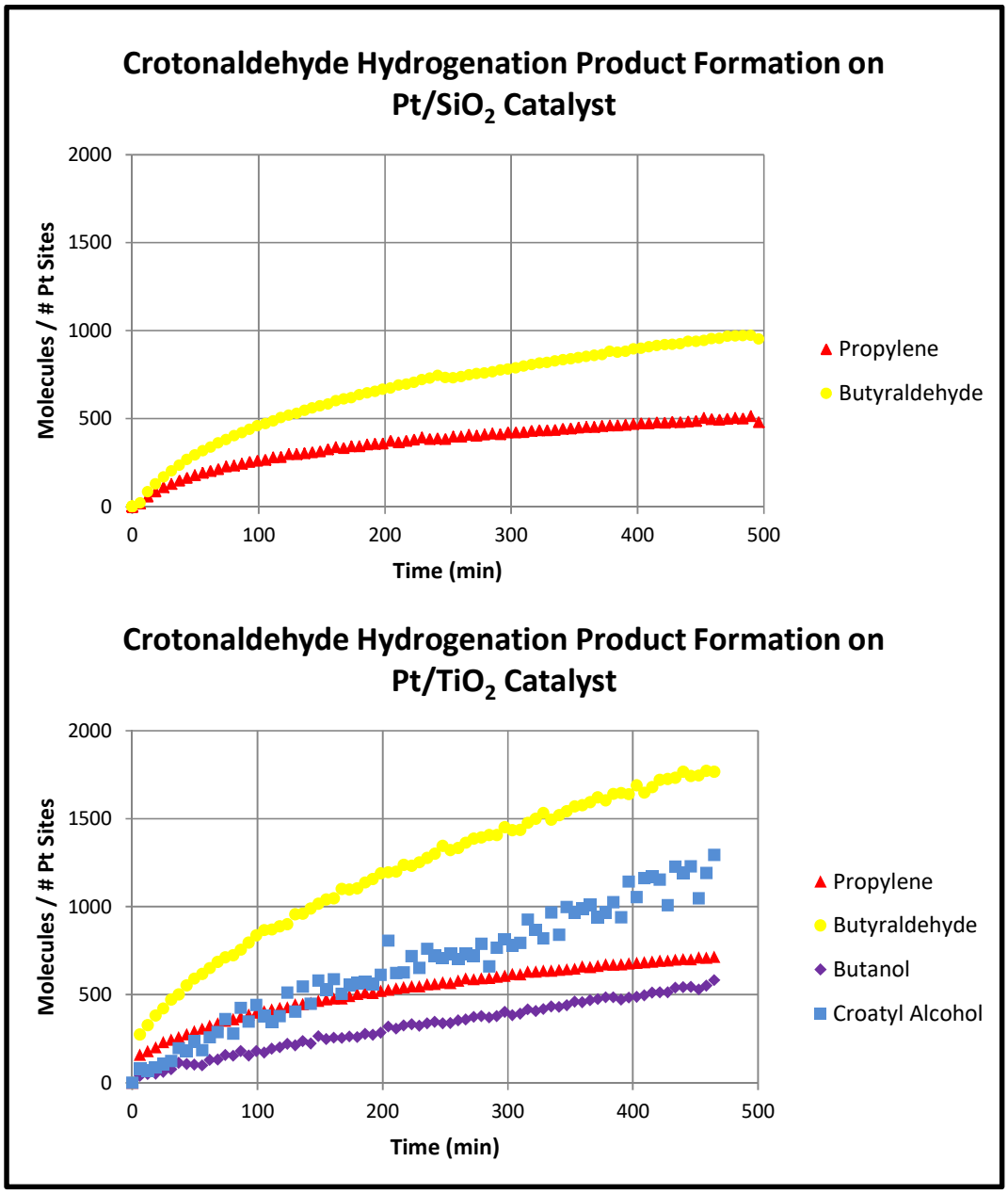

Figure 5.3 Reaction rate data for crotonaldehyde hydrogenation for the two catalysts, Pt/SiO_2 and Pt/TiO_2. All reactions are carried out in a batch mode reactor with 1 Torr Crotonaldehyde, 100 Torr H_2 and 669 Torr He, with a catalyst temperature of 120 °C. Note that on both catalysts propylene and butyraldehyde production decrease over the first 200 minutes of reaction by roughly 70%. In contrast crotyl alcohol and butanol production shows much less deactivation, only 30% over the course of the reaction. Deactivation is due to poisoning of the Pt surface by CO. The substantially lesser deactivation in the production of crotyl alcohol and butanol indicates that the formation of these products is not highly dependent on Pt active sites, but rather interfacial or TiO_2 surface sites.

5.3.2 Sum Frequency Generation Vibration Spectroscopic Studies

In order to better understand the mechanism by which TiO_2 enhances the rate of C=O bond hydrogenation Sum Frequency Generation Vibrational Spectroscopy is employed to determine surface reaction intermediates. Figure 5.4 shows the SFG spectra for (A) Pt/SiO_2, and (B) Pt/TiO_2 all under crotonaldehyde hydrogenation reaction conditions, along with proposed adsorption geometries and reaction intermediates. The Pt/SiO_2 spectrum shows two features at 2860 and 2915 cm^{-1} consistent with previous work on Pt single crystal surfaces by Kliewer et. al. [19] The peak at 2915 cm^{-1} is assigned to a CH_3 stretch and the peak at 2860 is assigned to an aldehyde CH stretch. It has been shown previously that aldehyde stretches, usually near 2800 cm^{-1}, can be shifted into this range when adsorbed on a surface.[24] This assignment is in agreement with the proposed η_2 adsorption mode, which is believed to be the intermediate responsible for the formation of butyraldehyde. The clear similarities between the SFG spectra taken on the Pt/SiO_2 and Pt (111) single crystal further support the claim that the SiO_2 support plays no active role in the hydrogenation of crotonaldehyde on Pt.

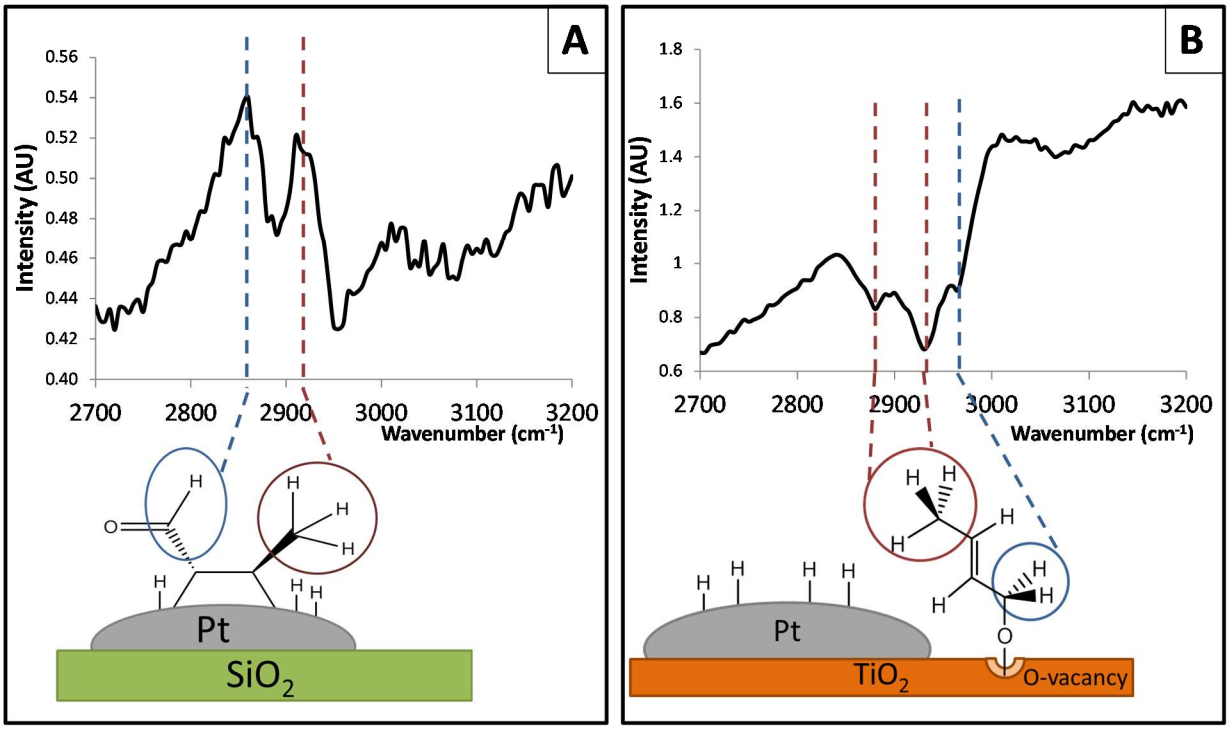

Figure 5.4 SFG spectra for (A) Pt/SiO_2 and (B) Pt/TiO_2 under reaction conditions of 1 Torr crotonaldehyde, 100 Torr hydrogen and 669 Torr argon at a catalyst temperature of 120°C. Assignment of these spectra, explained in the text, yields the accompanying surface intermediates.

The spectrum of Pt/TiO_2, Figure 5.4B, shows several intense negative features at 2880, 2930 and 2965 cm^{-1}. Both the strength and sign of these peaks are due to the increased non-resonant component of the signal from Pt/TiO_2 in the presence of hydrogen. Hydrogen spillover from Pt to TiO_2 serves to reduce the surface of the TiO_2 to TiO_{2-x}, which in turn makes it more

metallic. Additionally this surface reduction increases the number of O-vacancy sites. The non-resonant component of SFG is largely the result of free-carrier motion at the surface of a sample. As more O-vacancies are formed on the TiO_2 surface the free carrier concentration increases as evidenced by increased surface conductivity[25], and subsequently the non-resonant component of the SF signal is larger. This serves as a marker for the chemical and electronic structure of the oxide surface and supports our hypothesis that O-vacancies are the active catalytic sites. The increased non-resonant contribution can serve to elevate the baseline level in SFG spectra and also enhance the intensity of resonant features due to the relationship between the non-resonant and resonant components of $\chi^{(2)}$ and the SFG intensity. The resonant features observed are out of phase with this non-resonant background and thus present as negative peaks.

The reported spectrum in Figure 5.4B is remarkably similar to the same region in the crotyl alcohol gas phase IR spectrum and is indicative of a crotyl-oxy intermediate bound to the TiO_2 surface by the aldehyde O atom. The features at 2880 and 2930 cm^{-1} are assigned to the CH_3 symmetric and asymmetric stretching modes respectively.[26] The stretch at 2965 cm^{-1} is assigned to the CH_2 asymmetric stretching mode of the O bound C.[27]

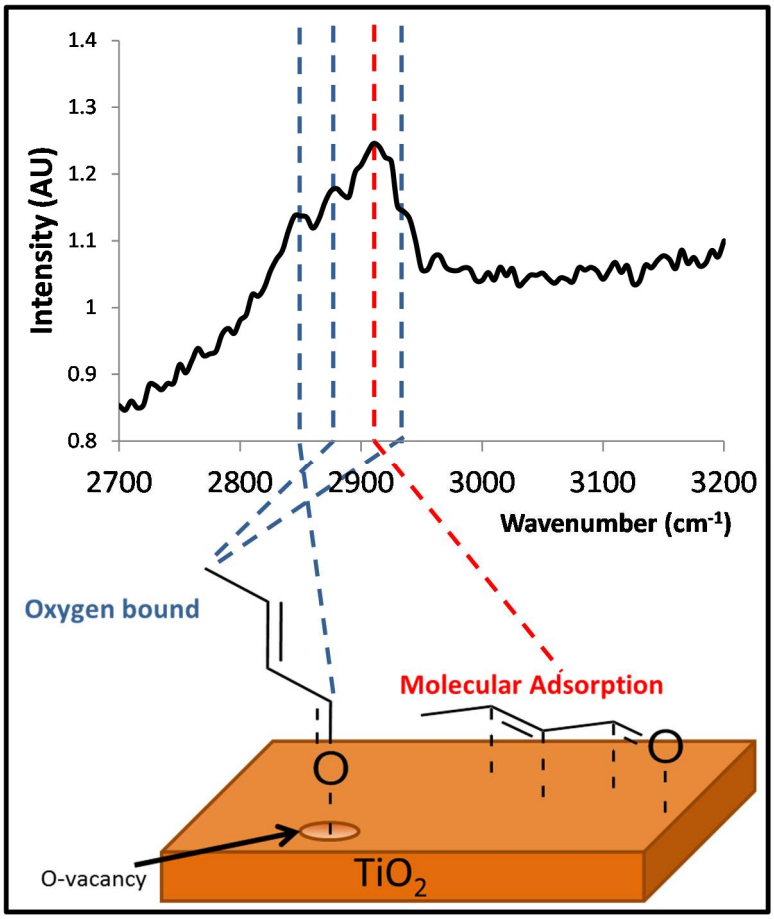

Figure 5.5 SFG spectrum for TiO_2 without Pt under reaction conditions of 1 Torr crotonaldehyde, 100 Torr hydrogen and 669 Torr argon at a catalyst temperature of 120°C.

The spectrum obtained from TiO_2 without Pt nanoparticles, Figure 5.5, shows three peaks at 2850, 2880 and 2910 cm^{-1} and a shoulder centered near 2930 cm^{-1}. These features are attributed to two distinct adsorption modes. The first, which accounts for the peak at 2910 cm^{-1}, is a molecular adsorption mode. In all spectra obtained from any substrate without Pt at temperatures ranging from 25°C to reaction temperature, 120°C, a stretch is observed at this frequency. Due to its presence at these various conditions we attribute it to a non-reactive molecular adsorption mode. The second adsorption mode present on the TiO_2 surface is a species that is bound to the surface only via the aldehyde O atom. This mode allows the crotonaldehyde to stand vertically on the surface and the additional three vibrational modes are indicative of this species. The stretches at 2880 and 2930 cm^{-1} are assigned to the CH_3 symmetric and asymmetric stretching modes, respectively, and the mode at 2850 cm^{-1} is assigned to the aldehyde CH stretch. The CH_3 group assignments closely match the crotonaldehyde gas phase spectrum in which the CH_3 symmetric stretch appears at 2880 cm^{-1} and the asymmetric stretch appears at 2938 cm^{-1}. The similarity between these stretches on the TiO_2 surface and those in the gas phase indicate limited interaction of the methyl group with the TiO_2 surface, as such interactions can shift the peaks by 20-40 cm^{-1}. The aldehyde CH stretch is shifted significantly from its gas phase frequency due to the strong interaction of the aldehyde group with the TiO_2 surface. It is clear from the spectrum that, in the absence of Pt, this oxygen bound species has not undergone any hydrogenation as indicated by the lack of any CH_2 stretching modes which would appear if either the C=C or the C=O double bonds were hydrogenated. We believed that this oxygen bound species is bound to TiO_2 at O-vacancy sites on the TiO_2 surface. It has been shown previously that aldehyde adsorption on TiO_2 is strongly favored at O-vacancies on the TiO_2 surface via the aldehyde O, and that this binding results in an electron transfer from a reduced Ti^{3+} cation at the O-vacancy site to the adsorbed molecule.

Comparison of the Pt/TiO_2 spectrum with the spectrum of TiO_2 alone, Figure 5.5, shows the aldehyde stretch disappears and a CH_2 stretch appears in the presence of Pt, indicating hydrogenation of the carbonyl C by H spillover from the Pt to the TiO_2. The result of this initial hydrogenation step is a crotyl-oxy surface intermediate, shown in Figure 5.4B, which is the precursor to the crotyl alcohol product.

As stated previously it is believed that the Ti^{3+} atoms at oxygen-vacancy sites bind strongly to the aldehyde oxygen and activate the aldehyde carbon for hydrogenation by a charge transfer process, drawing analogy to acid-base catalysis. The charge transfer process described previously[4] where in the excess electron at the Ti^{3+} site forms a covalent Ti-O bond with the aldehyde oxygen, results in a charge on the aldehyde carbon as the C=O bond becomes a C-O σ bond. This charged carbon is highly reactive and quickly reacts with the atomic hydrogen present on the surface. In the previous case of furfural the adsorption of the aldehyde group at this Ti^{3+} site resulted in an energy decrease of the system by 1.35 eV as determined by DFT calculations. Addition of the hydrogen at the carbonyl carbon lowered the energy of the system by an additional 0.2 eV. The adsorption and initial single hydrogen addition are believed to be very fast and result in a fairly stable surface species, which we observe by SFG. The subsequent hydrogen addition at the aldehyde O to form an O-H bond and adsorption of a new reactant molecule at

this site would likely provide the energy required to desorb the molecule as a product. In light of this and the reaction data previously presented, which clearly demonstrates that for the Pt/TiO_2 catalyst the change in selectivity is due to *additional* activity toward the alcohol products as compared to the Pt/SiO_2, we are confident that the SFG spectrum observed for Pt/TiO_2 is that of a reactive surface species.

5.4 Conclusions

It has been shown for crotonaldehyde hydrogenation that the support for Pt particles has a substantial impact on the selectivity and activity of a catalyst. Pt particles on SiO_2 show few, if any, differences in both their catalytic selectivity and observed surface intermediates when compared to Pt single crystals, confirming that SiO_2 plays no active role in the catalytic reaction. When Pt nanoparticles are supported on TiO_2, substantial changes in the catalytic activity and selectivity are observed along with accompanying changes to the SFG spectrum. The Pt/TiO_2 catalyst has nearly 4x the activity of the Pt/SiO_2 and is over 50% selective toward the alcohol products. SFG Vibrational Spectroscopy is utilized to probe the molecular species present on the surface of these catalysts under reaction conditions. The spectrum observed on Pt/SiO_2 is remarkably similar to that obtained on a Pt (111) single crystal under the same conditions and leads to the same assignment of a species which is an intermediate for the formation of butyraldehyde. Analysis of the SFG spectra for TiO_2 with Pt leads to the conclusion that crotonaldehyde binds to the TiO_2 surface through oxygen vacancy sites, activating the molecule for hydrogen addition at the aldehyde carbon. A crotyl-oxy species is observed on the TiO_2 surface, which is the intermediate for the formation of crotyl alcohol.

5.5 Experimental Methods

5.5.1 Catalyst Preparation

The catalyst samples used in this study, shown schematically in Figure 1, are two-dimensional model catalysts consisting of colloidally synthesized platinum nanoparticles deposited on thin film TiO_2 and SiO_2 supports. The as-synthesized platinum particles are encapsulated by polyvinylpyrrolidone (PVP) which prohibits contact between the platinum and the supporting oxide. Removal of this capping layer is necessary to bring the two materials into contact which in turn allows for interaction of the metal and oxide, shown to be essential for the this support effect to be observed.

The platinum nanoparticles were synthesized from PVP (MW: 29,000 Da) and chloroplatinic acid hexahydrate in ethylene glycol, yielding spherical particles of 4.6±2.8 nm diameter as determined by Transmission Electron Microscopy (TEM).

These synthesized particles were deposited on two supports, SiO_2 and TiO_2. The SiO_2 support was a Si (100) wafer with a 500nm thermally grown oxide layer. The TiO_2 support consisted of a 50nm TiO_2 thin film deposited by electron beam evaporation on the previously mentioned thermal oxide wafer. This film was subsequently annealed at 773 K in O_2 to ensure

proper stoichiometry. Analogous samples were prepared on transparent quartz discs for use in SFG spectroscopic studies. The quartz itself served as the SiO_2 support. A 50nm thin film of TiO_2 deposited by electron beam evaporation and subsequently annealed at 773 K in O_2 served as the TiO_2 support. In both cases SiO_2 samples were also prepared using an Electron Beam Evaporated thin film of SiO_2 and no differences were observed in catalytic or spectroscopic tests when compared to the thermal oxide wafer and quartz disc surfaces.

Platinum nanoparticles were deposited on all the above support materials by the Langmuir-Blodgett method. To summarize this method, a suspension of Pt nanoparticles in chloroform was dispersed on the water (18MΩ) surface of a Langmuir-Blodgett trough (Kibron MTX) and the chloroform allowed to evaporate. This sparse film is then compressed by motorized barriers while the surface pressure is monitored by a Pt/Ir alloy probe attached to a microbalance. The film is compressed to a packed monolayer at which point the submerged substrate is pulled from the water and the nanoparticle film transfers to it. All samples for this study were prepared at a surface pressure of 35 mN/m. Coverage of support by the Pt nanoparticles was approximately 40% as determined by TEM. Before deposition of nanoparticles all substrates were cleaned for one hour in Nochromix.

Immediately before reaction or spectroscopic studies, samples were exposed to UV light in air for 3 h in order to photodecompose the PVP capping layer and in turn activate the metal-support interaction between the Pt and TiO_2. Two low-pressure mercury (Hg) lamps (Lights Sources Inc., model number GPH357T5VH/4P) were used as the UV source; the Hg lamp emitted two lines: 184 and 254 nm. The two lamps were positioned parallel to each other 2.5 cm apart in a clean Al box. The sample was positioned 1.2 cm below the lamps. This cleaning is the combined effect of direct photodecomposition of the PVP as well as oxidation of the PVP by ozone produced by the 184 nm Hg line.

5.5.2 Measurement of Selectivity and Activity

Determination of reactivity and selectivity of the Pt/SiO_2 and Pt/TiO_2 catalysts was achieved using a stainless steel, batch mode catalytic reactor. A boron nitride substrate heater was used to heat the catalysts to the reaction temperature. Gas mixing was achieved through the use of a metal bellows recirculation pump. In all crotonaldehyde hydrogenation reactions 1 Torr of crotonaldehyde, 100 Torr of H_2 and 659 Torr of He were dosed into the reactor. Each sample was run for 8 hrs and the gas mixture was sampled at regular time intervals and the composition analyzed with a gas chromatograph equipped with a flame-ionization detector in order to monitor reaction progress. Hydrogenation reactions of the partial hydrogenation products, crotyl alcohol and butyraldehyde were also carried out using the same conditions. The total conversion of crotonaldehyde over the course of a reaction was kept below 15%.

In order to quantify the number of Pt sites on each catalyst, and thus calculate the turnover frequencies (TOF), ethylene hydrogenation was utilized. Ethylene hydrogenation has been shown to be insensitive to support material and type of platinum site. By measuring a reaction for a sample and dividing it by a known turnover frequency it is possible to determine the number of platinum active sites on a catalyst. The reaction rates for crotonaldehyde

hydrogenation were normalized using the number of metal active sites to give a turnover frequency for each catalyst. The total number of Pt sites per cm^2 of catalyst ranged from $0.8x10^{15}$ to $1.1x10^{15}$ and catalysts of approximately 1.5 cm^2 were used. Coverage of the substrate area by platinum particles for all samples was approximately 40% as determined by TEM.

Reaction rates toward each product of crotonaldehyde hydrogenation were determined by a fit of the peak area versus time, these rates, divided by the number of active sites, give a TOF toward each product. The total TOF of a catalyst was defined as the sum of the TOFs for each product. Selectivity toward a given product was determined by dividing the TOF for that product by the total TOF for all products.

5.5.3 Sum-Frequency Generation Vibrational Spectroscopy

Sum-Frequency Generation Spectroscopy probes the second order non-linear susceptibility tensor $\chi^{(2)}$. The $\chi^{(2)}$ tensor is zero for centrosymmetric media, so processes which probe $\chi^{(2)}$ are selective to interfaces or surfaces, where inversion symmetry is broken. Thus SFG vibrational spectroscopy is well suited to obtain vibrational information from molecules adsorbed on a surface. In this study SFG was used to obtain spectra of the reaction intermediates on Pt/SiO_2 and Pt/TiO_2 catalysts under the same conditions used for the catalytic reaction studies.

For the SFG experiments an active/passive mode-locked Nd:YAG laser (Continuum Leopard D-20) was used to give 20 ps pulses of 1064 nm light at a repetition rate of 20 Hz. The fundamental 1064 nm output was passed through an optical parametric generator/amplifier to give a second harmonic visible beam (VIS) of 532 nm and a tunable infrared beam (IR) tunable from 2700 – 3600 cm^{-1}. The IR and VIS beams, each with 100 µJ per pulse, were overlapped spatially and temporally on the surface of the catalyst surface deposited on a quartz window as described above. This window was pressed against a prism in order to direct the beams to the sample surface. An index matching gel was used to minimize reflection at the quartz-quartz interface. The sum-frequency signal generated on the sample was then collected and measured by a photomultiplier tube. A gated integrator was used to improve signal to noise. Spectra were collected by scanning the IR frequency across the range of interest. All spectra were collected in the ppp polarization.

The sample mount used for SFG experiments allows for exposure of the sample surface to a recirculating gas mixture and allows for the sample temperature to be controlled between RT and >350 °C. All reported spectra were recorded while the sample surface was exposed to the same mixture of reactant gases as was used in the catalytic test at a catalyst temperature of 120 °C.

5.6 References

(1) A. Hervier, L. R. Baker, K. Komvopoulos, G. A. Somorjai, *J. Phys. Chem.C* **2011**, *115*, 22960–22964.

(2) L. R. Baker, A. Hervier, H. Seo, G. Kennedy, K. Komvopoulos, G. A. Somorjai, *J. Phys.Chem. C* **2011**, *115*, 16006–16011.

(3) M. A. Vannice, *Top. Catal.* **1997**, *4*, 241–248.

(4) L. R. Baker, G. Kennedy, M. van Spronsen, A. Hervier, X. Cai, S. Chen, L.-W. Wang, G. A. Somorjai, *J. Am. Chem. Soc.* **2012**, *134*, 14208–14216.

(5) M. Englisch, A. Jentys, J. A. Lercher, *J. Catal.* **1997**, *166*, 25 – 35.

(6) S. D. Lin, D. K. Sanders, M. A. Vannice, *Appl. Catal., A* **1994**, *113*, 59 – 73.

(7) A. Boffa, C. Lin, A. T. Bell, G. A. Somorjai, *J. Catal.* **1994**, *149*, 149–158.

(8) Y. Yamada, C.-K. Tsung, W. Huang, Z. Huo, S. E. Habas, T. Soejima, C. E. Aliaga, G. A. Somorjai, P. Yang, *Nat. Chem.* **2011**, *3*, 372–376.

(9) J. G. Santiesteban, D. C. Calabro, W. S. Borghard, C. D. Chang, J. C. Vartuli, Y. P. Tsao, M. A. Natal-Santiago, R. D. Bastian, *J. Catal.* **1999**, *183*, 314 – 322.

(10) W. C. Conner, J. L. Falconer, *Chem. Rev.* **1995**, *95*, 759–788.

(11) E. V. Benvenutti, L. Franken, C. C. Moro, C. U. Davanzo, *Langmuir* **1999**, *15*, 1–7.

(12) B. J. Morgan, G. W. Watson, *J. Phys. Chem. C* **2009**, *113*, 7322–7328.

(13) A. Boffa, C. Lin, A. Bell, G. Somorjai, *Catal. Lett.* **1994**, *27*, 243–249.

(14) W. P. Jencks, *Acc. Chem. Res.* **1980**, *13*, 161–169.

(15) J. Greeley, J. K. Nørskov, M. Mavrikakis, *Annu. Rev. Phys. Chem.* **2002**, *53*, 319–348.

(16) A. Dandekar, M. A. Vannice, *J. Catal.* **1999**, *183*, 344–354.

(17) C. G. Raab, J. A. Lercher, *J. Mol. Catal.* **1992**, *75*, 71–79.

(18) M. Abid, V. Paul-Boncour, R. Touroude, *Appl. Catal., A* **2006**, *297*, 48–59.

(19) C. J. Kliewer, M. Bieri, G. A. Somorjai, *J. Am. Chem. Soc.* **2009**, *131*, 9958–9966.

(20) P. Mäki-Arvela, J. Hájek, T. Salmi, D. Y. Murzin, *Appl. Catal., A* **2005**, *292*, 1 – 49.

(21) K. M. Bratlie, L. D. Flores, G. A. Somorjai, A. L. Flores, L. Flores, L. Flores, *J. Phys.Chem. B* **2006**, *110*, 10051–10057.

(22) C. J. Kliewer, M. Bieri, G. A. Somorjai, *J. Phys. Chem. C* **2008**, *112*, 11373–11378.

(23) C. J. Kliewer, C. Aliaga, M. Bieri, W. Huang, C.-K. Tsung, J. B. Wood, K. Komvopoulos, G. A. Somorjai, *J. Am. Chem. Soc.* **2010**, *132*, 13088–13095.

(24) J. Haubrich, D. Loffreda, F. Delbecq, P. Sautet, A. Krupski, C. Becker, K. Wandelt, *J. Phys.Chem. C* **2009**, *113*, 13947–13967.

(25) H. Seo, L. R. Baker, A. Hervier, J. Kim, J. L. Whitten, G. A. Somorjai, *Nano Lett.* **2011**, *11*, 751–756.

(26) A. Jayaprakash, V. Arjunan, S. P. Jose, S. Mohan, *Spectrochim. Acta, Part A* **2011**, *83*, 411–419.

(27) B. Silvi, J. P. Perchard, *Spectrochim. Acta, Part A* **1976**, *32*, 11–22.

Chapter 6

In Situ Spectroscopic Investigation into the Active Sites for Crotonaldehyde Hydrogenation at the Pt Nanoparticle Co_3O_4 Interface

6.1 Abstract

The hydrogenation of crotonaldehyde by platinum nanoparticles supported on cobalt oxide was used as a reaction to probe the effect of the interface between the two materials on the activity and selectivity of the catalyst. Four potential products can be formed by this reaction, propylene, butyraldehyde, crotyl alcohol and butanol. When Pt nanoparticles are supported on SiO_2, an inert support, only propylene and butyraldehyde are formed. However, when Pt is supported on cobalt oxide the alcohols make up roughly 40% of the total activity, indicating cobalt oxide plays a pivotal role in the reaction, much like other active supports such as TiO_2. To elucidate the mechanism of alcohol formation *in-situ* Sum Frequency Generation Vibrational Spectroscopy (SFG) and Ambient Pressure X-Ray Photoelectron Spectroscopy (AP-XPS) were utilized to probe the reactant adsorption and intermediate formation, and the chemical state of the materials under working catalytic conditions. The SFG data indicates that crotonaldehyde adsorbs on the oxide surface, likely through the aldehyde oxygen as well as on the Pt surface through the alkene group. AP-XPS results show that the surface of the Co_3O_4 support becomes partially reduced under the reaction conditions and Pt exists in its metallic state. Taking these results together it is proposed that the crotonaldehyde adsorbs at reduced oxide surface sites and that this adsorption mode is responsible for the production of alcohol products. A platinum nanoparticle density dependence study was also undertaken to change abundance of interface sites and study their effect on the reaction. The selectivity between the two alcohol products was altered as a function of the Pt nanoparticle density, higher selectivity toward butanol and lower toward crotyl alcohol with increasing density, while propylene and butyraldehyde selectivities were constant with respect to density. Based upon the data presented it is proposed that butanol is preferentially formed at the metal-oxide interface, while crotyl alcohol is formed at oxide surface sites by reaction with spillover hydrogen.

6.2 Introduction

Modification and control of catalytic properties by a seemingly inert support has been a focus of catalytic research for decades.[1,2] A number of studies have shown that by changing the support one can change the activity and selectivity of a number of catalytic reactions including, but not limited to, alkane reforming[3], hydrogenation of organic molecules,[4,5] oxidation of carbon monoxide,[6] and oxidation of methanol[7]. In most of these cases, the oxide support does little to no chemistry on its own but when combined with the active metal the result is dramatically different from the metal alone. Several explanations have been offered in the literature[8] to explain these effects depending on the reaction and materials at hand but few can be generalized to many reactions or material systems. The aim of this work is to establish a general mechanism for the selective hydrogenation of aldehyde groups by Pt supported on reducible metal oxides. In the previous chapter the role of titanium dioxide as a support was studied and here that work is expanded to cobalt oxide (Co_3O_4).

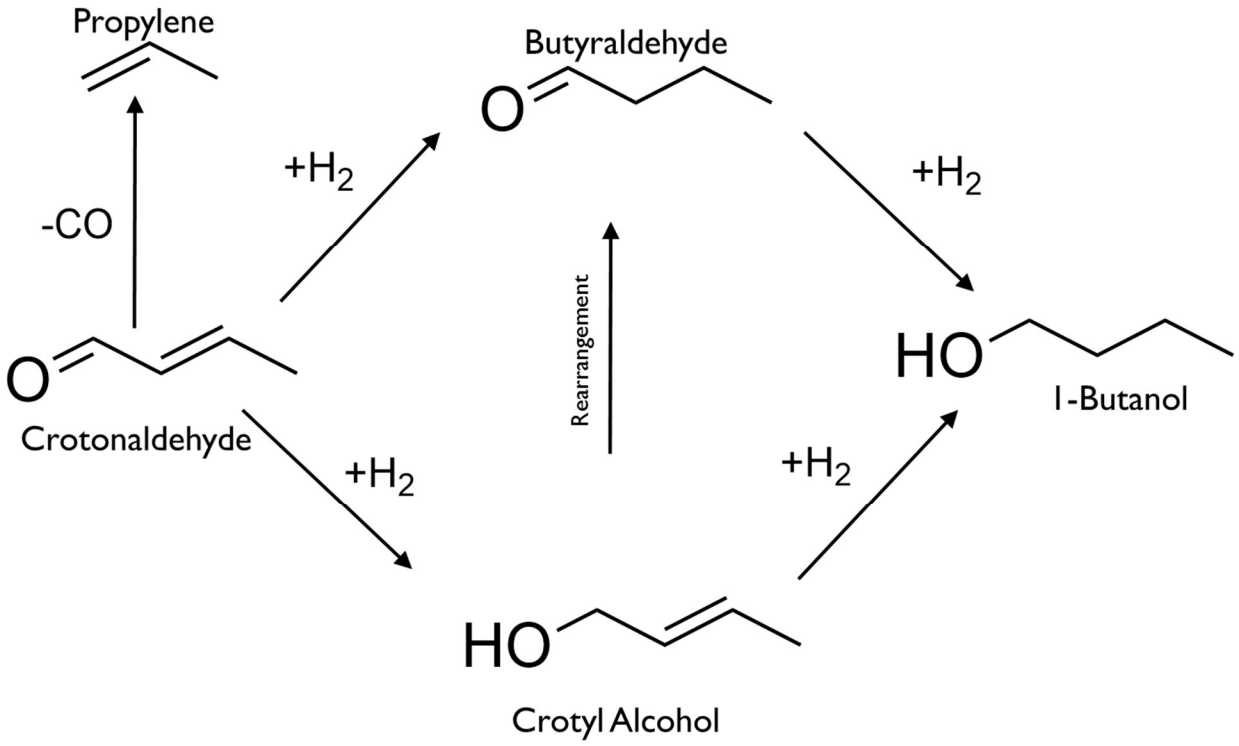

Scheme 6.1 Possible reaction pathways for the hydrogenation of crotonaldehyde

Crotonaldehyde hydrogenation is chosen here as a probe reaction as it allows for clear distinction between reaction pathways that have been shown to be sensitive to metal nanoparticle size[9] as well as support material. [10,11] As seen in Scheme 6.1 crotonaldehyde can hydrogenate into three

products, butyraldehyde, crotyl alcohol, and butanol, or decarbonylate to make propylene. The most desired product of this reaction is crotyl alcohol as it, and other unsaturated alcohols, are valuable intermediates in the production of value added fine chemicals and fragrances. As has been documented previously platinum single crystal surfaces[12] or platinum nanoparticles supported on SiO_2[5] produce primarily propylene and butyraldehyde under the conditions used in this work. Through interaction with the support, in this case cobalt oxide, the aldehyde group can be activated and alcohols are formed. This type of interaction has been documented previously for TiO_2[5,10,13] as the support but some questions remain about the exact nature of the active site and the state of the active materials. Chief among these questions is the location of the active site for alcohol production. Three distinct possibilities exist: (1) alcohols are formed on the Pt surface which has been altered by an electronic interaction with the support, (2) alcohols are formed at the interface between platinum and the oxide, or (3) alcohols are formed on the oxide surface with atomic hydrogen that spills over from the metal surface following dissociation.

This work proposes a direct adsorption of the reactant, crotonaldehyde, on the oxide surface, which is not active on its own. The crotonaldehyde adsorbed on cobalt oxide can then react with spillover hydrogen from the platinum or additionally interact directly with the platinum surface at the interface through the carbon-carbon double bond. These two possibilities would in theory responsible for the crotyl alcohol and butanol products respectively. To arrive at this proposal, a study was undertaken that allows one to vary the concentration of platinum nanoparticles on a flat cobalt oxide thin film substrate which in turn changes the relative abundance of interface versus oxide sites. The catalytic results show a clear dependence of the selectivities toward the two alcohols as a function of Pt NP density, as the density increases, thus more interface and fewer oxide sites, butanol formed more selectively at the expense of crotyl alcohol. This catalyst preparation also allows for study by Sum Frequency Generation Vibrational Spectroscopy (SFG) and Ambient Pressure X-Ray Photoelectron Spectroscopy (AP-XPS) experiments to be conducted. The development and use of *in-situ* characterization techniques for catalysis and surface chemistry application has been a focus of research for the last two decades[14] and here two techniques are utilized that yield a fairly complete picture of the surface of our catalyst under reaction conditions. Using SFG one can study how the molecules adsorb on the surface of the metal and oxide, independent of one another and in combination, and correlate these surface intermediate species to the reaction performance. It is found that the crotonaldehyde adsorbs strongly on the cobalt oxide surface under reaction conditions, likely through the aldehyde oxygen. With AP-XPS one can determine the composition and state of the catalyst surface under reactive conditions. Using this technique it was found that the Pt surface is fully reduced to its metallic state and the Co_3O_4 surface has been partially reduced, likely to Co(II), under the reaction conditions. By using a well controlled catalyst preparation and these spectroscopic techniques a full picture of the working catalyst is obtained.

6.3 Results and Discussion

6.3.1 Catalytic Results

Figure 6.1 shows a comparison of the activity toward each of the four observed products for Pt on Co_3O_4 and previously reported data for Pt on SiO_2 and TiO_2.[5] As seen in the figure Pt on SiO_2 produces exclusively butyraldehyde and propylene at 120°C, results which closely mirror those from Pt single crystal reaction studies.[12] This indicates that SiO_2 plays no active role in the reaction. In contrast, both the Pt supported on TiO_2 and Co_3O_4 show dramatic increases in total activity as compared to the Pt/SiO_2 and for both a large part of that added activity is toward the alcohol products, which are not observed on Pt/SiO_2. The dramatic increase in activity, 3-4x increase for Pt/TiO_2 and 8x increase for Pt/Co_3O_4, indicates that there are additional sites available for reaction on the cobalt and titanium oxide supported catalysts and that these sites are active primarily for the formation of alcohols. The increased butyraldehyde formation on the Pt/Co_3O_4 and Pt/TiO_2 can be explained by the fact that a platinum mediated rearrangement pathway exists for the conversion of crotyl alcohol to butyraldehyde. This rearrangement path was observed previously[5] and was shown to be independent of the oxide. It is possible that this rearrangement could occur through the readsorption of previously formed crotyl alcohol molecules from the gas phase or by the migration and subsequent rearrangement of surface intermediates. However it cannot be stated conclusively which is the case from this work since butyraldehyde is produced by a direct process as well as this indirect one.

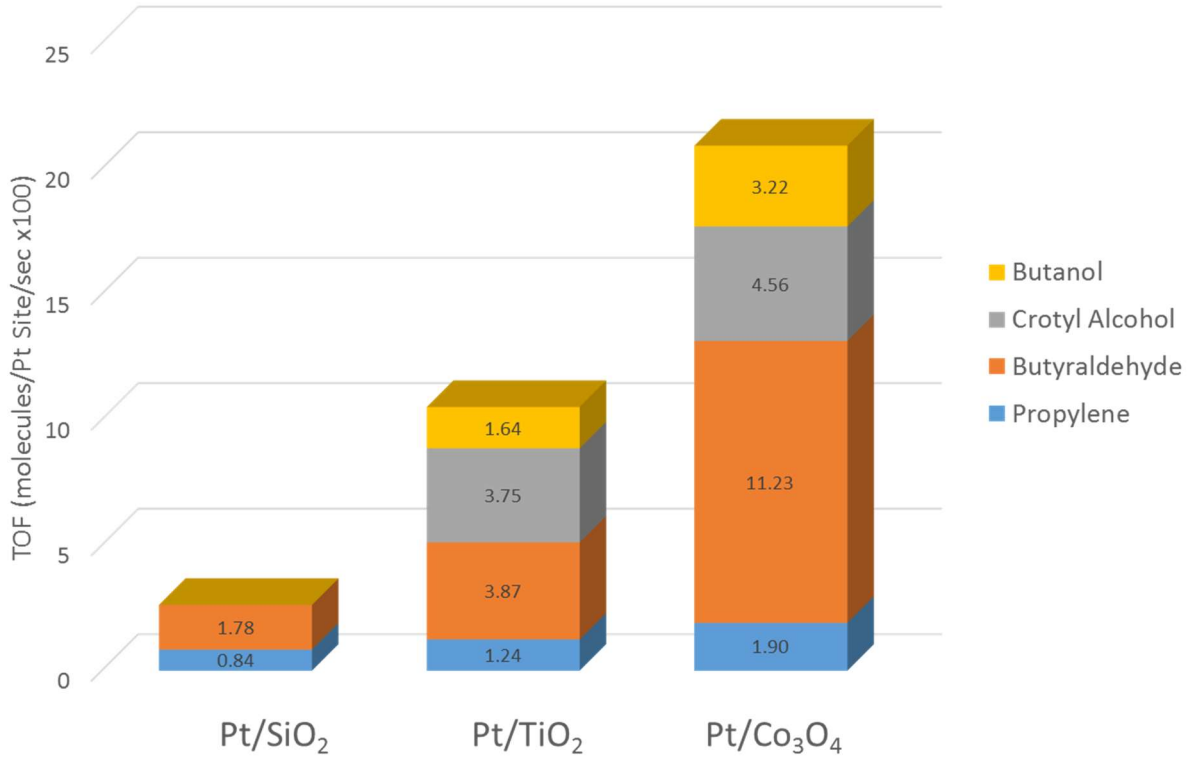

Figure 6.1 A comparison of the activity toward each product for crotonaldehyde hydrogenation on Pt supported on SiO_2, TiO_2, and Co_3O_4. SiO_2 plays no role in the catalytic

reaction and thus this point represents the activity of the Pt alone. Cobalt and titanium oxide both influence the reaction greatly by increasing the total activity and opening new reaction pathways toward the alcohol products. In all cases the the Pt films were prepared with a roughly 27% coverage of the oxide surface, deposited at a surface pressure of 30mN/m by the Langmuir-Blodgett method.

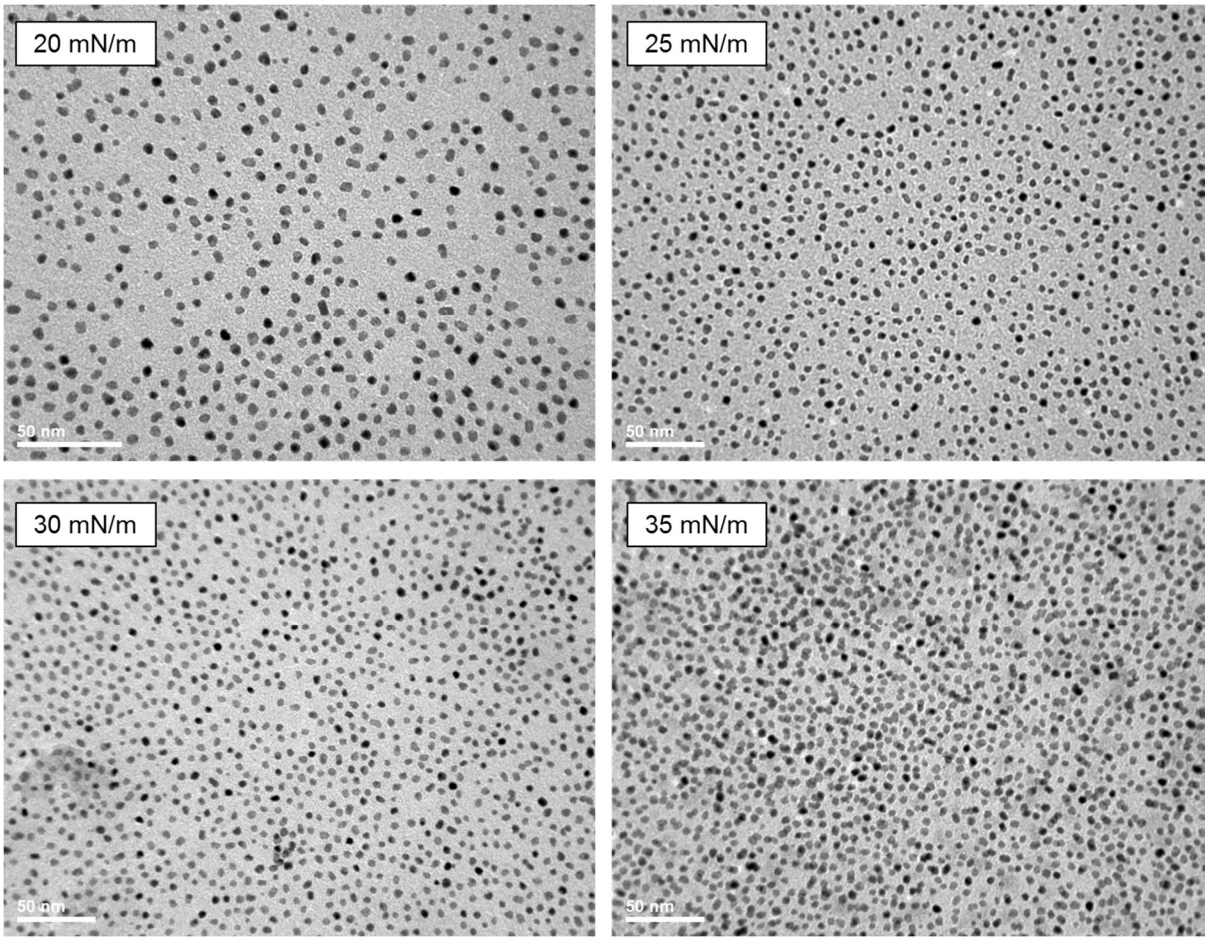

Figure 6.2 Transmission Electron Microscopy Images obtained for each of the four density nanoparticle films studied for crotonaldehyde hydrogenation. The average particle diameter was determined to be 4.6±0.4 nm. From these and twelve other images the percent coverage of the substrate by the nanoparticles was determined to be 17, 21, 27, and 32% for the Langmuir Blodgett surfaces pressures of 20, 25, 30, and 35 mN/m respectively.

In order to elucidate the role of each component, platinum and cobalt oxide, and the interface between the two, a study was subsequently undertaken in which the density of the platinum nanoparticle films was systematically varied. Catalysts were prepared with Langmuir-Blodgett films of platinum nanoparticles with surface pressures of 20, 25, 30, and 35 mN/m which yielded coverages of the substrate between 17-32% as determined by transmission electron microscopy, and summarized in figure 6.2. A trend can be observed in the selectivity between the two alcohol

products, crotyl alcohol and butanol as shown in figure 6.3. As the density of the particle film is increased, a decrease in the crotyl alcohol selectivity, and an increase in the butanol selectivity is observed. Across this range of particle densities the selectivity toward the other main product, butyraldhyde, increases slightly as well. This can be explained by the increase in Pt sites relative to oxide/interface sites as the density is increased. As described previously[5] it is believed that butanol is produced by a concerted hydrogenation of both double bonds rather than by the sequential hydrogenation of one group, followed by desorption/readsorption and the hydrogenation of the other. Additionally, in the case of platinum supported on TiO_2 it was proposed that hydrogenation of the aldehyde group was achieved through adsorption of the aldehyde oxygen on the oxide surface and hydrogenation by hydrogen spilling over from the platinum. We hold these ideas to be true for the case of cobalt oxide as well and propose that butanol production likely occurs very close to the Pt/Co_3O_4 interface, where the aldehyde group can interact with the oxide and the alkene group can interact with the Pt metal surface thus both bonds would be hydrogenated before desorption. It is proposed the crotyl alcohol is likely produced by adsorption of the aldehyde group on the surface of the oxide with platinum providing spillover hydrogen to reduce the aldehyde to an alcohol. With these proposed mechanisms sense can be made of the density dependent selectivity. As the density of platinum increases the amount of exposed oxide surface decreases, and the amount of interface sites increases. A larger number of interface sites is correlated with a higher activity toward butanol and a decrease in exposed oxide surface to a decrease in crotyl alcohol production. This implies there are at least three unique types of reaction sites on a Pt/Co_3O_4 catalyst, metal sites, oxide sites and interface sites, each of which can be correlated to a different reaction product.

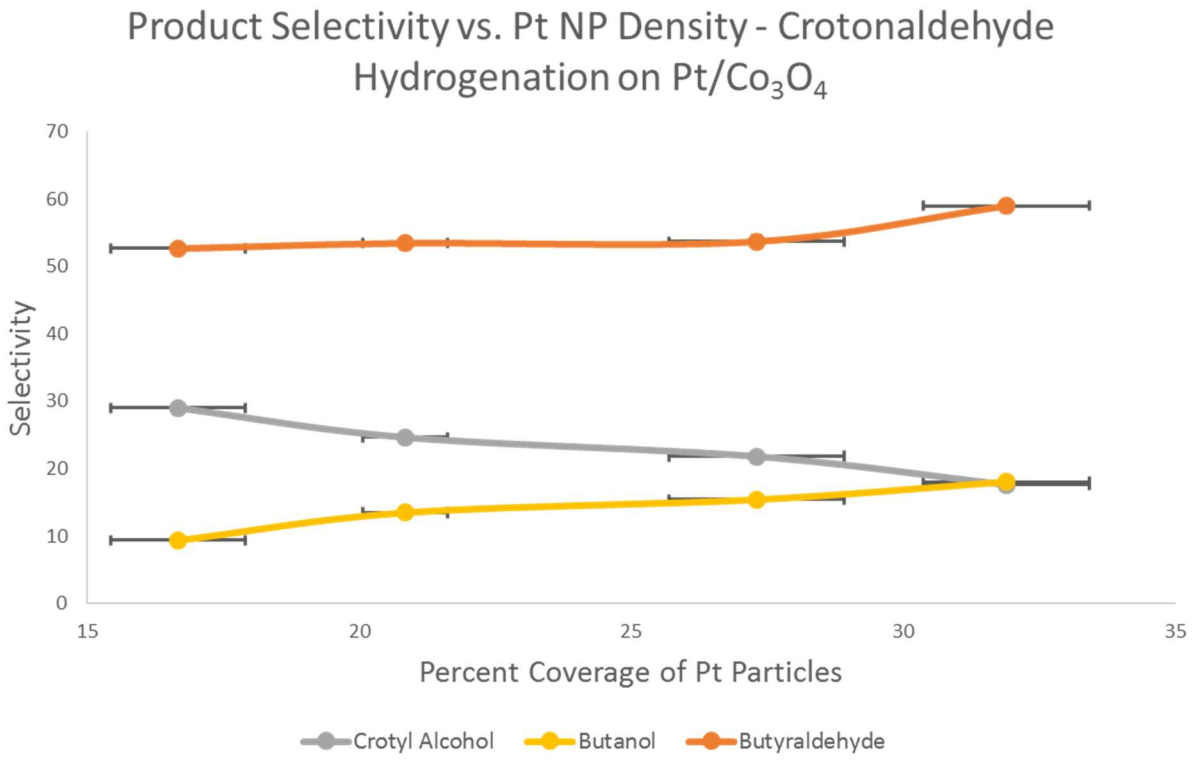

Figure 6.3 Selectivity toward the two alcohol products and butyraldehyde as a function of the Pt nanoparticle coverage on the cobalt oxide film. Here opposing trends for the crotyl alcohol and butanol are observed. As NP density is increased the selectivity toward butanol increases at the expense of the crotyl alcohol. Error bars represent the standard deviation obtained by quantifying multiple TEM images from different areas of the same sample.

6.3.2 Sum Frequency Generation Vibrational Spectroscopy

Sum Frequency Generation Vibrational Spectroscopy, an *in-situ* surface specific technique, is utilized here to understand how the reactant molecules interact with the catalyst surface under working catalytic conditions and correlate these interactions with the reaction results. Spectroscopic studies were done on cobalt oxide films with and without platinum nanoparticle films. This allowed us to decouple the support and metal signals to an extent and determine the extent to which the oxide alone interacts with the reactants. Figure 6.4 shows SFG spectra for cobalt oxide without Pt and Pt/Co_3O_4 under crotonaldehyde hydrogenation conditions at 120°C. In the case of the oxide without platinum three peaks at 2875 cm^{-1}, 2940 cm^{-1}, and 2970 cm^{-1} are assigned as the symmetric, asymmetric and Fermi resonance peaks of the CH_3 group. These peak positions are largely unchanged relative to the gas phase[15] peaks implying that there is no substantial interaction between the CH_3 group and the surface, as such interaction would cause a shift in position. Furthermore, the spectral features are assigned to these stretches since it is not expected for the molecule to have undergone any degree of hydrogenation on the Co_3O_4 surface without Pt as there would be no source of atomic hydrogen, thus no CH_2 stretches should be observed.

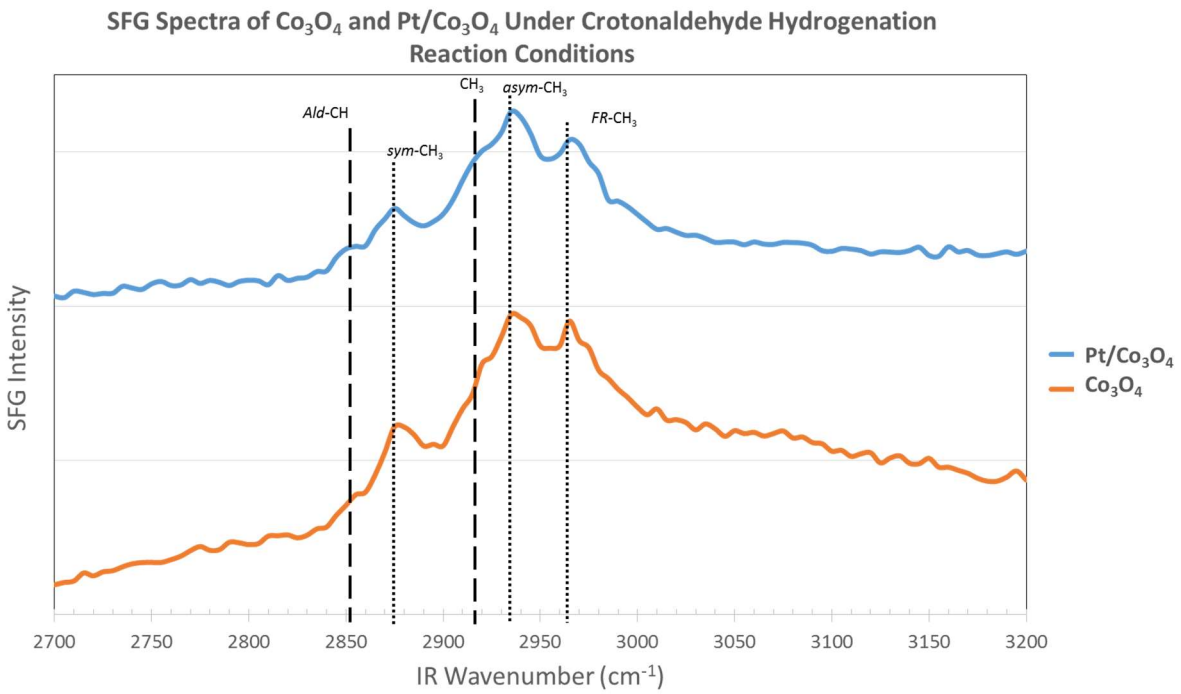

Figure 6.4 Sum Frequency Generation Vibrational Spectra of cobalt oxide with and without Pt nanoparticles under reaction conditions (1 Torr Crotonaldehyde 100 Torr H_2, 670 Torr He, 120°C). The Pt film was deposited by the Langmuir Blodgett method with a surface pressure of 30mN/m resulting in roughly 27% coverage of the support by Pt. The three features marked with the fine dotted line are assigned to a species adsorbed on the oxide surface via the aldehyde group. The two features marked with the heavier dotted line are assigned to crotonaldehyde adsorbed on Pt as a precursor to butyraldehyde.

Adsorption and reaction of crotonaldehyde and hydrogen on platinum single crystals has been previously reported by Kliewer et. al.[12] and the spectral assignments presented there have been shown to correlate well with the results for Pt nanoparticles on SiO_2[5]. These results allowed us to assign two features observed in the Pt/Co_3O_4 spectrum at 2850cm^{-1} and 2920cm^{-1}, to CH and CH_3(s) stretches of a crotonaldehyde molecule adsorbed on the Pt surface through the carbon-carbon double bond. This intermediate is believed to be the precursor to the formation of butyraldehyde, the major product for the Pt/SiO_2 catalyst and Pt single crystal surface. It may appear that these features are present in the Co_3O_4 spectra as well but they are quite close to the noise level of the spectrum and are clearly more intense in the Pt/Co_3O_4 spectrum. In the Pt/Co_3O_4 spectrum there are five identified features in total, three belonging to crotonaldehyde adsorbed on the oxide surface and two belonging to crotonaldehyde adsorbed on the platinum surface. However this spectrum is dominated by the features assigned to the Co_3O_4 surface with Pt adsorbed species giving rather small contributions comparatively. This would suggest the cobalt oxide surface has an abundance of sites available for adsorption of the crotonaldehyde. From this it can concluded that the cobalt oxide surface, while not active for the reaction on its

own, can play a key role in controlling how the molecules interacts with the catalyst surface and can provide additional reaction pathways that are not available to the Pt nanoparticles supported on inert supports. This is further supported by the fact that not only is the Pt/Co_3O_4 more selective toward the alcohol products, it is also far more active than the Pt/SiO_2 catalyst.

6.3.3 Ambient Pressure X-Ray Photoelectron and X-Ray Absorption Spectroscopies

Ambient Pressure X-Ray Photoelectron Spectroscopy (AP-XPS) was employed to determine the oxidation state of the platinum and cobalt constituents at various stages of pretreatment and under reaction conditions. These experiments were performed using catalysts prepared using the same methods as the catalytic and SFG studies but using a doped Si wafer to minimize the effect of charging. The samples were treated with UV irradiation for three hours prior to being loaded into the XPS chamber. The results, summarized in figure 6.5, show that immediately following UV treatment the surface of the platinum nanoparticles is substantially oxidized according to the fit of the Pt 4f edge. This is to be expected as the UV lines used are known to produce ozone, which readily oxidizes and removes the organic capping agent, as well as the Pt surface. At room temperature hydrogen was introduced into the sample chamber following the vacuum spectra and the sample was then incrementally heated, taking spectra at various temperatures up to 240°C. At room temperature in hydrogen the platinum surface remains predominantly oxidized. When heated to the reaction temperature of 120°C in hydrogen the platinum became fully reduced to the metallic state and remained metallic as the temperature was increased further.

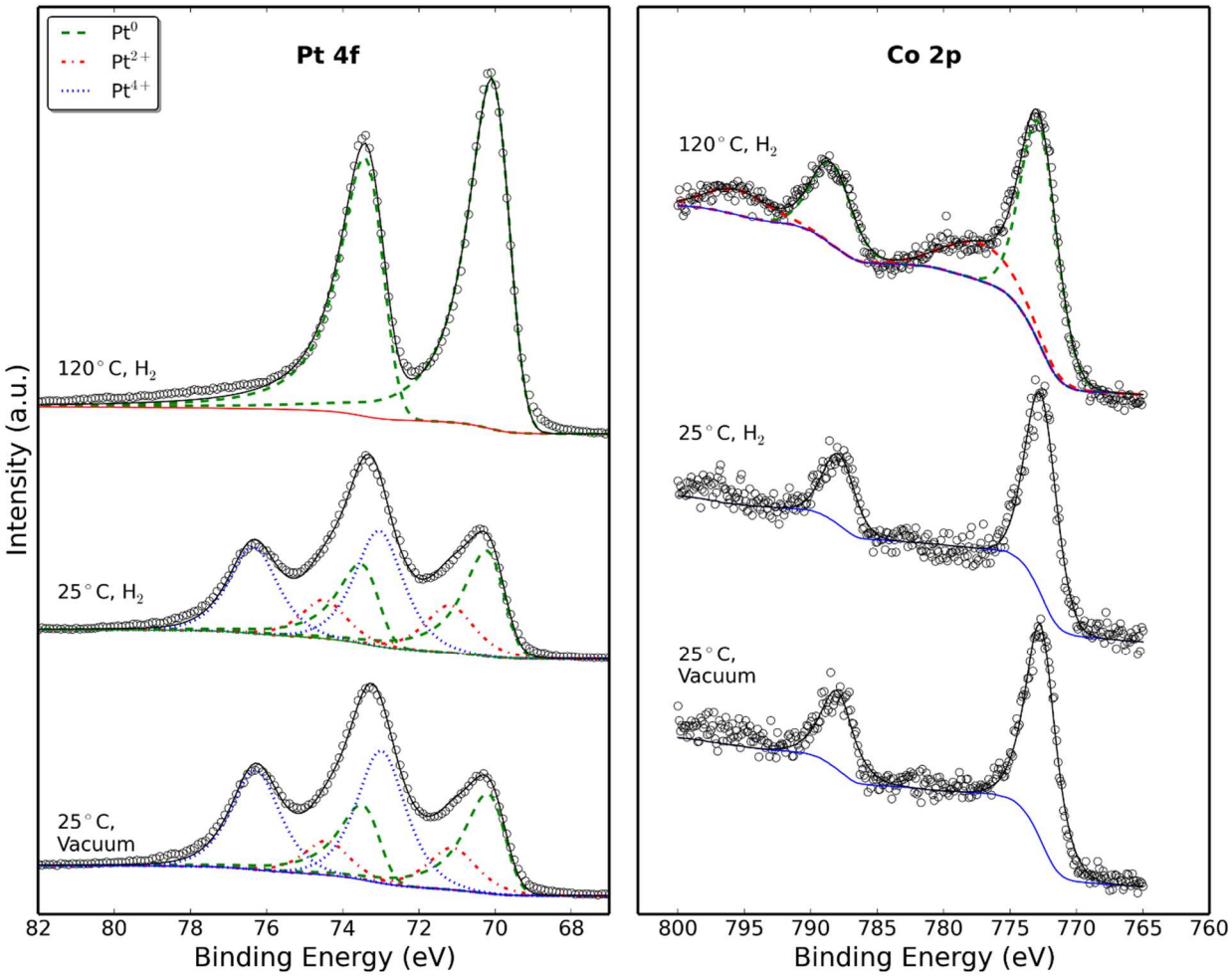

Figure 6.5 Ambient Pressure X-Ray Photoelectron Spectra of the Pt 4f and Co 2p edges. Figure on the left shows the Pt 4f edge under three conditions. Immediately following the UV treatment the Pt is partially oxidized. When exposed to hydrogen at room temperature the Pt remains oxidized however once heated to the reaction temperature of 120C the Pt is fully metallic. Cobalt 2p spectra on the left show changes in the cobalt oxidation state at reaction temperature and in hydrogen versus immediately after UV treatment and hydrogen at room temperature. The appearance of satellites in the 120C in H_2 spectrum indicates the surface of the Co_3O_4 support is partially reduced. The reduced surface is what is exposed during reaction and likely has a role in the increased activity and selectivity.

In figure 6.5 the Cobalt 2p edge is shown for two conditions, vacuum at 25°C immediately after UV treatment and under hydrogen at 120°C for a Pt/Co_3O_4 catalyst. The major change here is the appearance of the satellite peaks near the oxide features under hydrogen. These satellites are indicative of CoO while the as-prepared film is in the Co_3O_4 state. This is evidence that the oxide surface undergoes reduction under the reaction conditions. Considering this reduction occurs far below the bulk reduction temperature of cobalt oxide it is likely due to the presence of atomic hydrogen spilling over from the Pt surface. Experiments were undertaken using *in-situ* X-Ray

Absorption Spectroscopy in the fluorescence mode to measure the bulk cobalt oxide structure. The results, figure 6.6, show that at 120°C the bulk of the material remains in the spinel Co_3O_4 state, indicating that the reduction observed by AP-XPS is a surface effect. This is additional evidence that the oxide support can be active through a mechanism involving hydrogen spillover. Hydrogen spillover mechanisms have been shown previously, for example, in the case of carbon dioxide reduction.[16]

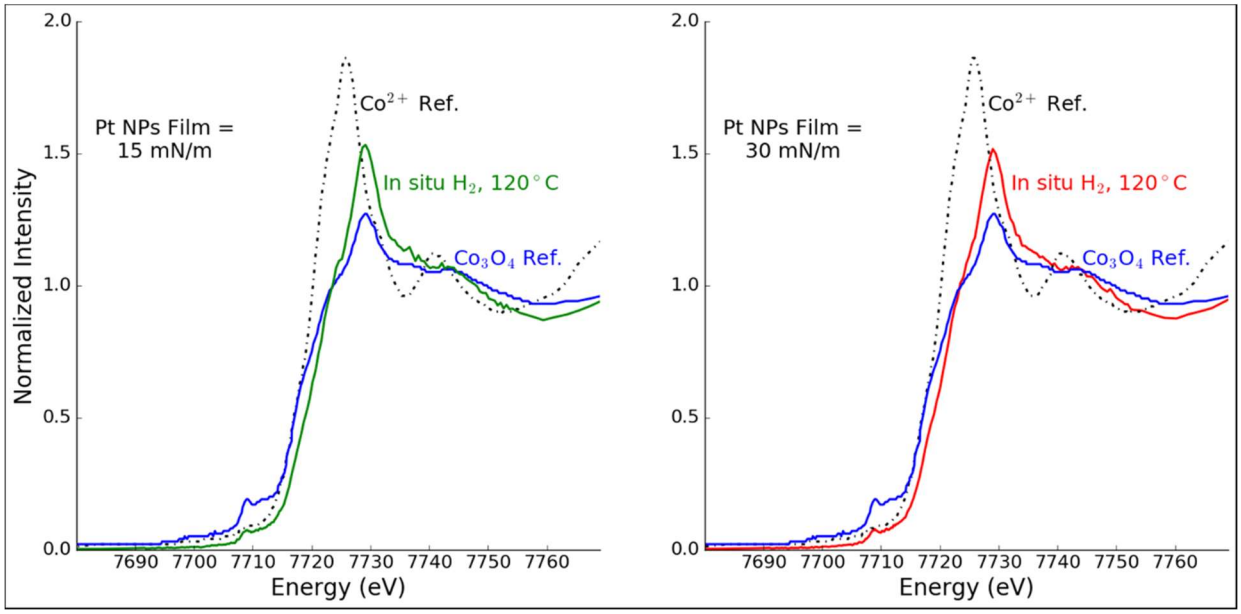

Figure 6.6 Near-Edge X-Ray Absorption Fine Structure spectra for the cobalt K-edge for Pt nanoparticles of two film densities supported on cobalt oxide under reactive gas conditions in the fluorescence mode. The in-situ spectra were taken at a catalyst temperature of 120°C under a flow of hydrogen. This was done to mimic the reducing reaction gas mixture for crotonaldehyde hydrogenation. The in-situ spectra show features closely resembling those of the spinel Co_3O_4 reference spectrum, specifically the pre-edge feature and the position of the white line, and are substantially different from the CoO reference spectrum. This goes to show that while the surface of the cobalt oxide is reduced to Co^{2+}, as shown by AP-XPS measurements, the bulk of the film remains predominantly in the Co_3O_4 structure.

6.4 Conclusions

In summary it has been established that Pt nanoparticles supported on Co_3O_4 give a dramatically enhanced activity and altered selectivity for crotonaldehyde hydrogenation when compared to Pt supported on SiO_2. The cobalt oxide support behaves similarly to another active support, TiO_2, for this reaction, generating a large amount of the alcohol products. To understand the mechanism of the reaction *in-situ* Sum Frequency Generation Vibrational Spectroscopy and Ambient Pressure X-Ray Photoelectron Spectroscopy were employed. The SFG results suggest that two species exist on the Pt/Co_3O_4 surface, a Pt bound precursor to butyraldehyde, and a

Co_3O_4 bound precursor to the alcohols. The results obtained by AP-XPS show that under reaction relevant conditions, 120°C and 100mTorr H_2, the Pt particles are fully reduced to the metallic state and the cobalt oxide surface is partially reduced, likely to Co^{2+}. This reduction of the oxide occurs at a significantly lower temperature than would be expected for the bulk oxide and suggests atomic hydrogen spills over onto the oxide to allow for this low temperature reduction. This reduced surface contains sites for the adsorption and reaction of crotonaldehyde selectively to the alcohol products. By varying the density of the Pt nanoparticle film on the cobalt oxide support for reaction studies a trend was observed in the selectivity between the two alcohol products, crotyl alcohol and butanol. As the density of the film increased the butanol selectivity increased and the crotyl alcohol selectivity decreased. To explain this result a mechanism is proposed where butanol is formed at the interface between the Pt and Co_3O_4 such that the aldehyde group can interact with the oxide and the alkene group can interact with the Pt metal. It is thus believed that crotyl alcohol is formed by adsorption at an oxide site through the aldehyde group, sufficiently far away from the Pt particle as to prevent interaction of the alkene with the metal. Crotyl alcohol is then formed by reaction with hydrogen spilling over from the Pt surface. These mechanisms are summarized in scheme 1. These proposed mechanisms are in line with previous work on Pt/TiO_2[4,5] and as such this is believed to be a general mechanism for activation of aldehyde groups by reducible oxide supports.

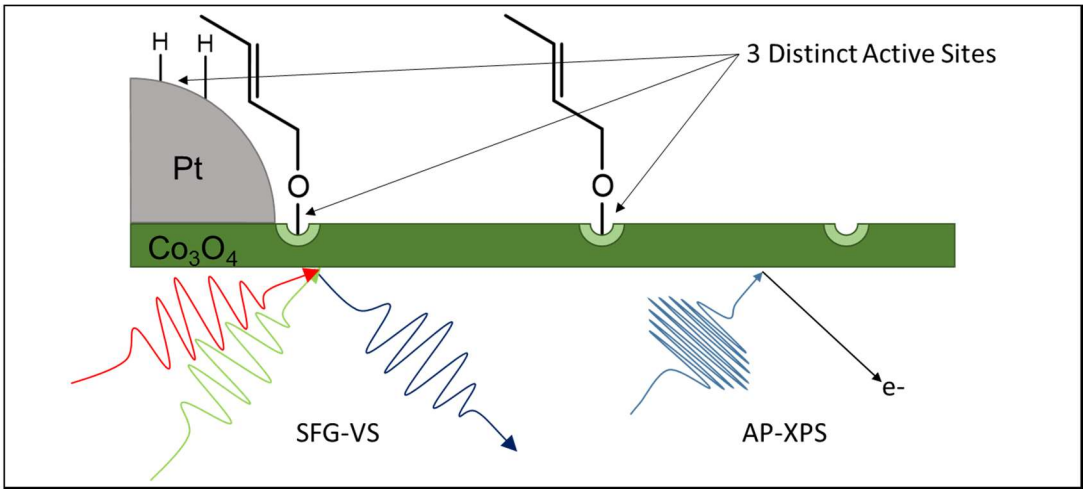

Scheme 1

6.5 Experimental Methods

6.5.1 Catalyst Preparation

The catalysts used for this study consisted of colloidally synthesized platinum nanoparticles supported on cobalt oxide thin films prepared by atomic layer deposition (ALD). Thin films were fabricated using an Oxford FlexAl-Plasma Enhanced Atomic Layer Deposition (ALD) apparatus in the Molecular Foundry at Lawrence Berkeley National Lab. Using

Bis(cyclopentadienyl) cobalt(II) as the gas-phase metal precursor, a substrate temperature of 300°C and alternating precursor and oxygen plasma cycles thin films of spinel (Co_3O_4)[17] cobalt oxide were produced with a thickness of 30nm for all applications.

Platinum nanoparticles with an average diameter of 4.6nm were synthesized using the polyol method as described previously[18]. In short chloroplatinic acid hexahydrate and polyvinyl pyrrolidone were dissolved in ethylene glycol in a 1:4 ratio by mass. The solution was then heated to 180°C for one hour under an argon atmosphere. The resulting dark brown solution was then mixed with acetone to precipitate the particles from solution. The particles were dissolved in ethanol and subsequently washed 3 times using ethanol and hexane.

The resulting particles were deposited onto two-dimensional substrates (silicon oxide wafers for catalytic tests and quartz windows for spectroscopic study which had been coated with the previously mentioned cobalt oxide films), using a Langmuir-Blodgett Trough as described previously[5]. Langmuir-Blodgett deposition allows for control of the nanoparticle density on the substrate by varying the surface pressure of a water surface coated with the nanoparticle solution maintained during deposition. Catalysts were prepared with surface pressures ranging between 20-35 mN/m resulting in a 17-32% coverage of the substrate by platinum nanoparticles. Figure 2 shows Transmission Electron Microscopy images of the four different density films. These images show a clear trend between LB pressure and particle coverage. Several images for each pressure were used to determine the percent coverages.

Following deposition of the nanoparticles the combined Pt/Co_3O_4 catalyst is treated with ozone producing UV light, in a home built treatment chamber consisting of two low-pressure mercury (Hg) lamps (Lights Sources Inc., model number GPH357T5VH/4P) which emit two lines: 184 and 254 nm. This serves to remove the PVP capping ligand from the particles and subsequently initiates contact between the metal particle and oxide. This contact has been previously reported as critical for the support to influence the reaction rate and selectivity.[4] After this UV treatment the catalyst is ready for catalytic or spectroscopic measurement.

6.5.2 Measurement of Catalytic Performance

Catalyst reactivity and selectivity was measured using a stainless steel, batch mode, gas phase reactor. The reactor consists of a one liter chamber, boronitride resistive heater, thermocouple, metal bellow recirculation pump, and gas manifold for dosing reaction gases. For all crotonaldehyde hydrogenation reactions 1 Torr of crotonaldehyde, 100 Torr of hydrogen and 669 Torr of helium were dosed into the reactor. Each reaction was run for eight hours, and the gas mixture was sampled approximately every five minutes and analyzed by a gas chromatograph equipped with a flame ionization detector and Cyclodex B capillary column. The catalysts temperature was 120°C unless otherwise noted. Reaction rates are calculated by plotting the normalized GC peak area for each gas versus time. Total conversion is kept low (below 10%) over the eight hour reaction time in order for a steady state approximation to be made. Reported rates are taken after initial deactivation, attributed to CO poisoning of the Pt surface.

To obtain a turnover frequency (TOF, Product Molecules Produced per Pt Site per second) the reaction rates are normalized to the number of Pt surface atoms as determined from a

measurement of the ethylene hydrogenation activity for each catalyst. Since ethylene hydrogenation is a structure insensitive reaction a known TOF[19] can be used to calculate the number of Pt sites from a measured reaction rate. Conditions for all ethylene hydrogenation reactions was 10 Torr ethylene, 100 Torr Hydrogen and 660 Torr He at 25°C.

6.5.3 Sum Frequency Generation Vibrational Spectroscopy

Sum Frequency Generation Vibrational Spectroscopy (SFG-VS) is a nonlinear spectroscopic technique that allows for vibrational spectra to be collected specifically from surfaces and interfaces. Rather than probing the molecular dipole (Infrared Absorption) or polarizability (Raman Spectroscopy) SFG probes the molecular hyperpolarizability. The hyperpolarizability (β) can be represented as the product of the molecular dipole (μ) and molecular polarizability (α).

$$\beta_{abc} = \mu_c \cdot \alpha_{ab}$$

By the rule of mutual exclusion we know that a molecule possessing centrosymmetry cannot have a vibrational mode with both a nonzero dipole moment and a nonzero polarizability, thus SFG can only occur when centrosymmetry is broken, most importantly, at interfaces between phases. This property makes SFG exceedingly useful for selectively obtaining vibrational spectra from molecules adsorbed at a gas-solid interface. The SFG signal is generated when two beams, a visible beam with a fixed wavelength and an infrared beam with a tunable wavelength, are overlapped at the interface. The process can be thought of as a combined infrared absorption and anti-Stokes Raman scatter yielding a photon whose frequency is the sum of the inputs beams. The signal intensity will increase when the wavelength of the infrared beam is resonant with a vibrational mode of a molecule at that interface, thus giving a spectrum of SFG Intensity vs. IR Wavelength.

This was accomplished using an active/passive mode-locked Nd:YAG laser (Continuum Leopard D-20) which produces 20 ps pulses of 1064 nm light at a repetition rate of 20 Hz. The fundamental 1064 nm output was passed through an optical parametric generator/amplifier (Laservision) to give a second harmonic visible beam (VIS) of 532 nm and amid-infrared beam (IR) tunable from 2700 – 3600 cm^{-1}. Spectroscopic experiments are performed in the total internal reflection geometry as shown in supplement figure S1. The IR and VIS beams, each with 200 μJ power per pulse, were overlapped spatially and temporally at the surface of the catalyst deposited on a quartz window as described above, which was pressed against a quartz prism in order to direct the beams. An index matching gel consisting of deuterated polystyrene and deuterated decalin was used to prevent reflection at the prism-window interface. The SF signal was collected using a PMT accompanied by a gated integrator to improve the signal quality. Using a homebuilt cell the surface was heated and a recirculating mixture of the reaction gases is passed over the catalyst.

6.5.4 X-Ray Photoelectron Spectroscopy

X-Ray Photoelectron Spectroscopy, performed in vacuum and in Ambient Pressure modes, allows for the characterization of composition of the catalyst surface and determination

of surface oxidation states. Ambient Pressure X-Ray Photoelectron Spectroscopy (AP-XPS) was performed at beamline 9.3.2 of the Advanced Light Source at Lawrence Berkeley National Lab. This beamline has a tunable x-ray source (240-900eV) and a differentially pumped hemispherical analyzer that allows for the introduction of gas to the sample at pressures up to several Torr. Catalysts for XPS study were prepared in the same manner as those for catalytic tests, however the wafer used was a highly p-doped wafer rather than one with a thermally grown silicon oxide in order to reduce the charging of the surface. A thorough description of the beamline can be found elsewhere.[20] Analysis and fitting of the XPS spectra was performed using CasaXPS.

6.5.5 Transmission Electron Microscopy

Microscopy experiments were performed using a JEOL 2100-F 200 kV Field-Emission Analytical Transmission Electron Microscope in the Molecular Foundry at Lawrence Berkeley National Laboratory. Image analysis was performed using ImageJ.

6.5.6 Near Edge X-Ray Absorption Fine Structure Spectroscopy (NEXAFS)

In situ NEXAFS spectroscopy was performed at the Advanced Light Source Beamline 10.3.2 at Lawrence Berkeley National Laboratory. Experiments were carried out using fluorescence yield detection in the QuickXAS mode using a homebuilt cell described previously.[21] Deadtime correction, pre-edge removal and post-edge normalization of the near edge spectra (up to 250 eV past the absorption threshold at the Co K edge) were carried out with software developed at the beamline.[22]

6.6 References

(1) Tauster, S.; Fung, S.; Baker, R.; Horsley, J. *Science* **1981**, *211*, 1121–1125.

(2) Schwab, G. M.; Koller, K. *J. Am. Chem. Soc.* **1968**, *90*, 3078-3080.

(3) An, K.; Alayoglu, S.; Musselwhite, N.; Na, K.; Somorjai, G. A. *J. Am. Chem. Soc.* **2014**, *136*, 6830–6833.

(4) Baker, L. R.; Kennedy, G.; van Spronsen, M.; Hervier, A.; Cai, X.; Chen, S.; Wang, L.-W.; Somorjai, G. A. *J. Am. Chem. Soc.* **2012**, *134*, 14208–14216.

(5) Kennedy, G.; Baker, L. R.; Somorjai, G. A. *Angew. Chem.* **2014**, *126*, 3473–3476.

(6) An, K.; Alayoglu, S.; Musselwhite, N.; Plamthottam, S.; Melaet, G.; Lindeman, A. E.; Somorjai, G. A. *J. Am. Chem. Soc.* **2013**, *135*, 16689-16696.

(7) Hervier, A.; Baker, L. R.; Komvopoulos, K.; Somorjai, G. A. *J. Phys. Chem. C* **2011**, *115*, 22960–22964.

(8) Park, J. Y.; Baker, L. R.; Somorjai, G. A. *Chem. Rev.* **2015**, *115*, 2781-2817.

(9) Grass, M.; Rioux, R.; Somorjai, G. *Catal. Lett.* **2009**, *128*, 1–8.

(10) Englisch, M.; Jentys, A.; Lercher, J. A. *J. Catal.* **1997**, *166*, 25 – 35.

(11) Vannice, M. A.; Sen, B. *J. Catal.* **1989**, *115*, 65–78.

(12) Kliewer, C. J.; Bieri, M.; Somorjai, G. A. *J. Am. Chem. Soc.* **2009**, *131*, 9958–9966.

(13) Dandekar, A.; Vannice, M. A. *J. Catal.* **1999**, *183*, 344–354.

(14) Han, H.-L.; Melaet, G.; Alayoglu, S.; Somorjai, G. A. *ChemCatChem* **2015**, *7*, 3625-3638.

(15) Jayaprakash, A.; Arjunan, V.; Jose, S. P.; Mohan, S. *Spectrochim. Acta, Part A* **2011**, *83*, 411–419.

(16) Beaumont, S. K.; Alayoglu, S.; Specht, C.; Kruse, N.; Somorjai, G. A. *Nano Lett.* **2014**, *14*, 4792-4796.

(17) Donders, M. E.; Knoops, H. C. M.; van, M. C. M.; Kessels, W. M. M.; Notten, P. H. L. *J. Electrochem. Soc.* **2011**, *158*, G92-96.

(18) Rioux, R. M.; Song, H.; Hoefelmeyer, J. D.; Yang, P.; Somorjai, G. A. *J. Phys. Chem. B* **2005**, *109*, 2192–2202.

(19) Kuhn, J. N.; Tsung, C.-K.; Huang, W.; Somorjai, G. A. *J. Catal.* **2009**, *265*, 209–215.

(20) Grass, M. E.; Karlsson, P. G.; Aksoy, F.; Lundqvist, M.; Wannberg, B.; Mun, B. S.; Hussain, Z.; Liu, Z. *Rev. Sci. Instrum.* **2010**, *81*, 053106-1 - 053106-6.

(21) Alayoglu, S.; Beaumont, S. K.; Melaet, G.; Lindeman, A. E.; Musselwhite, N.; Brooks, C. J.; Marcus, M. A.; Guo, J.; Liu, Z.; Kruse, N.; Somorjai, G. A., *J. Phys. Chem. C* **2013**, *117*, 21803-21809.

(22) Marcus, M. A.; MacDowell, A. A.; Celestre, R.; Manceau, A.; Miller, T.; Padmore, H. A.; Sublett, R. E. *J. Synchrotron Radiat.* **2004**, *11*, 239-247.

Chapter 7

Encapsulation of Pt Nanoparticles by Cobalt Oxide and its Effect on the Hydrogenation of Crotonaldehyde Studied by *in-situ* Vibrational and X-Ray Spectroscopies

7.1 Abstract

In this work two-dimensional nanoparticle catalysts composed of colloidally synthesized Pt nanoparticles and cobalt oxide thin films were studied for the catalytic hydrogenation of crotonaldehyde. While studying the surface chemical states of the catalyst materials under reactive gas conditions using ambient pressure x-ray photoelectron spectroscopy (AP-XPS) it was discovered that following exposure to hydrogen at 513 K and a subsequent exposure to oxygen at 573 K the platinum signal was no longer observed in the XPS spectrum and could not be recovered using subsequent gas treatments. This unexpected result suggested the Pt particles had been encapsulated by the oxide support to such an extent that the Pt photoelectron escape depth was smaller than the thickness of the cobalt encapsulation layer. Following this observation, the catalytic performance of the encapsulated catalyst was studied for the hydrogenation of crotonaldehyde. It was found that the encapsulated catalyst, while having a lower exposed Pt surface area, was substantially more active than the as prepared catalyst for all products, however the product selectivity was dramatically altered, with the selectivity toward butyraldehyde increasing from 53% to 73%. This increase in selectivity correlated well with vibrational spectra obtained by sum frequency generation (SFG) spectroscopy. An enhancement in the intensity of the features attributed to a surface intermediate for butyraldehyde production was observed relative to the intensities of features attributed to intermediates of other products. Taking these data together suggests the encapsulation layer of cobalt oxide is at minimum 2 nm in thickness but porous as to allow the diffusion of reactant and product molecules to and from the Pt surface.

7.2 Introduction

Since the discovery of synergistic catalytic effects arising from metal/oxide interfaces in 1968 by Schwab,[1] continuing with the discovery of the strong metal-support interaction (SMSI) by Tauster and Fung in 1978,[2] through to the present day there has been extensive work aimed at uncovering the nature of interactions between catalytic metal nanoparticles and their supports. One of the earliest explanations for the effects observed by Tauster and Fung, where in the hydrogen adsorption on Pt supported by TiO_2 dropped following a high temperature reduction, was the encapsulation of the metal particles by the reduced oxide support.[3] It is generally accepted that this encapsulation occurs as a means of reducing the surface energy of a surface by decorating a high surface energy metal by a low surface energy oxide.[4] From the observations of Tauster and Fung and general intuition it would be thought that following this encapsulation the catalyst would lose activity, since the active metal sites are being blocked. However Vannice and Twu showed that despite the encapsulation a Pt/TiO_2 catalyst in the SMSI state was dramatically more active than Pt supported on other oxides or without the SMSI inducing treatment for the methanation of carbon monoxide.[5]

As an extension of the work presented in Chapter 6, the present work demonstrates the encapsulation effect for a new material system, Pt supported on cobalt oxide (Co_3O_4), and its impact on the hydrogenation of ethylene and crotonaldehyde. The encapsulation is first evidenced by ambient pressure XPS experiments first employed to monitor the surface oxidation states of the Pt and Co_3O_4 as they are exposed to reaction relevant conditions (elevated temperatures in H_2). Upon reoxidation of the catalyst the Pt signal is not observed, indicative of an overlayer formation.[6] Reaction studies revealed that, as in the case of Tauster and Fung's work, the amount of available Pt surface area had been decreased by the encapsulation, yet the activity for crotonaldehyde hydrogenation, like for the methanation of carbon monoxide, was dramatically increased and the selectivity was altered. Sum frequency generation vibrational spectroscopy was then employed to the influence of the encapsulation on the adsorption of the crotonaldehyde reactant molecule and the formation of intermediate species. Through the combination of these studies we can conclude that the cobalt oxide overlayer forms in such a way that increases the amount of interface sites, decreases the available Pt sites, and is porous as to allow for molecular diffusion to and from the Pt surface. Possibilities are given to explain the increase in total activity and change in selectivity for crotonaldehyde hydrogenation, however the results presented are insufficient to determine the exact reason for the changes.

7.3 Results and Discussion

7.3.1 Ambient Pressure X-Ray Photoelectron Spectroscopy

In this study the Pt/Co_3O_4 catalyst was prepared according to the method outlined above and introduced into the XPS chamber. The catalyst was then exposed to 100 mTorr of H_2 gas and heated incrementally to 513 K, a temperature still below the bulk reduction temperature of Co_3O_4, but which was shown to induced reduction of the cobalt surface. Following this the catalyst was re-oxidized by exposure to 100 mTorr of O_2 at 573 K to return the cobalt oxide surface to its initial state. Figure 7.1 shows the Pt 4f and Co 3p edges for this series of conditions.

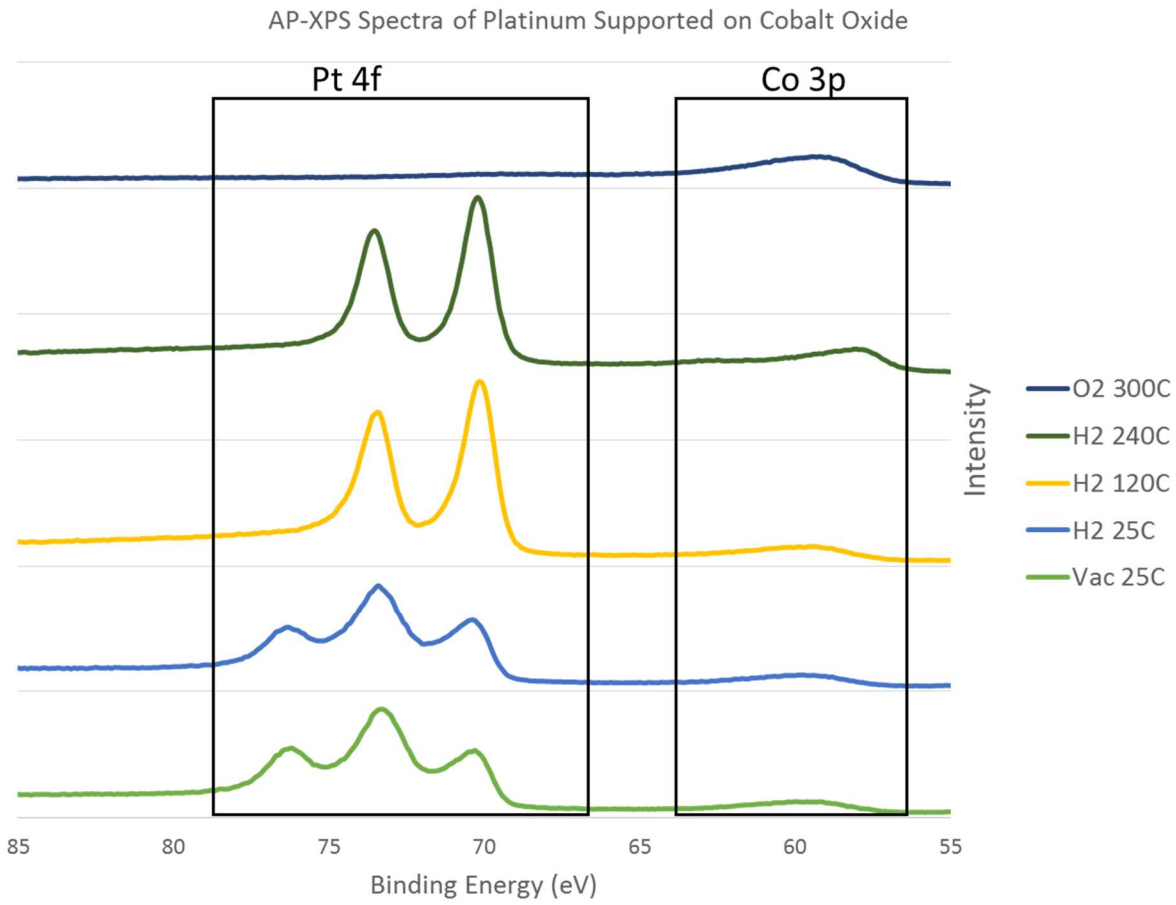

Figure 7.1 Ambient Pressure XPS spectra of the Pt 4f and Co 3p edges under a series of gas and temperature conditions. The progression of the spectra starts at the bottom and proceeds up. Immediately following the UV treatment the Pt is seen to be partially oxidized and is subsequently reduced upon heating to 120°C (393 K). After heating to 240°C (513 K) in H_2 the chamber was evacuated and oxygen is introduced and heated to 300°C (573 K). Under these conditions the Pt signal disappears and the Co signal increases slightly in intensity.

Upon the introduction of O_2 to the system at 573 K following the reduction of the cobalt surface by H_2 a surprising observation was made, the Pt signal completely vanished from the AP-XPS spectrum. Two possible explanations can be offered to explain this result; (1) the Pt has been removed from the catalyst, e.g. by evaporation, or (2) the photoelectrons generated by the Pt cannot escape from the sample surface. Possibility (1) is unlikely considering the temperature conditions used, leaving possibility (2). In order to explain this one must understand certain fundamental aspects of XPS. The signal obtained from XPS comes in the form of photoelectrons emitted by an atom following excitation by the x-ray. These photoelectrons typically have kinetic energies in the range of 100-1000 eV. When escaping from a solid material, electrons with this range of kinetic energies can travel a distance on the order of 1 nm before being deflected by the solid and losing the information contained in its initial kinetic energy. Thus if the Pt particles became decorated or covered by more than approximately 2 nm of cobalt oxide the Pt generated

photoelectrons would not reach the detector. This explanation has support from literature where in there are several examples of catalyst decoration by a supporting oxide. This is one of the primary mechanisms offered to explain the strong metal-support interaction (SMSI) first proposed by Tauster and Fung. It is generally accepted that the driving force for this encapsulation is the minimization of surface energy, and this effect is typically observed when low surface energy oxides (i.e. titania, ceria) are used to support high surface energy metals (i.e. Pt, Rh, Pd).[7] Additionally, these encapsulation phenomena have been shown to greatly impact the adsorption behavior of gas phase molecules and catalytic properties of the resulting material. As such a study was undertaken to verify that this was in fact a case oxide encapsulation of a metal nanoparticle and what effect this would have on the crotonaldehyde hydrogenation behavior of the catalyst.

7.3.2 Catalytic Reaction Studies

For catalytic tests analogous samples to those studied by AP-XPS were prepared and the encapsulation was initiated by *ex-situ* treatments in hydrogen and oxygen at the same temperatures but by flowing the gases at a pressure of 760 torr through a tube furnace for 1hr at each condition. The encapsulation was verified by lab XPS performed in vacuum and, as expected, no Pt signal was observed after the treatment, while it was detectable prior.

To investigate the effect of this treatment on the amount of available platinum surface the rate of ethylene hydrogenation was measured and using a known turnover frequency the number of exposed surface Pt atoms can be calculated.[8] Using this method we found that before the treatment the catalyst possessed 6.0×10^{14} Surface Pt atoms/cm^2, and following the treatment this value dropped to 4.8×10^{14} Surface Pt atoms/cm^2. A drop in available Pt surface would be expected following encapsulation by the oxide support but it is interesting to note that the vast majority (80%) of the Pt surface is still accessible by gas phase reactant molecules. This suggests a porosity to the overlayer that is sufficient to allow molecular diffusion but insufficient to allow for detectable levels of photoelectrons to escape. Additionally this serves as proof that the Pt particles remain on the catalyst following the reduction/oxidation cycle, disproving possibility (1) given above.

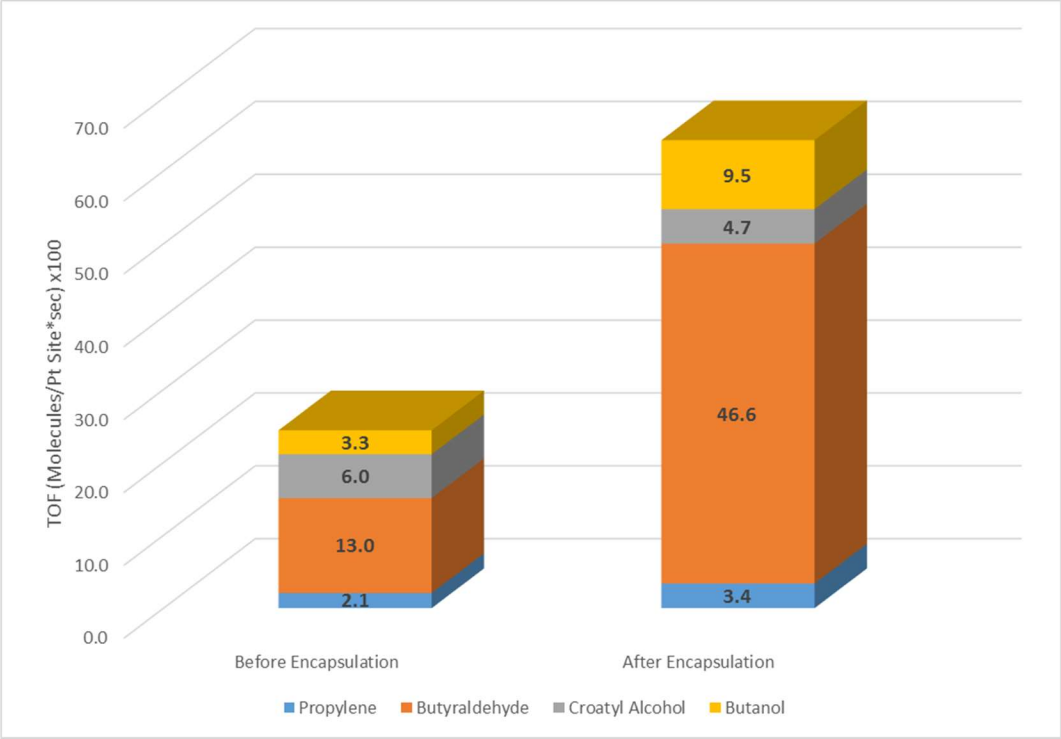

Figure 7.2 Turnover frequency results for the Pt/Co_3O_4 catalyst after only UV treatment, and after UV + Reduction/Oxidation treatment. The rate of formation for each of the four products are shown as indicated in the legend. Reactions were conducted with 1 Torr crotonaldehyde, 100 Torr H_2 and 669 Torr He at a catalyst temperature of 393 K.

The results for the catalytic hydrogenation of crotonaldehyde over the Pt/Co_3O_4 catalyst before and after encapsulation are summarized in figure 7.2. The total activity after reduction/oxidation treatment resulting in the encapsulation is, quite surprisingly, more than double than after the UV treatment alone, with the largest portion of that increased activity going toward butyraldehyde. The increased production of butyraldehyde and butanol come at a small loss of activity toward crotyl alcohol, however this loss in crotyl alcohol activity cannot explain the magnitude of the increase in butyraldehyde production. Previous work has shown an interplay between the production of butanol and crotyl alcohol based upon the relative abundance of interface sites as compared to oxide surface sites.[9] In this work we proposed that butanol is likely formed at the interface between Pt and Co_3O_4. This could be used to explain the change in butanol and crotyl alcohol activities here as encapsulation would increase the total number of interface sites relative to the starting catalyst, thus increasing the production of butanol. The dramatic increase in the production of butyraldehyde, however, remains rather difficult to explain. In order obtain more insight into effect the encapsulation has on this reaction pathway we turn to sum frequency generation vibrational spectroscopy.

7.3.3 Sum Frequency Generation Vibrational Spectroscopy

For the SFG studies catalysts were prepared in an identical manner to those for catalytic testing but deposited onto an optical quartz window to allow for spectroscopic study as outlined in the methods section. They underwent the same hydrogen/oxygen treatment as outlined in

section 7.4.2 to initiate the encapsulation. Figure 7.3 contains spectra in the CH vibrational region of the SFG spectrum for the Pt/Co_3O_4 catalyst under crotonaldehyde hydrogenation reaction conditions before and after the encapsulation inducing treatment.

Five distinct features are identified in both spectra, two assigned to a Pt bound crotonaldehyde molecule believed to be the precursor for the production of butyraldehyde (aldehyde CH at 2855 cm^{-1} and CH_3 at 2915 cm^{-1}), and three (symmetric CH_3 at 2875 cm^{-1}, asymmetric CH_3 at 2940 cm^{-1} and fermi resonance CH_3 at 2970 cm^{-1}) assigned to a cobalt oxide bound crotonaldehyde molecule, bound through the aldehyde group, believed to be the precursor to alcohol formation.[9] The presence all of all features in both spectra is expected as the species formed by each catalyst are the same, but the relative intensities of these features can give insight into the catalytic behavior observed above.

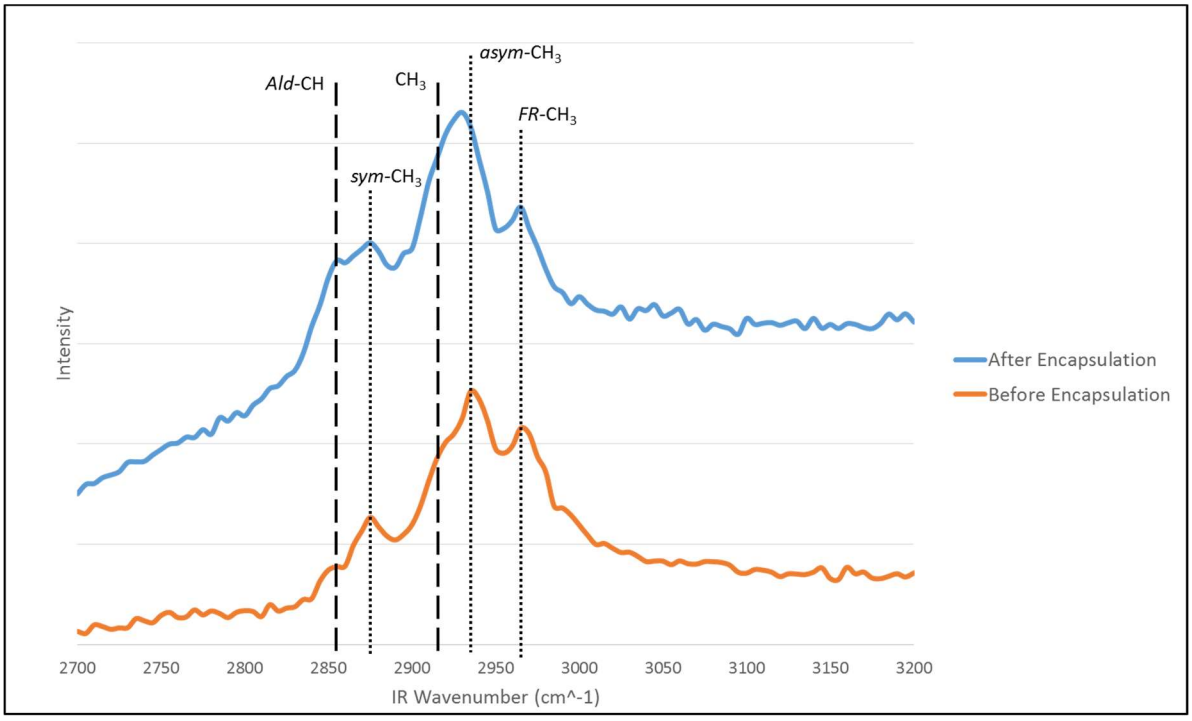

Figure 7.3 Sum frequency generation vibrational spectra of the Pt/Co_3O_4 catalyst under crotonaldehyde hydrogenation reaction conditions. Conditions are 1 torr crotonaldehyde, 100 torr hydrogen and 669 torr helium with a catalyst temperature of 120°C (393 K). Five features are assigned for both spectra. The aldehyde-CH stretch and CH_3 stretch marked by the thick dotted line are assigned to a Pt bound surface intermediate for the formation of butyraldehyde. The symmetric, asymmetric and fermi-resonance CH_3 features marked with the fine dotted line are assigned to a cobalt oxide bound intermediate to alcohol formation. A dramatic increase in the intensity of the features assigned to the Pt bound butyraldehyde intermediate is observed following encapsulation of the metal by the oxide.

As shown in figure 7.3 the intensity those features assigned to the butyraldehyde intermediate are increased substantially for the catalyst that has undergone the encapsulation treatment, while the features assigned to the oxide bound intermediate species are relatively

unchanged. These results correlate rather directly with the observed trends in catalytic activity. The total activity toward the alcohol products increases slightly, by 52%, following encapsulation while the production of butyraldehyde increases by nearly 260%. The primary conclusion to be gained from the SFG spectra is that the increased butyraldehyde production directly correlates with an increased coverage of the Pt surface by the butyraldehyde precursor species. Furthermore this implies that the mechanism for butyraldehyde remains unchanged as a change in mechanism would likely result in new spectral features. We observe no new features and thus we can assume butyraldehyde is still produced through the Pt dependent pathway described by Kliewer et. al.[10] The precise mechanism for this enhancement, however, cannot be determined by the above experiments alone. Multiple possible explanations could be argued for, including steric influence of the porous overlayer influencing molecular adsorption on the surface, electronic interactions between oxide and metal upon treatment, or additional surface carbon removal by the hydrogen oxygen treatment exposing sites which are far more active, however based upon the experiments here a firm conclusion cannot be made.

7.4 Conclusions

In summation it has been found that under rather mild conditions (513 K in H_2, 573 K in O_2) Pt nanoparticles supported on cobalt oxide (Co_3O_4) will become encapsulated by a cobalt oxide overlayer, causing Pt to be undetectable by XPS. This is indicative of an overlayer of at least 1-2 nm in thickness. After this encapsulation has been initiated the Pt surface remains accessible and only a small portion of the Pt surface area is blocked by the presence of oxide layer as evidenced by the ethylene hydrogenation activity before and after encapsulation. When used for the hydrogenation of crotonaldehyde the encapsulated catalyst shows an improved activity as compared to the non-encapsulated catalyst with the majority of this increased activity directed toward the butyraldehyde product, and a smaller portion to butanol. Surface vibrational spectra obtained by sum frequency generation show an enhancement in the intensity of those features attributed to a crotonaldehyde molecule adsorbed to the Pt as an intermediate to butyraldehyde which indicates that the primary pathway for butyraldehyde production is further activated by the encapsulation, rather than that product being formed through a new reaction pathway. The exact cause of this enhancement remains undetermined but possible mechanism are proposed.

7.5 Experimental Methods

7.5.1 Catalyst Preparation

The catalysts prepared for this work consisted of colloidally synthesized platinum nanoparticles supported by thin films of cobalt oxide (Co_3O_4) formed by atomic layer deposition.

The thin films were prepared with an Oxford FlexAl-Plasma Enhanced Atomic Layer Deposition (ALD) apparatus in the Molecular Foundry at Lawrence Berkeley National Lab. Bis(cyclopentadienyl) cobalt(II) served as the gas-phase metal precursor and oxygen plasma was used as an oxidizer. A substrate temperature of 300°C and alternating precursor and oxygen plasma cycles produced thin films of spinel (Co_3O_4) cobalt oxide with a thickness of 30 nm. The oxide structure was confirmed by XPS.

Platinum nanoparticles of 4.6 nm diameter were synthesized using the polyol method. In short chloroplatinic acid hexahydrate and polyvinylpyrrolidone were dissolved in ethylene glycol in a 1:4 ratio by mass. The solution was then heated to 180°C for one hour under an inert argon atmosphere. To the resulting solution acetone was added to precipitate the particles. The particles were then dispersed in ethanol and subsequently washed 3 times using alternating washes of ethanol and hexane to remove excess capping agent.

The resulting particles were deposited onto flat substrates (silicon oxide wafers for catalytic tests and quartz windows for spectroscopic study which with cobalt oxide films), using a Langmuir-Blodgett Trough. Langmuir-Blodgett deposition allows for the deposition of well controlled monolayers of nanoparticles to be deposited on the target substrate ensuring maximal interaction of the nanoparticle and support.

Following deposition of the nanoparticles the combined Pt/Co_3O_4 catalyst was treated with UV light in a home built treatment chamber consisting of two low-pressure mercury (Hg) lamps (Lights Sources Inc., model number GPH357T5VH/4P) which emit two lines: 184 and 254 nm. The UV light removes the capping agents by the combined action of ozone produced by the 184 nm line and photoexcitation of the Pt-PVP bond by the 254 nm line.

In order to initiate the encapsulation effect observed in the AP-XPS experiments the prepared catalyst was treated in a tube furnace t 513 K in hydrogen then subsequently at 583 K in oxygen. The encapsulation of the Pt particles by the cobalt oxide was confirmed by lab XPS.

7.5.2 Measurement of Catalytic Performance

Catalyst reactivity and selectivity was measured using a stainless steel, batch mode, gas phase reactor. The reactor consists of a 1 L chamber, boronitride resistive heater, thermocouple, metal bellow recirculation pump, and gas manifold for dosing reaction gases. For all crotonaldehyde hydrogenation reactions 1 Torr of crotonaldehyde, 100 Torr of hydrogen and 669 Torr of helium were dosed into the reactor. Reactions were run for eight hours, and the gas mixture was sampled approximately every five minutes and analyzed by a gas chromatograph equipped with a flame ionization detector and Cyclodex B capillary column. The catalysts temperature was 120°C. Reaction rates are calculated by plotting the normalized GC peak area for each gas versus time. Total conversion is kept low (below 10%) over the eight hour reaction time to minimize the formation of secondary products.

To obtain a turnover frequency (TOF, Product Molecules Produced per Pt Site per second) the reaction rates are normalized to the number of Pt surface atoms as determined from a measurement of the ethylene hydrogenation activity for each catalyst. Furthermore the ethylene hydrogenation rate can be used to measure the degree to which the encapsulation blocks Pt surface sites. Since ethylene hydrogenation is a structure insensitive reaction a known TOF can be used to calculate the number of Pt sites from a measured reaction rate. Conditions for all ethylene hydrogenation reactions was 10 Torr ethylene, 100 Torr Hydrogen and 660 Torr He at 25°C.

7.5.3 Sum Frequency Generation Vibrational Spectroscopy

Sum Frequency Generation (SFG) Vibrational Spectroscopy is a nonlinear optical spectroscopic technique that allows for vibrational spectra to be collected specifically from surfaces and interfaces. This property makes SFG exceedingly useful for selectively obtaining

vibrational spectra from molecules adsorbed at a gas-solid interface. The SFG signal is generated when two beams, a visible beam with a fixed wavelength and an infrared beam with a tunable wavelength, are overlapped spatially and temporally at the interface. The process can be thought of as a combined infrared absorption and anti-Stokes Raman scatter yielding a photon whose frequency is the sum of the inputs beams. The signal intensity increases when the when the infrared beam is resonant with a vibrational mode of a molecule at that interface, thus giving a spectrum of SFG Intensity vs. IR Wavelength.

This was accomplished using an active/passive mode-locked Nd:YAG laser (Continuum Leopard D-20) which produces 20 ps pulses of 1064 nm light at a repetition rate of 20 Hz. The fundamental 1064 nm output was passed through an optical parametric generator/amplifier (Laservision) to give a second harmonic visible beam (VIS) of 532 nm and a mid-infrared beam (IR) tunable from 2700 – 3600 cm^{-1}. Spectroscopic experiments are performed in the total internal reflection geometry. The IR and VIS beams, each with 200 μJ power per pulse, were overlapped spatially and temporally at the surface of the catalyst deposited on a quartz window as described above, which was pressed against a quartz prism in order to direct the beams. An index matching gel consisting of deuterated polystyrene and deuterated decalin was used to prevent reflection at the prism-window interface. The SF signal was collected using a photomultiplier tube detector accompanied by a gated integrator to improve the signal quality. Using a homebuilt cell the surface was heated and a recirculating mixture of the reaction gases is passed over the catalyst.

7.5.4 X-Ray Photoelectron Spectroscopy

X-Ray Photoelectron Spectroscopy, performed in vacuum and in Ambient Pressure modes, allows for the characterization of the surface composition of the catalyst and determination of surface oxidation states. Ambient Pressure X-Ray Photoelectron Spectroscopy (AP-XPS) was performed at beamline 9.3.2 of the Advanced Light Source at Lawrence Berkeley National Lab.[11] This beamline utilizes the tunable nature of the synchrotron based x-rays (240-900eV) and a differentially pumped hemispherical analyzer, which allows for the introduction of gas to the sample at pressures up to several Torr, to study the dynamic surface states that can arise when a system is exposed to a reactive environment. Catalysts for XPS study were prepared in the same manner as those for catalytic tests, however the wafer used was a highly p-doped wafer in order to increase the conductivity of the sample and reduce the charging of the surface, which would result in shifting of the XPS features. Analysis and fitting of the XPS spectra was performed using CasaXPS.

7.6 References

(1) Schwab, G. M.; Koller, K. *Journal of the American Chemical Society* **1968**, *90*, 3078.

(2) Tauster, S. J.; Fung, S. C.; Garten, R. L. *Journal of the American Chemical Society* **1978**, *100*, 170.

(3) Baker, R. T.; Prestridge, E. B.; Garten, R. L. *Journal of Catalysis* **1979**, *56*, 390.

(4) Qin, Z. H.; Lewandowski, M.; Sun, Y. N.; Shaikhutdinov, S.; Freund, H. J. *The Journal of Physical Chemistry C* **2008**, *112*, 10209.

(5) Vannice, M. A.; Twu, C. C. *Journal of Catalysis* **1983**, *82*, 213.

(6) Sadeghi, H. R.; Henrich, V. E. *Journal of Catalysis* **1984**, *87*, 279.

(7) Tauster, S.; Fung, S.; Baker, R.; Horsley, J. *Science* **1981**, *211*, 1121.

(8) Kuhn, J. N.; Tsung, C.-K.; Huang, W.; Somorjai, G. A. *Journal of Catalysis* **2009**, *265*, 209.

(9) Kennedy, G.; Melaet, G.; Han, H.-L.; Ralston, W. T.; Somorjai, G. A. *ACS Catalysis* **2016**, *6*, 7140.

(10) Kliewer, C. J.; Bieri, M.; Somorjai, G. A. *Journal of the American Chemical Society* **2009**, *131*, 9958.

(11) Grass, M. E.; Karlsson, P. G.; Aksoy, F.; Lundqvist, M.; Wannberg, B.; Mun, B. S.; Hussain, Z.; Liu, Z. *Rev Sci Instrum* **2010**, *81*, 053106.